Polycationic polymers in nucleic acid delivery: Membrane interaction and cellular responses

by

Rahul Rattan

A dissertation submitted in partial fulfillment
of the requirements for the degree of
Doctor of Philosophy
(Biomedical Engineering)
in the University of Michigan
2013

Doctoral Committee:

Professor Mark M. Banaszak Holl, Chair
Research Assistant Professor Anna U. Bielinska
Professor David H. Kohn
Professor Bradford G. Orr

Devoted to Smita Rattan
Your memory is my inseparable keepsake

Acknowledgements

This work would not have been completed without help, mentorship, friendship and support of many. Writing acknowledgment is unbelievably difficult and I tried my best to express my gratitude. Unfortunately to err is human and in all likelihood I will miss someone, if that person is you reading this I hope I get a chance to thank you in person.

First and foremost I am thankful to Mark Banaszak Holl for his support and guidance. His optimism and ingenious insights have made this work possible. I still remember the time I would "walk-in" his Chemistry office knocking on his door, he will always had time to discuss my work. I also appreciate his understanding when I spend long hours away from lab working on Endocutter and encouragement to include Endocutter as my thesis chapter.

I am thankful to Anna Bielinska who took me under her wing and taught me how to do real Science. Her critical thinking and analytical understanding of biology played an indispensible role in my work.

I'm grateful to Brad Orr for his helpful suggestions and perspective that as an engineer and physics enthusiast I valued and enjoyed greatly. I find myself at awe of his teaching skills and how easily he could explain complex physics principles.

I would like to express my gratitude to James R. Baker, Jr., M.D. for his helpful comments and guidance regarding my projects. His knowledge pool, keen intellect and extensive biology expertise have helped me at multiple points in my projects.

I would also like to take this opportunity to thank David Kohn for serving on my committee and helping me realize the broader picture related to my projects.

I have also been fortunate enough to have labmates like Becky Lahti Matz and Lisa Prevette and deeply appreciate their support and encouragement over the years of my graduate school. I would like to extent this gratitude to all Banaszak Holl group members who patiently listened to my data presentations and gave me valuable feedback.

I would like to thank Alina Kotlyar for her excellent lab management skills. She made sure I have all the reagents and material required for my work, her accommodating nature created an inviting and fun atmosphere to work in. I was also lucky to tap into Jolanta Kukowska-Latallo's molecular biology expertise; she was always available to help me with my molecular biology questions.

I would also take this opportunity to thank my Endocutter team: Taarif Jafferi, Zachary Weingarden, Raghunath Katragadda, Robert Stoler, M.D., Aileen Huang-Saad, David Olson, Toby Donajkowski, Joe Elmunzer, M.D. and Daniel Hazekamp. Working on Endocutter with a team like you was one of the highlights of my graduate career.

I would like to express my gratitude to my first tutor and sister Kavita Taneja. Words will fall short to explain her role in what and where I am today. I can't thank

her enough for all the time she invested in me making sure that I do well on my exams when she was falling short on hers. I owe you everything I am today.

I am forever thankful and indebted to my sister Smita Rattan for her support in my endeavors. You will forever be loved and cherished.

I would also like to thank Kaitlin M. Hanlon, D.O. and Hanlon family for their love, support, care and inspiration.

Lastly but most importantly, I am thankful to my parents and my sister Amita Rattan for their unconditional love and support. Their unwavering belief, perseverance and sacrifices have immensely helped me achieve what I am today.

Table of Contents

List of Figures

List of Tables

Abstract

Polycationic polymers in nucleic acid delivery: Membrane interaction and cellular responses

by

Rahul Rattan

In order to optimize the design of gene delivery vector systems using polycationic polymers, their internalization pathway needs to be extensively studied. In chapter 2, Generation 7 (G7) poly(amidoamine) (PAMAM) dendrimers (G7-NH_2) with amine termination were prepared to investigate polymer/cell membrane interaction. C6 cells were employed in this experiment because of their unique characteristic of inherently lacking GM_1 but still possessing downstream requirements for successful GM_1 mediated endocytosis. This resulted in the reported binary experiment where C6 cells without and with GM_1 did not show differential G7-NH_2 uptake supporting the hypothesis that GM_1 mediated endocytosis is not the primary pathway for G7-NH_2 internalization. In addition to understanding uptake mechanisms, efforts to improve the polymer-based vector systems have assumed that cells play a passive role and don't actively respond to these polymer vector systems. In chapter 3, I will show how cells respond to different polymer systems by activating different levels of cytosolic nucleases and how this nuclease activity can be measured with the help of Molecular Beacon (MB). We also learn that membrane porosity is not the reason for nuclease activation. This nuclease activation decreases gene expression, ultimately decreasing polymer efficiency. In doing this, I show that it is possible to screen multiple polymer-based vector systems, thereby increasing the probability of identifying and designing an efficient polymer vector system. In chapter 4, I will concentrate on DNA degradation characteristics of these cytosolic nucleases. High-throughput sequencing was used to identify and quantify degradation patterns of these cytosolic nucleases on a plasmid. We will also see that S1 nuclease (a known nuclease) has similar degradation pattern as cytosolic nucleases. Designing polymer vector systems that protect these labile sites on DNA can improve gene expression.
In chapter 6, invention of The Endocutter, a gastrointestinal device that cuts clots, cuts costs and saves lives is described. This device was designed to be compatible with both single and dual channel endoscope for easy adaptation. Endocutter is easy to use and has been shown to be safe and efficient in removing blood clots both in-vitro and in-vivo systems (http://www.youtube.com/watch?v=gxnB_kuzOsQ)

Chapter 1

Introduction

1.1 Nucleic Acid Delivery Systems

Nucleic acid transfection and expression play an important role in everyday molecular biology experiments. [1] Delivery of oligonucleotides, including antisense DNA (asDNA), silencing RNA (siRNA), and plasmid DNA (pDNA) is a promising strategy in the field of medicine with possible applications including diagnosis, vaccines and disease management.[2] The big range of applications and potential impact on common, life threatening diseases like diabetes mellitus and metastatic neoplasm,[2] led to a predicted pharmaceutical industry of $16.8 billion/year by 2020-2025;[3] however, almost 15 years after this prediction gene therapy is only a small fraction of this multi-billion dollar market projection. Despite the outstanding promise of this technology, there are no FDA-approved vector systems for nucleic acid delivery in humans. This lack of market availability and penetration arises primarily because of safety and efficiency issues for current nucleic acid delivery systems.[4, 5] In addition to gene therapy, many other nucleic acid manipulation techniques like asDNA and siRNA can greatly benefit from safe and efficient delivery

systems.[2, 4] There are two categories of nucleic acid delivery systems but they each have their tradeoffs:

1.1.1 Viral Based Systems

Viral based systems are good at providing gene expression. However, they pose significant health and safety concerns because of their use of infective viruses like adenoviruses, retroviruses, etc.[6, 7] Viral based vector systems take advantage of the virus's inherent ability to transfect cells. These systems are composed of a benign part of the viral genome in conjunction with the transgene to help facilitate transgene expression into the host cell. This technique has various caveats:

1.1.1.1 The target locus of the host's genome where the transgene is integrated cannot be confidently predetermined.[7] If the target locus expresses an important transcript then the integration can lead to a nonfunctional transcribe which ultimately can lead to a precarious state for the host.

1.1.1.2 The viral based system, like any other system that utilizes foreign agents, can lead to activation of the host's immune response. Not only can that lead to a potentially fatal immune hyper-reaction in the host, but can also block future gene therapy treatment with the same agent. [7]

1.1.2 Non-Viral Based Systems

Non-viral based systems, because of their small size and lack of traditional immunogenic epitopes, lack non-specific immune responses. However they are not as efficient for gene expression as viral based systems. [8, 9] Some examples of non-

viral based systems are electroporation, gene gun, and cationic polymeric systems such as PAMAM dendrimer and PEI (Poly(ethyleneimine)), and lipids. Non-viral systems are efficient at delivering the transgene into the cells and can also protect the nucleic acid from cytosolic degradation, but they lack a dedicated transport mechanism within cells that leads to their inefficiency in providing transgene expression. [8, 9] Additionally, they lack the ability to integrate the gene into the host's genome. [9]

1.1.2.1 Low Transgene Expression with Non-Viral Vector Systems

A polycationic polymer like the PAMAM dendrimer can provide a high level of customization with its defined molecular architecture and high surface moieties to volume ratio, without activating an aggressive immune response. [10-13] This makes it an optimum vector system.[9, 14] Many studies have investigated cellular uptake mechanism for viral and non-viral vector systems.[15-17] They both are thought to enter via energy dependent endocytosis pathways that can lead to their localization inside an endosome. [8, 18] Before these endosomes become lysosomes, the two vector systems are thought to escape via different mechanisms. Viral systems have a dedicated mechanism to transfer nucleic acid into the nucleus, but polyplexes are not known to have such a mechanism. [19] This is thought to contribute to the inefficiency of non-viral systems in providing transgene expression. This problem has been studied for several years, but researchers have always attributed it to the uptake mechanism and endosomal escape. [19] Recent work by Lechardeur et al. [20] and Pollard et al. [21] argues otherwise. Their studies show that cytosolic nucleases contribute to degradation of transported DNA

lowering overall expression of transgene. Chapter 2 will concentrate on PAMAM dendrimer interaction with cell plasma membrane and test a specific internalization pathway PAMAM dendrimer proposed to be active for uptake into cells. In chapter 3, I will identify and evaluate effects of cytosolic nuclease activity on gene expression and also how choice of polymer used in polyplexes relates to the activity. In chapter 4, I will characterize cytosolic nucleases and use sequencing to study their degradation sites on a plasmid DNA.

1.2 The Role of Ganglioside GM1 in Cellular Internalization Mechanisms of Poly(amidoamine) Dendrimers (Chapter 2)

In order to optimize the design of gene delivery vector systems using polycationic polymers, their internalization pathway needs to be extensively studied. [10, 12, 16, 17] PAMAM dendrimer, with their defined molecular architecture and controlled synthesis, provide a unique opportunity for understanding these specific internalization pathways in great detail.[11, 13, 22] There are studies in literature supporting the hypothesis that PAMAM dendrimer are internalized via polycationic endocytosis mechanisms such as clathrin and GM_1 mediated endocytosis. [23] But there are many also contradictory and inconclusive experiments existing in literature. [24-28] In the first chapter I will present a binary way to address this hypothesis. This study showed that polycationic polymer, contrary to some studies in literature, does not internalize via GM_1 mediated endocytosis. Additionally this study was repeated with polyplexes where the hypothesis had been shown to stay true. [29] This conclusion helped narrow down possible internalization pathways

for PAMAM dendrimers, informing better design for novel polymer based nucleic acid delivery systems.

1.3 Polyplex-Induced Cytosolic Nuclease Activation leads to Differential Transgene Expression (Chapter 3)

Nucleic acid delivery based therapeutics like DNA, asDNA, siRNA are severely limited by absence of safe and efficient delivery systems. Non-viral nucleic acid delivery systems like PAMAM dendrimers and other provide certain advantages like low toxicity, high surface moieties to volume ratio but don't provide the level of efficiency viral systems do. As mentioned above, this low efficiency has been attributed to uptake mechanisms, endosomal escape and nuclear transport by polymer systems. [8, 15-17] In studying the above-mentioned bottlenecks, it is assumed that 1) cells do not actively respond to the introduction of polymer/DNA complexes (polyplexes), and 2) if a cell does respond it responds in a fashion independent of polymer employed. In chapter 3, I will address our hypothesis that polyplexes induce a cellular response (cytosolic nucleases), which in turn decreases the downstream transgene expression.. And how nuclease activation is dependent on the polymer employed to make polyplexes. This knowledge can help in designing efficient polymeric nucleic acid delivery system that decreases cytosolic nucleases activation leading to increase in downstream gene expression.

1.4 Quantification of Cytosolic Plasmid DNA Degradation Using High-Throughput Sequencing: Implications for Gene Delivery (Chapter 4)

Hypothesis tested in this chapter: S1 nuclease type nucleases are part of the cytosolic nuclease milieu and cytosolic nucleases attack certain plasmid regions more than others. High-throughput sequencing is employed to study the downstream effects of nuclease activation on the transported DNA. High-throughput sequencing was used in this study to identify and quantify labile sites on a plasmid DNA. S1 nuclease was used in this study to both validate sequencing data comparison with published agarose gel work but also because of interest in better understanding of the S1 nuclease plasmid DNA cleavage pattern. High-throughput sequencing not only provided more labile sites than previously known but also provided information regarding relative degree of degradation for labile site and their location on the plasmid. This study can help in designing efficient polymer vector systems that protect these labile sites from degradation and in turn improving expression.

1.5 References

1. Mastrobattista, E., W.E. Hennink, and R.M. Schiffelers, *Delivery of Nucleic Acids.* Pharmaceutical Research, 2007. **24**(8): p. 1561-1563.
2. Scholz, C. and E. Wagner, *Therapeutic plasmid DNA versus siRNA delivery: Common and different tasks for synthetic carriers.* Journal of Controlled Release, 2012. **161**: p. 554-565.
3. Hess, P. and D. Cooper, *Impact of Pharmacogenomics on the Clinical Laboratory.* Molecular Diagnosis, 1999. **4**(4): p. 289-298.
4. Liu, C. and N. Zhang, *Nanoparticles in gene therapy principles, prospects, and challenges.* Prog Mol Biol Transl Sci, 2011. **104**: p. 509-662.
5. D., L. and L. G.L., *Intracellular Barriers to Non-Viral Gene Transfer.* Current Gene Therapy, 2002. **2**(2): p. 183-194.

6. Osterman, J.V., A. Waddell, and H.V. Aposhian, *DNA and Gene Therapy: Uncoating of Polyoma Pseudovirus in Mouse Embryo Cells.* Proceedings of the National Academy of Sciences, 1970. **67**(1): p. 37-40.
7. Deyle, D.R. and D.W. Russell, *Adeno-assciated virus vector integration.* Current Opinion in Molecular Therapeutics, 2009. **11**(4): p. 442-447.
8. Pack D, W., et al., *Design and development of polymers for gene delivery.* Nature Reviews Drug Delivery, 2005. **4**: p. 581-593.
9. Smedt, S.C.D., J. Demeester, and W.E. Hennink, *Cationic Polymer Based Gene Delivery Systems.* Pharmaceutical Research, 2000. **17**(2): p. 113-126.
10. Li, S. and L. Huang, *Nonviral gene therapy: promises and challenges.* Gene Therapy, 2000. **7**: p. 31-34.
11. Hong, S., et al., *Physical interactions of nanoparticles with biological membranes: the observation of nanoscale hole formation.* CHemical Health and Safety, 2006. **13**: p. 16-20.
12. Abdallah, B., L. Sachs, and B.A. Demeneix, *Nonviral gene transfer: Applications in developmental biology and gene therapy.* Biol. Cell, 1995. **85**: p. 1-7.
13. Hong, S., et al., *The interaction of polyamidoamine (PAMAM) dendrimers with supported lipid bilayers and cells: hole formation and the relation to transport.* Bioconjugate Chem., 2004. **15**: p. 774-782.
14. Dufès, C., I. Uchegbu, and A.G. Schätzlein, *Dendrimers in gene delivery.* Advanced Drug Delivery Reviews, 2005. **57**(15): p. 2177-2202.
15. Zhang, S.B., et al., *Cationic compounds used in lipoplexes and polyplexes for gene delivery.* Journal of Controlled Release, 2004. **100**: p. 165-180.
16. Jevprasesphant, R., et al., *Transport of dendrimer nanocarriers through epithelial cells via the transcellular route.* Journal of Controlled Release, 2004. **97**: p. 259-267.
17. Kopatz, I., J.S. Remy, and J.P. Behr, *A model for non-viral gene delivery: through syndecan adhesion molecules and powered by actin.* Journal of Gene Medicine, 2004. **6**: p. 769-776.
18. Lentz, T.B., S.J. Gray, and R.J. Samulski, *Viral vectors for gene delivery to the central nervous system.* Neurobiology of Disease, 2012. **48**(2): p. 179-188.
19. Al-Dosari, M.S. and X. Gao, *Nonviral Gene Delivery: Principle, Limitations, and Recent Progress.* American Association of Pharmaceutical Scientists Journal, 2009. **11**(4): p. 671-681.
20. Lechardeur, D., et al., *Metabolic instability of plasmid DNA in the cytosol: a potential barrier to gene transfer.* Gene Therapy, 1999. **4**(482-497).
21. Pollard, H., et al., *Ca2+-sensitive cytosolic nucleases prevent efficient delivery to the nucleus of injected plasmids.* The Journal of Gene Medicine, 2001. **3**: p. 153-164.
22. Jevprasesphant, R., et al., *Engineering of dendrimer surfaces to enhance transepithelial transport and reduce cytotoxicity.* Pharmaceutical Research, 2003. **20**: p. 1543-1550.
23. Manunta, M., et al., *Gene delivery by dendrimers operates via a cholesterol dependent pathway.* Nucleic Acids Research, 2004. **32**: p. 2730-2739.

24. Manunta, M., et al., *Gene delivery by dendrimers operates via different pathways in different cells, but is enhanced by the presence of caveolin.* Journal of Immunology Methods, 2006. **314**: p. 134-146.
25. Seib, F.P., A.T. Jones, and R. Duncan, *Comparisonof the endocytic properties of linear and branched PEIs, and cationic PAMAM dendrimers in B16f10 melanoma cells.* Journal of Controlled Release, 2007. **117**: p. 291-300.
26. Kandyba, A.G., A.M.S. Kozlov, O. G., and E.V. Dyatlovitskaya, *A comparative study of sphingolipids in transplanted melanomas with high and low metastatic activity.* Russian Journal of Bioorganic Chemistry, 2008. **34**: p. 230-233.
27. Kitchens, K.M., et al., *Endocytosis inhibitors prevent poly(amidoamine) dendrimer internalization and permeability across Ceco-2 cells.* Molecular Pharmaceutics, 2008. **5**: p. 364-369.
28. Perumal, O.P., et al., *The effect of surface functionality on cellular trafficking of dendrimers.* Biomaterials, 2008. **29**: p. 3469-3476.
29. Qi, R., et al., *The Mechanism of Polyplexes Internalization into Cells: Testing the GM1/Caveolin-1-Mediated Lipid Raft Mediated Endocytosis Pathway.* Molecular Pharmaceutics, 2010. **7**: p. 267-279.

Chapter 2

The Role of Ganglioside GM_1 in Cellular Internalization Mechanisms of Poly(amidoamine) Dendrimers[#]

2.1 Abstract

In this chapter, the hypothesis that GM_1 medicated endocytosis plays an important role in polyplex cellular internalization was addressed. Generation 7 (G7) poly(amidoamine) (PAMAM) dendrimers with amine, acetamide, and carboxylate end groups were prepared to investigate polymer/cell membrane interactions *in* V*itro*. G7 PAMAM dendrimers were used in this study because higher-generation of dendrimers are more effective in permeabilization of cell plasma membranes and in the formation of nanoscale holes in supported lipid bilayers than smaller, lower-generation dendrimers. Dendrimer-based conjugates were characterized by ^1H NMR, UV/vis spectroscopy, GPC, HPLC, and CE. Positively charged amine-terminated G7 dendrimers (G7-NH_2) were observed to internalize into KB, Rat2, and C6 cells at a 200 nM concentration. By way of contrast, neither negatively charged G7 carboxylate-terminated dendrimers (G7-COOH) nor neutral acetamide-terminated G7 dendrimers (G7-Ac) associated with the cell plasma membrane or internalized under similar conditions.

[#]Rahul Rattan and Seungpyo Hong are equal contribution authors for this publication. Cytotoxicity assays and GM_1 experiments with C6 cells were performed and analyzed by me.

G7-NH_2 dendrimers colocalized with CTB; however, experiments with C6 cells indicated that internalization of G7-NH_2 was not ganglioside GM_1 dependent. The G7/CTB colocalization was thus ascribed to an artifact of direct interaction between the two species. The presence of GM_1 in the membrane also had no effect upon XTT assays of cell viability or lactate dehydrogenase (LDH) assays of membrane permeability.

2.2 Introduction

Polycationic polymers such as poly(lysine)s, poly(ethyleneimine)s, diethylaminoethyl-dextrans, and poly(amidoamine) (PAMAM) dendrimers have demonstrated great potential to be exploited as gene transfer and drug delivery vectors.(*1-9*) Among those polycationic polymers, PAMAM dendrimers have attracted great scientific interest in the biomedical applications due to their excellent water-solubility and well-defined structure, molecular weight, and surface end groups. Demonstrated utility for practical applications, coupled with excellent monodispersity and chemical versatility, make PAMAM dendrimers an ideal material for exploring polymer-membrane interactions in greater detail.(*6, 8-10, 13, 15*)

The internalization mechanism of amine-terminated PAMAM dendrimers into cells has been explained as polycation-mediated endocytosis or leaky endocytosis.(*10-14*) In particular, co-localization studies with using choleratoxin subunit B (CTB)

suggested that ganglioside GM_1 played a major role in the initial interaction with the cell membrane and the subsequent internalization process for EA.hy 926 cells and Chinese hamster ovary (CHO) cells.(*16*) Furthermore, inhibition of internalization by methyl-β-cyclodextrin (MβCD) suggested that a lipid-raft mediated process may be a primary pathway for PAMAM dendrimer internalization into the cells. Subsequent studies with HeLa and HepG2 cells did not show an effect from MβCD but instead increased uptake and transfection efficiency were observed as a function of caveolin 1 expression.(*17*) These results were particularly interesting in light of other studies that had identified an "adsorptive" endocytosis that might involve a specific membrane component for B16f10 melanoma cells(*18*) which are also known to contain GM_1.(*19*) However, the generality of a caveolae-based endocytosis mechanism is called into question by studies on Caco-2 cells which support a clathrin-based mechanism, not a caveolae-mediated mechanism.(*20*) In addition, studies on A549 cells indicate the process is not either clathrin or caveolae based.(*21*)

An alternative to endocytic mechanisms of uptake is direct physical disruption of the membrane and the formation of nanoscale holes causing plasma membrane permeability. AFM observations have revealed that polycationic polymers cause nanoscale hole formation, expansion of pre-existing defects, or membrane thinning depending on physical properties of polymers such as structure, size, and terminal groups, as well as membrane composition and phase.(*6, 9, 22-25*) Particularly, efficiency of hole formation in supported lipid bilayers induced by PAMAM dendrimers was concluded to be proportional to molecular weight (G7 > G5 > G3) as

well as terminal end groups (amine > acetamide; i.e. charged > uncharged) of the dendrimers. Recent studies across a broad variety of cationic nanomaterials suggests that surface area is the single best correlate.(*26*) This observation agrees with *in vivo* studies carried out by Oberdörster et al.(*27*) AFM studies using supported lipid bilayers were consistent with our *in vitro* results exploring cell membrane permeability and dendrimer internalization.(*6, 8, 9*) Employing two tumor cell lines, KB and Rat2, cytosolic enzyme (LDH and luciferase) leakage, dendrimer internalization, and small molecule diffusion in and out of the cells were observed as a result of incubation with positively charged G7 PAMAM dendrimers as illustrated in Figure 2.1. We thus concluded that the cellular level data for the interaction of cationic PAMAM dendrimers with cell membranes was consistent with induction of nanoscale hole formation and that this process may be related to the internalization of these materials into the cell and/or the membrane permeability measured by dye diffusion and LDH assays.(*6, 8, 9*)

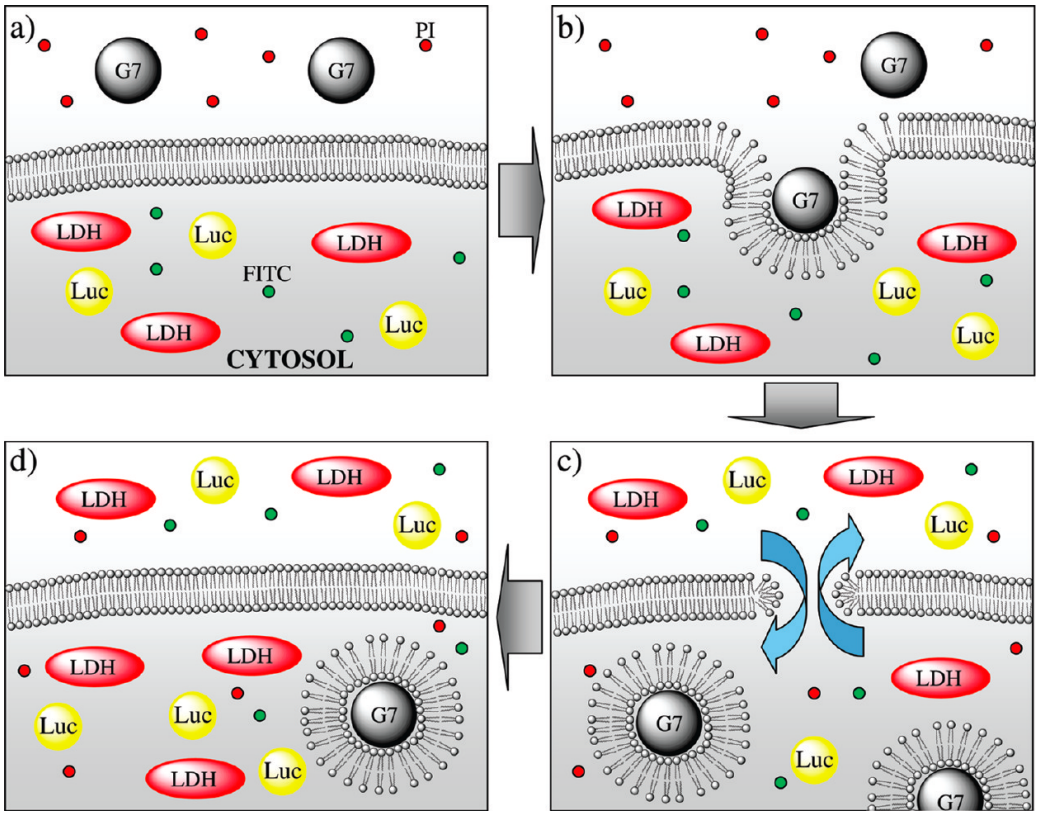

Figure 2.1. Schematic diagram of the proposed nanoscale hole formation mechanism induced by positively charged PAMAM dendrimers. The data supporting this schematic summary is presented in this paper as well as in our previous reports.

Considering the recent reports on endocytic internalization(*16-21*) and nanoscale hole formation,(*6, 8, 9, 26*) we decided to investigate the role of GM_1 in the interaction of PAMAM dendrimers with cells. Experiments were designed probing the roles of GM_1 in endocytosis and/or nanoscale hole formation. Experiments to test other key hypothesis such as clathrin pathways were also explored. For this study, G7 PAMAM conjugates were chosen because of their effectiveness in terms of both endocytosis and cell membrane disruption and because they had been observed to cause membrane permeability even at 4 ºC.(*6, 8, 9, 28, 29*) Three different types of G7 PAMAM dendrimer-AlexaFluor®488 conjugates (amine,

acetamide, and carboxylate terminated) were synthesized and characterized (Figure 2.2). The conjugates were then tested *in vitro* to explore dendrimer/cell interactions. The key findings in this paper are: 1) no evidence is found for a GM_1 dependence of G7 PAMAM dendrimer with respect to internalization via endocytosis or nanoscale hole formation 2) the presence of GM_1 in the membrane does not play a role in cell viability assays as measured by XTT 3) the presence of GM_1 in the membrane does not play a role in plasma membrane permeability assays as measured by LDH.

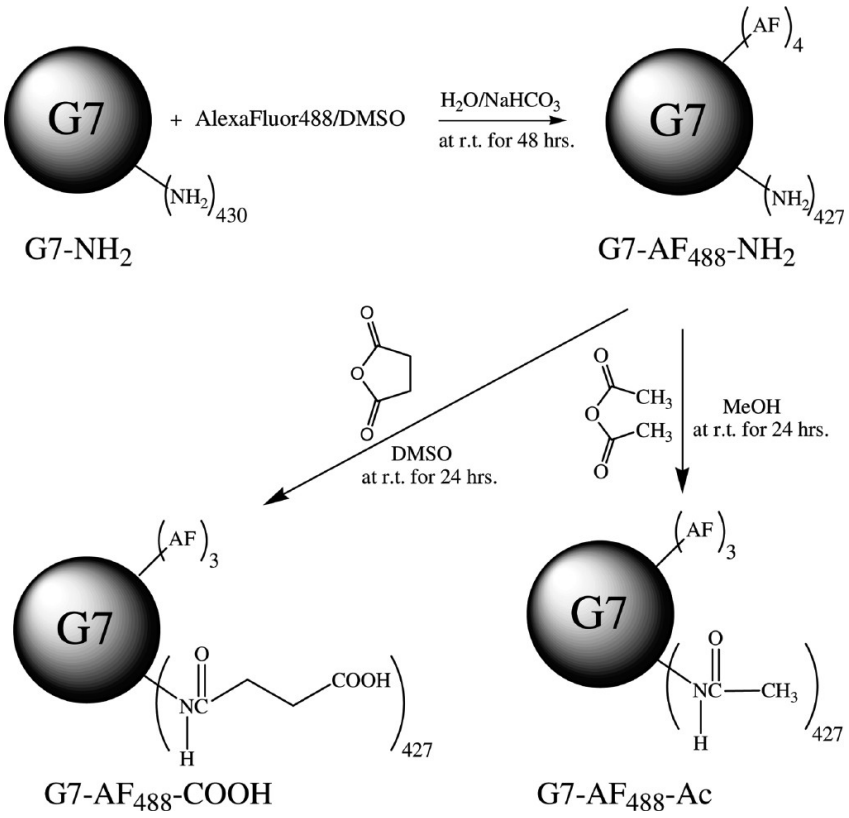

Figure 2.2. Synthetic routes for G7 PAMAM dendrimer conjugates with various surface end groups.

2.3 Experimental Methods

2.3.1 Materials

G7 and G5 PAMAM dendrimers were synthesized at the Michigan Nanotechnology Institute for Medicine and Biological Sciences and purified using ultrafiltration and dialysis before use. Alexa Fluor®488 carboxylated, succinimidyl ester (AF488) was supplied by Molecular Probes (Eugene, OR) and used without further purification. Tranferrin from human serum labeled by AlexaFluor®546 (TF-AF546), recombinant cholera toxin subunit B-Alexa Fluor®647 conjugate (CTB-AF647), and LysoTracker® Red DND-99 (LysoTracker) were provided by Molecular Probes. Methyl-β-cyclodextrin (MβCD), and GM_1-pyrene were purchased from Sigma-Aldrich (St. Louis, MO) and used without further purification. Materials for native PAGE were obtained from Invitrogen. All other chemicals were acquired from Aldrich and used as received. Water used in this work was purified by Milli-Q Plus 185 system and had a resistivity higher than 18.0 MΩ/cm.

2.3.2 Preparation of PAMAM Dendrimer Conjugates and Their Surface Modification

Two milligrams of AF488 (6.20 μM, 5 times excess to G7) dissolved in 400 μL DMSO were conjugated to 68 mg of the purified G7 PAMAM dendrimers (1.25 μM) under the presence of 2 mL of 1 M $NaHCO_3$ at room temperature for 48 hrs. The resulting reaction mixture was then dialyzed in water for 2 days and lyophilized for 2 days, followed by 5 times of ultrafiltration with water using an 80,000 molecular weight

cut-off membrane at 21 °C, 5000 rpm for 30 min each. Sixty milligrams of a yellowish powder (G7-AF488-NH_2) were finally obtained (yield: 86%). The average number of AF488 dye molecules present was determined by ^1H NMR and/or GPC. The materials used in these studies varied from 2.4 – 4 AF488 per dendrimer. Twenty-two milligrams of G7-AF488-NH_2 were allowed to react with 12 μL of acetic anhydride (50% mol excess to the conjugate) in 1.5 mL MeOH as a solvent at room temperature for 24 hrs. The reaction mixture was then purified by ultrafiltration at the same condition above with PBS (w/o Ca^{2+}, Mg^{2+}) and water subsequently 5 times for each. After lyophilization for 2 days, 16.25 mg of a yellowish powder (G7-AF488-Ac) was obtained (yield: 63%). Twenty milligrams of G7-AF488-NH_2 were also allowed to react with 11 mg succinic anhydride (50% excess to the conjugate) in 1.5 mL DMSO at room temperature for 24 hrs followed by ultrafiltration and lyophilization at the same condition used for preparation of G7-AF488-Ac. A yellowish powder (18.8 mg) was obtained (G7-AF488-COOH, yield: 67%). The synthetic routes for the three different conjugates are summarized in Figure 2.2. In addition, G5 PAMAM dendrimers used in the XTT assay (Figure 2.3) were also conjugated with 6-carboxy-tetramethylrhodamine (6-TAMRA) followed by acetylation as described earlier.(*30*)

2.3.3 Characterization of the Prepared PAMAM Based Conjugates: UV/Vis and ^{1}H NMR Spectroscopy

UV/Vis spectra of the G7 PAMAM conjugates were measured on Perkin Elmer UV/Vis spectrometer Lambda 20 (Wellesley, MA). Molar extinction coefficients of the dendrimer conjugates were also calculated by plotting maximum absorbance values against conjugate concentrations at 20, 40, 60, 80, and 100 μg/mL using the Lambert-Beer law (Table 2.1). ^{1}H NMR spectra were also taken in D_2O and were used to provide integration values for structural analysis using a Bruker AVANCE DRX 500 instrument.(*31*)

Table 2.1. Molar extinction coefficients, molar masses, and polydispersity indices of G7 conjugates

conjugates	molar extinction coeff. ($M^{-1}cm^{-1}$)[a]	theoretical molar mass[b]	molar mass (M_n)[c]	polydispersity (M_w/M_n)	HPLC peak width at half-height[d]
G7-NH_2	N/A	97 020	97 000	1.07 ± 0.02	0.52
G7-AF_{488}-NH_2	171 100	99 137	99 600	1.38 ± 0.03	0.62
G7-AF_{488}-Ac	147 130	116 903	116 300	1.06 ± 0.02	0.49
G7-AF_{488}-COOH	122 520	141 437	138 500	1.08 ± 0.02	0.57

[a] Molar extinction coefficients were obtained from the Lambert-Beer equation by plotting λ_{max} against corresponding concentrations of a conjugate (20, 40, 60, 80, and 100 μg/mL). R_2 values of the linear regressions were 0.9966-0.999. The coefficients were calculated on the basis of UV characteristic peaks of conjugated AF_{488} at 497 nm. [b] Calculated from the measured molecular weight of starting G7-NH_2 by assuming that the G7 PAMAM dendrimers have 4 AF488 moieties per dendrimer and 427 surface terminal groups according to the previously reported curve fit (*30*). Measured by GPC (M_n, Number average molecular weight; M_w, Weight average molecular weight). [d] Obtained from HPLC chromatograms.

2.3.4 Characterization of the Prepared PAMAM Based Conjugates: GPC and HPLC

The molar mass moments and molar mass distribution of each polymer sample were measured using gel permeation chromatography (GPC). The number average molecular weight (M_n) and polydispersity index (PDI), a commonly used measure of the breadth of the molar mass distribution defined as the ratio of the weight and number average molecular weights (M_w/M_n), of individual samples are listed in

Table 2.1. GPC experiments were performed using an Alliance Waters 2690 separation module (Waters Corp., Milford, MA) equipped with a Waters 2487 UV absorbance detector (Waters Corp.), a Wyatt Dawn DSP laser photometer (Wyatt Technology Corp., Santa Barbara, CA), an Optilab DSP interferometric refractometer (Wyatt Technology Corp.), and TosoHaas TSK-Gel Guard PHW 06762 (75×7.5 mm, 12 μm), G 2000 PW 05761 (300 × 7.5 mm, 10 μm), G 3000 PW 05762 (300 × 7.5 mm, 10 μm), and G 4000 PW (300 × 7.5 mm, 17 μm) columns. A detailed procedure of the GPC measurement was described elsewhere.(*9, 31*)

The reverse-phase (RP) HPLC system (Beckman Coulter, Fullerton, CA) consisting of a System GOLD 126 solvent module, a model 507 autosampler equipped with a 100 μL loop, and a model 166 UV detector were used in this study as well. A Jupiter C5 silica-based RP-HPLC column (250 × 4.6 mm, 300 Å) was purchased from Phenomenex (Torrance, CA). Two Phenomenex Widepore C5 safety guards (4 × 3 mm) were also installed ahead of the Jupiter column. The mobile phase for elution of G7-AF488 dendrimer conjugates with different terminal groups was a linear gradient beginning from 100:0 (v/v) water/acetonitrile (ACN) to 50:50 (v/v) water/ACN at a flow rate of 1 mL/min for 40 min. Trifluoroacetic acid (TFA) at 0.14 wt % concentration in water as well as in ACN was used as counter-ions to make the dendrimer surfaces hydrophobic. All the samples were dissolved into the aqueous mobile phase (water containing 0.14% TFA) at the concentration of 1 mg/mL. The detection of eluted samples was performed at 210 nm. The analysis was performed using Beckman's System GOLD Nouveau software.(*32*)

2.3.5 Characterization of the Prepared PAMAM Based Conjugates: Capillary Electrophoresis (CE)

An Agilent Technologies (Waldbronn, Germany) CE instrument was used in this work. Unmodified quartz capillaries were purchased from Polymicro Technologies (Phoenix, AZ, USA). The voltage was kept at 20 kV. On-capillary UV diode-array detection was used, operating at wavelengths of 210 nm, 250 nm, 280 nm and 495 nm. Samples were introduced by hydrodynamic injection at a pressure of 50 mbar.

For analysis of G7-AF488 conjugates with amino and acetamide terminal groups, silanized capillaries (i.d. 100 μm) with total length of 48.5 cm and effective length of 40 cm were employed following previous literature.(*33*) G7-AF488-NH_2 and G7-AF488-Ac conjugates were dissolved in pH 2.5 phosphate buffer and the sample solutions were adjusted to pH 2.5 using 0.1 M phosphoric acid to give a concentration of 1 mg/ml. All the conjugates contained 0.05 mg/mL 2,3-diaminopyridine (2,3-DAP) as an internal standard.

For analysis of G7-AF488 conjugate with carboxyl terminal groups, bare silica capillaries (i.d. 75 μm) with total length of 64.5 cm and effective length of 56 cm were used for the characterization of G7-AF488-COOH conjugates. The capillary temperature was maintained at 20 °C. Before use, the uncoated silica capillary was pretreated by rinsing with 1 M NaOH (15 min), deionized water (Purchased from Agilent) (15 min) and running buffer (15 min).(*33*) Before each injection, the capillary was rinsed with a similar sequence of each eluent. 20 mM borate buffer (pH 8.3) was used as the running buffer. G7-AF488-COOH conjugates were dissolved in the running buffer and the sample's pH was adjusted to 8.3 with 20 mM

sodium tetraborate solution to get a final concentration of 1 mg/mL. 4-Methoxybenzyl alcohol (MBA) (0.05 mg/mL) was used as a neutral marker.

2.3.6 Cell Lines

The KB, Rat2, and C6 cell lines were purchased from the American Type Culture Collection (ATCC, Manassas, VA) and grown continuously as a monolayer at 37 °C, and 5% CO_2. The KB cells were grown in RPMI 1640 medium (Mediatech, Herndon, VA). The Rat2 and C6 cells were grown in Dulbecco's modified Eagle's medium (DMEM, Gibco, Eggenstein, Germany). The RPMI 1640 and DMEM media were supplemented with penicillin (100 units/mL), streptomycin (100 μg/mL), and 10% heat-inactivated fetal bovine calf serum (FBS) before use.

2.3.7 XTT Cytotoxicity Assay

Cytotoxicity of the dendrimer conjugates used in this study was assessed by the overall activity of mitochondrial dehydrogenase by 2,3-bis(2-methoxy-4-nitro-5-sulfophenyl)-*2H*-tetrazolium-5-carboxanilide (XTT) assay (Cell Proliferation Kit II, Roche Molecular Biochemicals, Mannheim, Germany). KB, Rat2, and C6 cell lines (at a concentration of 5×10^4 cells/well) were prepared as monolayers in 96 well plates, followed by incubation with dendrimers in phosphate buffered saline (PBS) with Ca^{2+} and Mg^{2+} at 37 °C under 5% CO_2 for 4.5 hrs (2 h for C6 cells). Polymer solutions (supernatants) were then removed, followed by washing with PBS twice. Mitochondrial activities of the cells were spectrophotometrically measured at 492 nm using a Spectra Max 340 ELISA Reader (Molecular Devices, Sunnyvale, CA). Cell viability was then calculated based on optical density (OD) from untreated cells.

2.3.8 LDH Membrane Permeability Assay

Membrane permeability was tested via lactate dehydrogenase (LDH) leakage using the LDH assay kit (Promega, Madison, WI). The activity of LDH in extracellular media is taken as a measure of membrane porosity. C6 cells were seeded at a density of 5×10^4 cells/well in 96 well plates for overnight incubation at 37 °C and 5% CO_2. Dendrimers diluted in 100 µL PBS (w/ Ca^{2+}, Mg^{2+}) was added at specified concentrations into the 96 well plates and incubated at 37 °C and 5% CO_2 for 2 hrs after which the supernatant was removed and 50 µL was taken for the LDH assay (throughout the experiment boundary wells were not used). LDH activity was spectrophotometrically measured at 490 nm using an ELISA reader.

2.3.9 Confocal Laser Scanning Microscopy (CLSM)

A concentration of 1×10^5 cells/mL of KB and Rat2 cells was seeded on MatTek glass bottom petri dishes (35 mm) and incubated at 37 °C under 5% CO_2 for 24 hrs. The cell culture medium was removed and 2 mL of each dendrimer-AF488 conjugates in PBS (w/ Ca^{2+}, Mg^{2+}) solution was added into the appropriate dish. The dishes were incubated with added solutions either at 37 °C under 5% CO_2 for 1 hr or at 4 °C. For the low temperature experiment, cells were pre-incubated at 4 °C for 10 min before adding the dendrimer solutions. The conjugate-containing solutions were removed and the resulting cell monolayer was washed with PBS at least three times. Cells were fixed with 2% formaldehyde in the PBS (w/ Ca^{2+}, Mg^{2+}) at room temperature for 10 min, followed by washing with PBS twice.

For co-localization studies of dendrimers with CTB and transferrin on KB and Rat2 cells, dendrimer solutions were pre-mixed with markers, resulting in final

concentrations of 200 nM, 10 μg/mL, and 50 μg/mL for G7-AF488-NH_2, CTB-AF647, and TF-AF546, respectively. The mixed solutions were then added to KB and Rat2 cells and the cells were incubated at 37 ºC, 5% CO_2 for 1 hr.

For co-localization studies of CTB and G7-NH_2 dendrimers on C6 cells, cells were seeded in Fisherbrand 2 well microscope cover glass # 1.5 at 2.5 × 10^5 cells/mL density, with 1 mL complete media in each well. Cells were allowed to attach to the surface for 4 hrs after which wells were washed with PBS (w/ Ca^{2+}, Mg^{2+}) and then overnight incubated with media (w/o serum) containing GM_1-pyrene. Cells were then treated with 5 µg/mL CTB-AF647 for 1 hr or 500 nM G7-AF488-NH_2- for 2 hrs, washed with PBS, and imaged in PBS solution.

For co-incubation of KB cells with G7-AF488-NH_2 and fully acetylated G5 PAMAM-6-TAMRA conjugates (G5-6T-Ac),(*34*) KB cells were incubated with 100, 200, and 400 nM G7-AF488-NH_2 at 37 ºC for 30 min followed by addition of 1 μM G5-6T-Ac with additional incubation for 30 min.

Confocal and differential interference contrast (DIC) images were taken on an Olympus FV-500 confocal microscope using either a 60X, 1.5 NA or a 100X, 1.4 NA oil immersion objective. For the confocal images using three different AlexaFluors, the 488 nm line of an argon ion laser (for dendrimer conjugates), 543 nm line of a HeNeG laser (for transferrin and LysoTracker), or 633 nm line of a HeNeR laser (for cholera toxin) was used for excitation and the emission was filtered at 505-525, 560-600, 660 IF nm, respectively. Percentages of overlapping between two markers in the confocal images were quantified using Metamorph offline software version 6-3r7 provided by Molecular Devices (Downingtown, PA).

2.4 Results

2.4.1 Synthesis and Characterization of G7 PAMAM/AlexaFluor 488 Conjugates with Various Surface End Groups

G7 PAMAM dendrimers were conjugated with AF488 dye to allow confocal laser scanning microscopy (CLSM) studies. AF488 was chosen for this study because this fluorophore is known to exhibit brighter fluorescence and greater photostability than other spectrally similar fluorophores (300% more photostable than fluorescein (FITC) at 90 sec. exposure) as well as greater pH insensitivity between pH 4.0 and 10.0.(*35*) The synthesis scheme for the conjugates is illustrated in Figure 2.2. ^{1}H NMR spectra for all three conjugates are provided in Figure 2.S1. After conjugation with AF488, characteristic peaks for the conjugated dyes molecules appear in the range of δ 6.8-8.4 ppm. The ^{1}H NMR spectrum of G7-AF488-Ac (Figure 2.S1c) is consistent with the previously published spectra using G5 PAMAM.(*31*) UV/Vis spectra reveal that maximum absorbance of AF488 shifted from 495 to 497 nm after conjugation with the dendrimer. Calculated molar extinction coefficients decrease with the increase of molecular weights of the conjugates providing a rough guide when the surface modification from primary amine end groups to acetamide and carboxylate end groups is successfully performed (see Table 2.1).

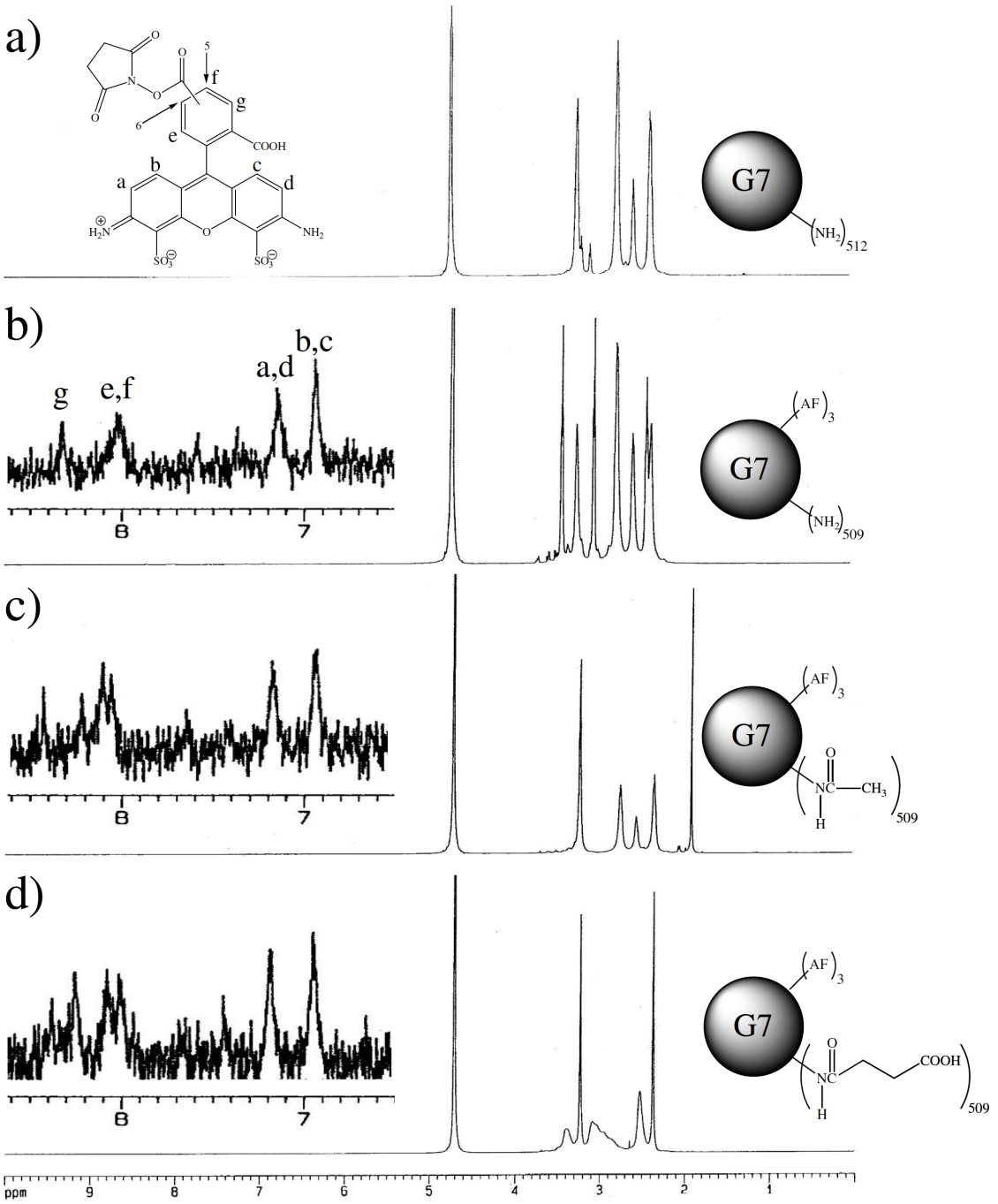

Figure 2.S1. 1H NMR spectra of a) starting G7 PAMAM dendrimers (G7-NH_2), b) G7-AF488 conjugates with amine end groups (G7-AF488-NH_2), c) G7-AF488 conjugates with acetamide end groups (G7-AF488-Ac), and d) G7-AF488 conjugates with carboxylate end groups (G7-AF488-COOH). Inset spectra are enlarged characteristic peaks of AlexaFluor®488.

HPLC chromatograms of the prepared G7 PAMAM dendrimer conjugates are provided in Figure 2.S2. All the conjugates exhibit a single peak and it is notable that no peak is present for free AF488 in the chromatograms. The peak widths at half-height of all the dendrimers are ranged from 0.49 to 0.62 min indicate that the dendrimer conjugates are relatively monodisperse compared to other types of condensation polymers with molecular weights of > 100,000 g/mol. This is consistent with GPC results presented in Table 2.1.(*32*) In order to provide an even more stringent assessment of polymer homogeneity, the same materials were characterized using CE.(*9, 33, 36-38*) The G7-NH_2 dendrimer exhibits multiple peaks which persists, with a change in relative magnitude, after conjugation with AF488 (Figure 2.S3b). After surface modification with acetamide and carboxylate groups is performed, the dendrimer conjugates produce sharper peaks although a multiple peak structure is still apparent for G7-AF488-Ac.

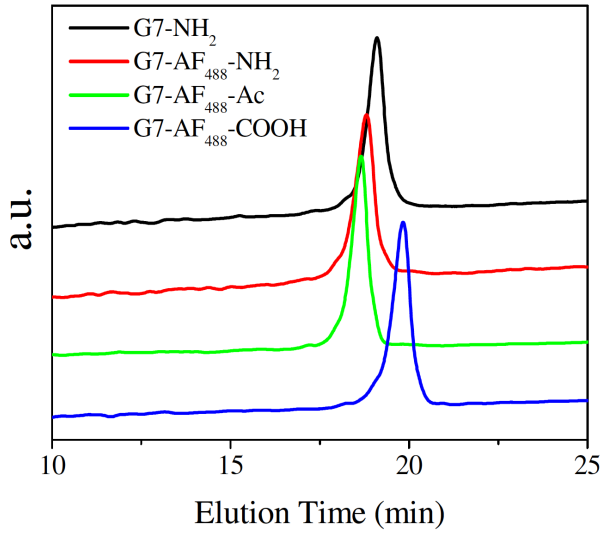

Figure 2.S2. HPLC chromatograms of the dendrimer based conjugates. All the curves are normalized based on the peak intensity of G7-NH_2.

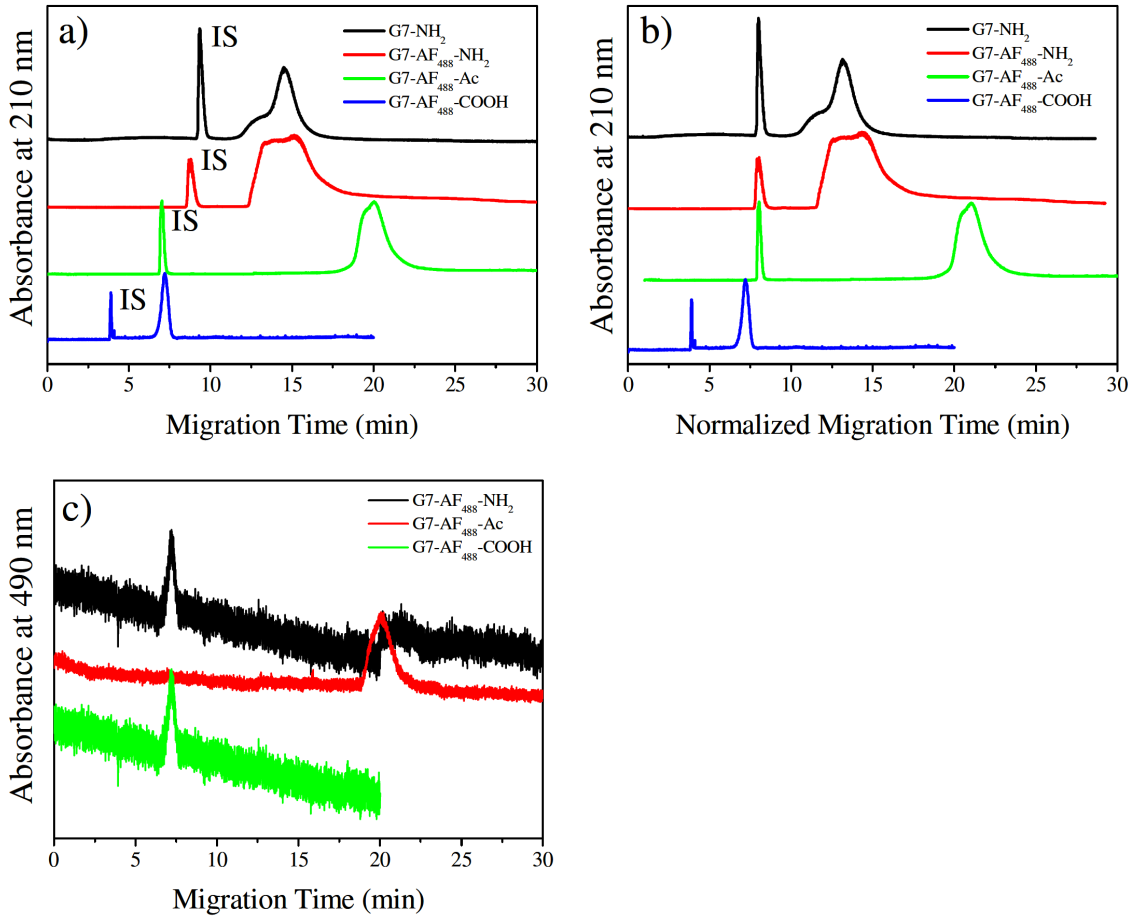

Figure 2.S3. a) CE electropherograms and b) their normalized electropherograms of the dendrimer based conjugates; G7-NH_2, G7-AF488-NH_2, G7-AF488-Ac, and G7-AF488-COOH measured at 210 nm (based on PAMAM dendrimers). Note that 2,3-diaminopyridine (2, 3-DAP) is used as an internal standard (IS) for G7-NH2, G7-AF488-NH_2, and G7-AF488-Ac. Thus only three curves are normalized in b) based on the IS peak appearance. For G7-AF488-COOH, 4-Methoxybenzyl alcohol (MBA) is used as a neutral marker. Also note that the data of G7-AF488-COOH is shown only up to a 20 min time point because no additional peak was observed thereafter. c) Electropherogram of G7-AF488-NH_2, G7-AF488-Ac, and G7-AF488-COOH measured at 490 nm (based on attached AF488). Peak heights are normalized based on the G7-AF488-NH_2

2.4.2 Cytotoxicity of Dendrimer Conjugates as Measured by XTT Assays

The cytotoxicity of the G7 PAMAM conjugates on KB, Rat2, and C6 cells *in vitro* was explored using XTT assay (Figure 2.3). The KB cell line, a variant of the human HeLa line, and the Rat2 cell line, a dermal fibroblast from Fisher Rat, were selected

because they are adherent and robust cell lines enabling us to employ various biological techniques. The C6 cell line was selected because it contains caveolin-1 but lacks GM_1 in the plasma membrane.

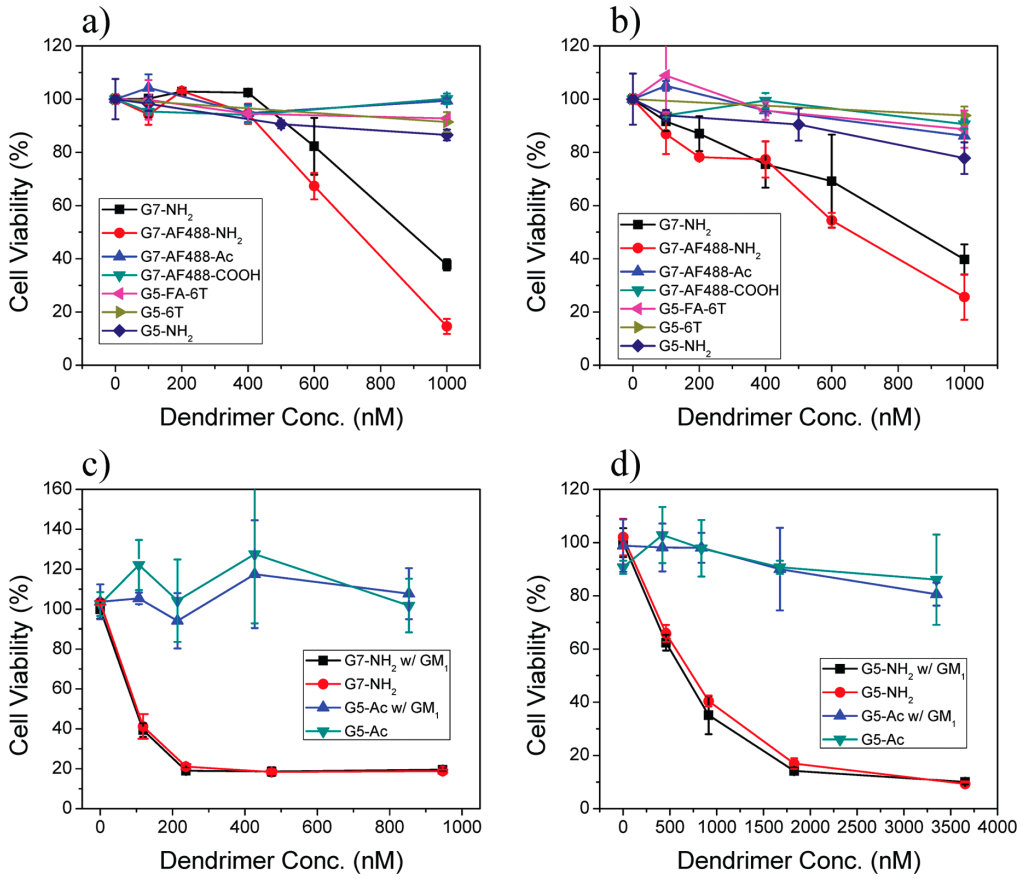

Figure 2.3. Percentage viability as measured by XTT assay when cells are treated with various G5 and G7 PAMAM dendrimers: a) KB cells, b) RAT-2 cells, c) C6 cells, and d) C6 cells. FA = folic acid. 6T = 6-Tamra.

Amine terminated G7 PAMAM dendrimers show a degree of cytotoxicity (~20% toxicity) starting at a concentration of ~400 nM whereas G5 PAMAMs are not cytotoxic at a concentration as high as 1 μM in both KB and Rat2 cells. These results are consistent with our previous report which concluded the cytotoxicity of the PAMAM dendrimers is highly dependent on size of the macromolecules.(*9*) Surface modification of the starting dendrimers significantly reduces their cytotoxicity. As

shown in Figure 2.3a and 2.3b, G7-AF488-Ac, G7-AF488-COOH, G5-6T-FA (cancer cell targeting dendritic nanodevices), and G5-6T-Ac do not show any significant toxic effect on the both cell lines at the concentration range used in the experiment. The effect of the presence of GM_1 in the cell plasma membrane on cytotoxicity was explored using the C6 cell line (Figure 2.3, panel C and D). The C6 cells exhibited a greater sensitivity to G5-NH_2 and G7-NH_2 exposure but no differential effect was observed as a function of the presence of GM_1 in the membrane.

2.4.3 The Induction of Membrane Permeability as Measured by LDH assays

The effect of GM_1 on the release of lactate dehydrogenase (LDH) was explored using C6 cells (Figure 2.4). LDH release was independent of the presence of GM_1 in the cell plasma membrane for exposure to G5-NH_2 and G7-NH_2. By way of contrast, the acetylated forms of the dendrimer, G5-Ac and G7-Ac, did not exhibit a concentration dependent release of LDH.

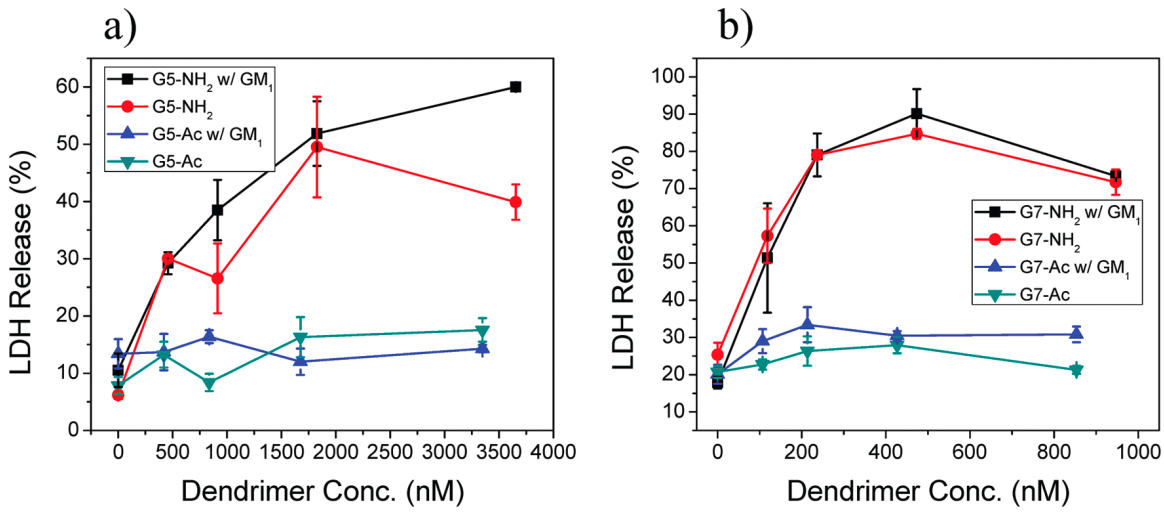

Figure 2.4. Percentage LDH release of C6 cells when treated with a) G5 and b) G7 PAMAM dendrimers.

2.4.4 CLSM Observation: Surface Group Dependence on Dendrimer Internalization

Figure 2.5 shows confocal images of Rat2 cells after exposure to G7-AF488-NH_2, G7-AF488-Ac, and G7-AF488-COOH at 37 ºC, 5% CO_2 for 1 hr. The cell nuclei were stained with DAPI and appear as blue fluorescence in the images. Figure 2.5d, 5e, and 5f are digitally zoomed-in images of Figure 2.5a, 5b, and 5c, respectively. As shown in Figure 2.5a and 5d, and confirmed by z-stack images, G7-AF488-NH_2 readily internalizes into the cells resulting in a punctate distribution of strong green fluorescence. On the other hand, surface modified dendrimers (G7-AF488-Ac and G7-AF488-COOH) do not interact with cell membrane or internalize into the cells (Figure 2.5b, c, e, and f). This is consistent with the XTT and LDH assay results shown in Figures 2.3 and 2.4 as well as previously published AFM results indicating that G7-NH_2 is the most active with supported lipid bilayers.(*24, 25*) These results stand in stark contrast to CHARM/MD studies that suggest that all three dendrimers should interact strongly with a lipid bilayer.(*39, 40*) To clearly show cell morphology, differential interference contrast (DIC) images of the cells incubated with G7-AF488-Ac and G7-AF488-COOH were overlapped with confocal fluorescence images in those images. Similar results were obtained using KB cells as well (data not shown).

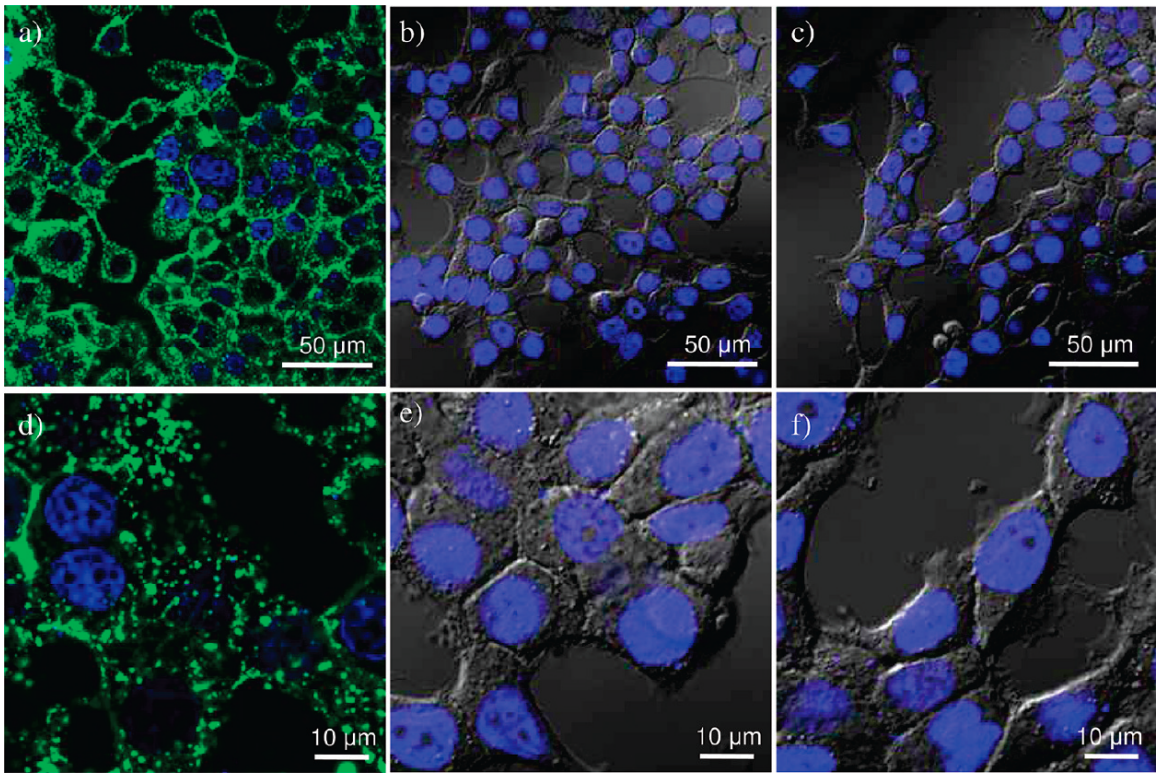

Figure 2.5. Confocal images of Rat2 cells after exposure to (a) G7-AF488-NH_2, (b) G7-AF488-Ac, and (c) G7-AF488-COOH at 37 °C for 1 h. The concentration of the dendrimer conjugates was at 200 nM. Images e, f, and g are digitally enlarged images of a, b, and c, respectively. Images b, c, e, and f are overlays of confocal and DIC images. Cell nuclei were stained by DAPI resulting in blue fluorescence in the images.

2.4.5 CLSM Observation: Effect of Low Temperature on G7-NH_2 Internalization

Figure 2.6 illustrates confocal images of Rat2 cells after incubation with G7-AF488-NH_2 and G5-FITC-NH_2 at both 37 ºC and 4 ºC. As shown in Figure 2.6e and f, G5-FITC-NH_2 penetrates into the cells at 37 ºC whereas they do not internalize but associate with cell plasma membranes at 4 ºC, which is in good agreement with previously published images.(*9*) Although G7-AF488-NH_2 internalization is reduced at the lowered temperature by ~60% as measured by FACS, the dendrimers

internalize into the cells not only at 37 ºC but also at 4 ºC as shown in Figure 2.6a and 6b. It can be more clearly observed in the zoomed-in image (Figure 2.6d). Z-stack images of Figure 2.6d also confirm internalization of the dendrimers (data not shown). The intracellular distribution pattern of fluorescence in Figure 2.6d is slightly different from that of Figure 2.6b. Less punctate distribution of the dendrimers in the cytosol is observed in Figure 2.6d (the low temperature case) as compared intracellular distribution of the dendrimers in Figure 2.6b.

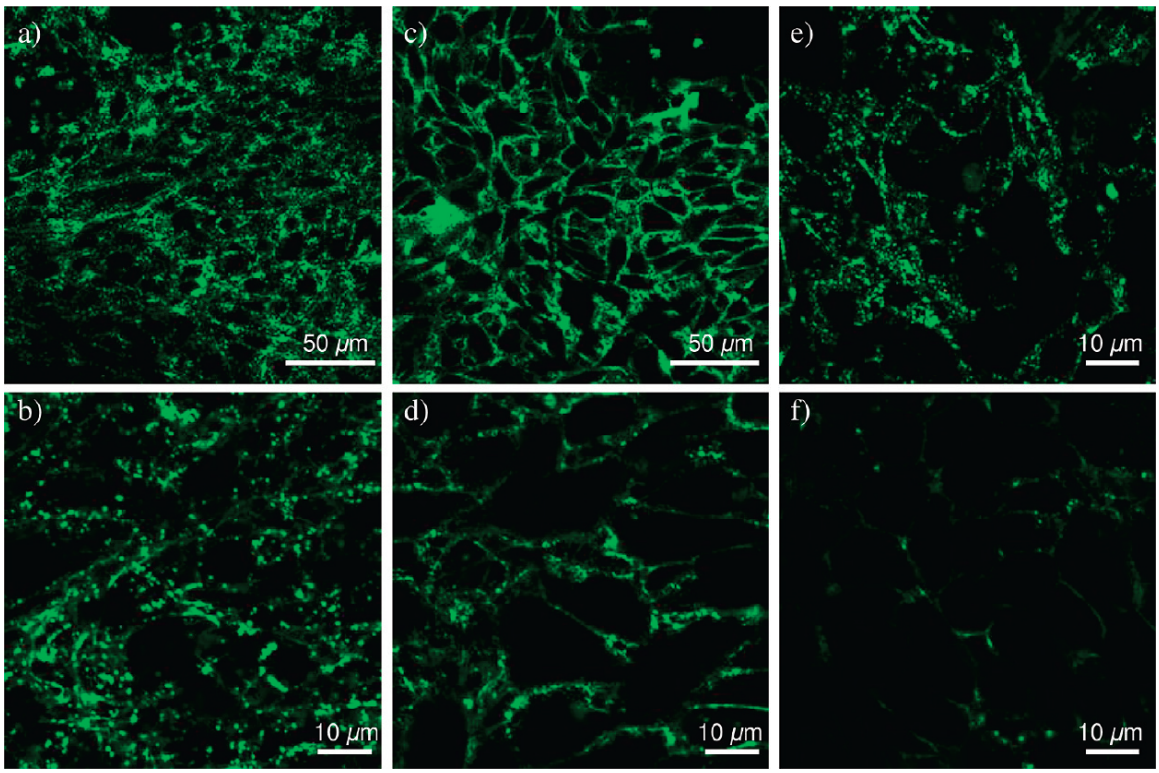

Figure 2.6. Confocal images of Rat2 cells after incubation with G7-AF488-NH_2 at (a) 37 °C and (c) 4 °C, both for 1 h. Images b and d are enlarged images of a and c, respectively. Concentration of the dendrimer conjugates was 200 nM. Note that G7-AF488-NH_2 penetrates into the cells even at the low temperature. Controls using G5-FITC-NH_2 at (e) 37 °C and (f) 4 °C.

2.4.6 CLSM Observation: Intracellular Co-localization of G7-NH_2 with Endocytic Markers

The generally reported endocytic pathways for large molecules such as biomedical polymers and cell-penetrating peptides (CPPs) include clathrin-dependent and lipid raft-mediated endocytosis.(*2, 41*) We employed commonly used endocytic markers, transferrin for clathrin dependent pathways and CTB for lipid raft-mediated endocytosis to explore the mechanism of dendrimer uptake.(*41, 42*) Direct observation of intracellular localization of the markers using CLSM was enabled by employing markers labeled by different AlexaFluors. As shown in Figure 2.7, G7-AF488-NH_2 (green fluorescence) is co-localized with CTB-AF647 (purple fluorescence) whereas intracellular localization of TF-AF546 is different from those of dendrimers and CTB in both KB and Rat2 cells. The quantified pixel counts for overlapped pixels using Metamorph software indicate the co-localization between G7-AF488-NH_2 and CTB-AF647 is 88% and 68% for KB and Rat2 cells, respectively. In contrast, co-localization as indicated by quantification of overlapped pixels for G7-AF488-NH_2 and TF-AF546 was 10 and 17 % for KB and Rat2 cells, respectively.

Co-localization with CTB is commonly taken as evidence for GM_1 interactions and a raft mediated endocytosis mechanism.(*41*) In order to directly test this hypothesis, internalization of CTB and G7-NH_2 was tested using C6 cells. In their native state, these cells contain little GM_1 in the plasma membrane. However, GM_1 can be added to the membrane via incubation. Consistent with previous reports in the literature,(*43*) CTB only internalized into C6 cells that had been pre-incubated with GM_1. However, G7-NH_2 internalized independent of the presence of GM_1 in the

plasma membrane (Figure 2.8). Recall that the results of both the XTT and LDH assays were independent of the presence of GM_1 in the C6 cell plasma membrane (Figures 2.3 and 2.4). The interaction of G7-NH2 dendrimer and CTB was explored using native poly(acrylamide) gel electrophoresis employing Coommassie blue staining. The band associated with CTB was no longer present upon mixing the dendrimer with the CTB at ratios from 1:5 to 5:1.

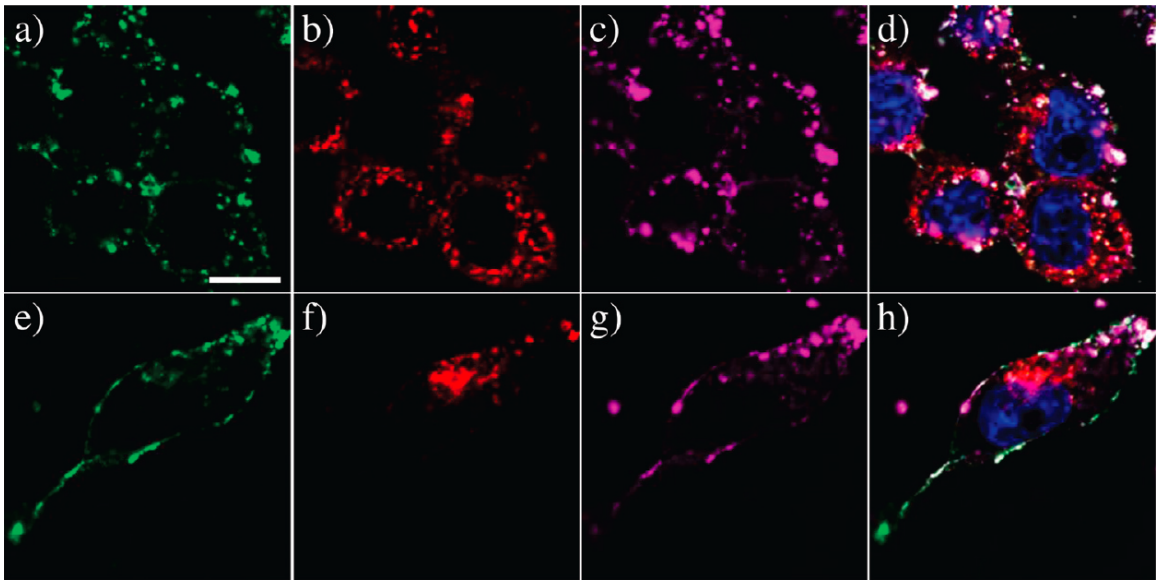

Figure 2.7. Confocal images of KB cells incubated for 1 h with (a) 200 nM G7-AF488-NH_2, (b) 50 μg/mL transferrin-AlexaFluor 546 (TF-AF546), and (c) 10 μg/mL cholera toxin subunit B-Alexa Fluor 647 (CTB-AF647) conjugates, and (d) a merged image of those. Green, red, and purple fluorescence, respectively, represent G7-AF488-NH_2, TF-AF546, and CTB-AF647. Images e, f, g, and h are a data set of Rat2 cells at the same condition with KB cells. Note that dendrimers are colocalized intracellularly with CTB in both cell lines. Bar: 10 μm.

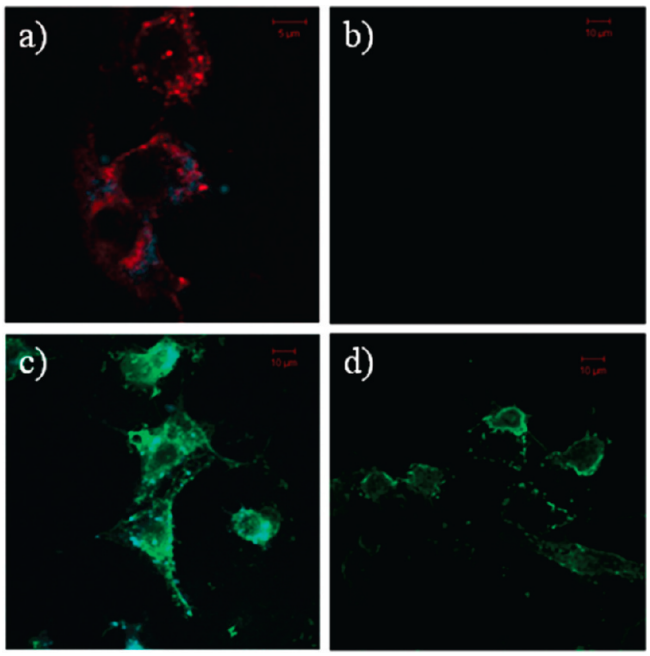

Figure 2.8. Confocal images of (a) C6 cells having GM_1-pyrene (blue) treated with Cholera toxin subunit B (CTB)-AF647(red), (b) C6 cells without GM_1 treated with CTB, (c) C6 cells having GM_1-pyrene (blue) treated with G7-NH_2-AF488 (green) PAMAM dendrimer, and (d) C6 cells without GM_1 treated with G7 dendrimer. All incubations were for 1 h. CTB is internalized only when GM_1 is present in the cell membrane. G7-NH_2 dendrimer is internalized independent of the presence of GM_1 in the cell membrane.

2.4.7 CLSM Observation: Diffusion of Neutral Dendrimers into cell?

Neutral dendrimers (G7-Ac and G5-Ac) do not interact with the cell membrane or internalize into the cell as indicated by LDH and XTT assays (Figures 2.3 and 2.4) and CLSM experiments (Figure 2.5). However, if holes of 5-25 nm were created in the membrane, G5-Ac might be expected to enter the cell via passive diffusion processes. Our previous studies have shown that LDH (135-140 kDa, ~ 4.3 nm diameter), propidium iodide, and fluorescein all diffusion across the membrane.(*6*) However, as illustrated in Figure 2.9, 100 nM G7-NH_2 is sufficient to give substantial internalization of dendrimer but 1 μM G5-6T-Ac still gives no detectable

internalization. Previous studies indicate that G7-NH_2 should be about 8 nm in diameter and the G5-6T-Ac should be about ~ 4-7 nm in diameter.(*24, 44*)

2.5 Discussion

2.5.1 Dendrimer/Membrane Interactions and Dendrimer Internalization

Amine-terminated (positively charged) G7 PAMAM dendrimers (G7-NH_2) exhibit cytotoxicity (Figure 2.3), cause LDH leakage (Figure 2.4), and internalize into cells (Figures 2.5-2.8) at <200 nM concentrations whereas charge neutral and negatively charged G7 PAMAM dendrimers do not. This is interesting because negatively charged PAMAM dendrimers (G7-AF488-COOH), suggested as a potential drug delivery vectors,(*45*) do not bind or internalize into cells at these concentrations (Figure 2.5c and f). We previously reported that G7-NH_2 PAMAM dendrimers caused more LDH leakage out of cells at 37 ºC than G5-NH_2 indicating that G7-NH_2 is more effective in membrane permeabilization or dendroporation. Furthermore, G7-NH_2 induces LDH leakage at 4 ºC whereas G5-NH_2 does not.(*9*) Confocal images also illustrate that G7-NH_2 internalizes into the cells at 4 ºC but G5-NH_2 does not (Figure 2.9). One might argue that the enhanced LDH leakage is caused by cell death since G7-NH_2 appears to be more cytotoxic than G5-NH_2 (Figure 2.4). In our concentration range (200 nM), however, G7-NH_2 exhibits minimal cytotoxic effects which are ~100% viability for KB and > 80% viability for Rat2. Consequently, the observed LDH assay and confocal data are taken as evidence for membrane permeabilization as opposed to cell death.

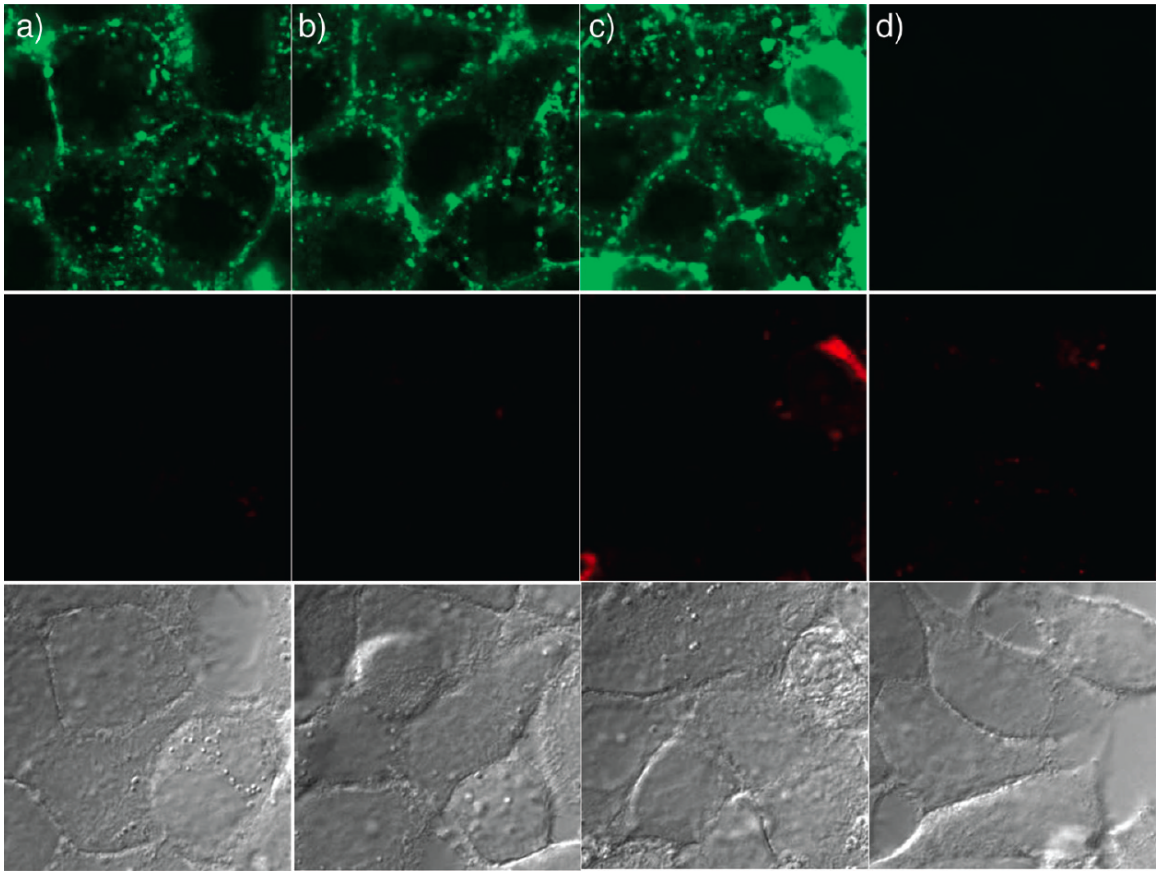

Figure 2.9. Confocal images of KB cells coincubated for 1 h with (a) 100 nM, (b) 200 nM, and (c) 400 nM G7-AF488-NH_2 and 1 μM G5-6T-Ac. Image d shows KB cells incubated with 1 μM G5-6T-Ac only. Note that red fluorescence should be detected if G7-AF488 NH_2 induces diffusion of G5-6T-Ac into the cells. However, no noticeable signal from G5-6T-Ac is observed. First row, green fluorescence channel detecting G7-AF488-NH_2; second row, red fluorescence channel detecting G5-6T-Ac; and third row, DIC images of each sample. Bar: 50 μm.

Low temperature has been used in a number of studies to investigate energy (or metabolic activities) dependency of proposed internalization mechanisms. Studies have been published for synthetic polymers and for CPPs.(*41, 42, 46*) The observation of G7-AF488-NH_2 internalization at 4 ºC can be explained by a number of possible mechanisms. One would be energy independent translocation mechanism as previously proposed for CPP internalization.(*47*) However, lowering temperature prevents G5-NH_2 internalization and partially inhibits G7-NH_2

internalization, indicating that dendrimer internalization is an energy dependent process. We will now consider two possible contributors to the energy-dependence of the nanoscale hole formation mechanism. First, the glass transition temperature (T_g) of the dendrimers may be responsible for the observed temperature dependence. Since the incubation temperature (4 ºC) is lower than T_g of both G5 and G7 PAMAM dendrimers (14-16 ºC),(*48*) chain flexibility of the dendrimer molecules should be significantly decreased. The decrease in dendrimer flexibility could impact the interaction with the plasma membrane creating a large barrier to micelle formation. Second, a phase change in the cell plasma membrane from the fluid phase (L_α) to low temperature gel phase (L^*_β)(*49*) would also inhibit nanoscale hole formation. It has recently been demonstrated using supported lipid bilayers that G7-NH_2 dendrimers only cause nanoscale hole formation in fluid phase membranes.(*23*) This is consistent with other reports indicating the membrane fluidity is related to transport properties in epithelial cells.(*50*)

There are several energy dependent pathways proposed for polycationic polymers including endocytosis *via* clathrin-coated pits(*51, 52*) and endocytosis *via* lipid rafts or caveolae.(*53, 54*) For this study we employed transferrin which is a commonly used marker for clathrin-mediated endocytosis and CTB which is a commonly used marker for clathrin-independent lipid raft (or caveolae) mediated endocytosis.(*41*) G7-AF488-NH_2 did not show substantial colocalization with transferrin (10% and 17% overlapping for KB and Rat2, respectively), indicating that G7-AF488-NH_2 internalization is not related to the clathrin-dependent pathway. Instead significant colocalization of G7-AF488-NH_2 with CTB-AF647 was observed (88% and 68%

overlapping for KB and Rat2, respectively). Co-localization with CTB implies that G7-AF488-NH_2 localizes in the cell with ganglioside GM_1. However, G7-AF488-NH_2 internalized into C6 cells independent of the presence of the GM_1 and G7-AF488-NH_2 did not co-localize with GM_1-pyrene. This indicates that the co-localization observed by us and others(*16*) is probably related to a dendrimer-CTB interaction and is not related to GM_1 interactions or a raft mediated endocytosis pathway. The LDH assays for C6 cells show no effect upon the presence or absence of GM_1 indicating the GM_1 is also not important for the mechanism of membrane permeabilization and nanoscale hole formation.

A substantial literature exists supporting polycationic endocytosis as a mechanism for the uptake of polycationic polymers into cells.(*16, 41, 55-58*) However, many inconclusive and contradictory experiments can be found in the literature and the details of the internalization mechanisms have remained elusive. In this paper, we provide direct evidence indicating a GM_1-dendrimer interaction is not involved in G7-AF488-NH_2 internalization. The best evidence supporting raft-mediated endocytosis for dendrimers, co-localization with CTB, is shown to instead result from a CTB-dendrimer interaction. Our results including nanoscale hole formation in supported lipid bilayers,(*23-25*) enzyme leakage and small molecule diffusion in and out of cells,(*6, 9*) and G7-AF488-NH_2 internalization at 4 ºC, do provide an alternative mechanism by which polycationic polymers, and nanoparticles more broadly,(*26*) may enter cells; the formation of nanoscale holes in the cell plasma membranes.(*8*) The data presented here, and published elsewhere by ourselves and others, does not indicate that the nanoscale hole mechanism should be considered

as a replacement for endocytosis mechanisms. Rather, it suggests a competitive process in which both mechanisms are operative. The nanoscale hole hypothesis does provide a straightforward explanation for data that is inconsistent with the endocytosis mechanism, both in this paper and in polycationic polymer endocytosis literature more generally.

2.6 References

1. Abdallah, B., Sachs, L., and Demeneix, B. A. (1995) Non-viral gene transfer: Applications in developmental biology and gene therapy. *Biology of the Cell 85*, 1-7.
2. Nori, A., and Kopecek, J. (2005) Intracellular targeting of polymer-bound drugs for cancer chemotherapy. *Advanced Drug Delivery Reviews 57*, 609-636.
3. Patri, A. K., Majoros, I. J., and Baker, J. R. (2002) Dendritic polymer macromolecular carriers for drug delivery. *Current Opinion in Chemical Biology 6*, 466-471.
4. Quintana, A., Raczka, E., Piehler, L., Lee, I., Myc, A., Majoros, I., Patri, A. K., Thomas, T., Mule, J., and Baker, J. R. (2002) Design and function of a dendrimer-based therapeutic nanodevice targeted to tumor cells through the folate receptor. *Pharmaceutical Research 19*, 1310-1316.
5. Gillies, E. R., and Frechet, J. M. J. (2005) Dendrimers and dendritic polymers in drug delivery. *Drug Discovery Today 10*, 35-43.
6. Hong, S., Bielinska, A. U., Mecke, A., Keszler, B., Beals, J. L., Shi, X., Balogh, L., Orr, B. G., Baker, J. R., and Banaszak Holl, M. M. (2004) The Interaction of Polyamidoamine (PAMAM) Dendrimers with Supported Lipid Bilayers and Cells: Hole Formation and the Relation to Transport. *Bioconjugate Chemistry 15*, 774-782.
7. Hong, S., Hessler, J. A., Banaszak Holl, M. M., Leroueil, P. R., Mecke, A., and Orr, B. G. (2006) Physical Interactions of Nanoparticles with Biological Membranes: The Observation of Nanoscale Hole Formation. *Chemical Health and Safety 13*, 16-20.
8. Leroueil, P. R., Hong, S. Y., Mecke, A., Baker, J. R., Orr, B. G., and Holl, M. M. B. (2007) Nanoparticle interaction with biological membranes: Does nanotechnology present a janus face? *Accounts of Chemical Research 40*, 335-342.
9. Hong, S. P., Leroueil, P. R., Janus, E. K., Peters, J. L., Kober, M. M., Islam, M. T., Orr, B. G., Baker, J. R., and Holl, M. M. B. (2006) Interaction of polycationic polymers with supported lipid bilayers and cells: Nanoscale hole formation and enhanced membrane permeability. *Bioconjugate Chemistry 17*, 728-734.

10. Zhang, S. B., Xu, Y. M., Wang, B., Qiao, W. H., Liu, D. L., and Li, Z. S. (2004) Cationic compounds used in lipoplexes and polyplexes for gene delivery. *Journal of Controlled Release 100*, 165-180.
11. Hussain, M., Shchepinov, M. S., Sohail, M., Benter, I. F., Hollins, A. J., Southern, E. M., and Akhtar, S. (2004) A novel anionic dendrimer for improved cellular delivery of antisense oligonucleotides. *Journal of Controlled Release 99*, 139-155.
12. Jevprasesphant, R., Penny, J., Attwood, D., and D'Emanuele, A. (2004) Transport of dendrimer nanocarriers through epithelial cells via the transcellular route. *Journal of Controlled Release 97*, 259-267.
13. Jevprasesphant, R., Penny, J., Attwood, D., McKeown, N. B., and D'Emanuele, A. (2003) Engineering of dendrimer surfaces to enhance transepithelial transport and reduce cytotoxicity. *Pharmaceutical Research 20*, 1543-1550.
14. Kopatz, I., Remy, J. S., and Behr, J. P. (2004) A model for non-viral gene delivery: through syndecan adhesion molecules and powered by actin. *Journal of Gene Medicine 6*, 769-776.
15. Liu, Z. H., Li, M. Y., Cui, D. F., and Fei, J. (2005) Macro-branched cell-penetrating peptide design for gene delivery. *Journal of Controlled Release 102*, 699-710.
16. Manunta, M., Tan, P. H., Sagoo, P., Kashefi, K., and George, A. J. T. (2004) Gene delivery by dendrimers operates via a cholesterol dependent pathway. *Nucleic Acids Research 32*, 2730-2739.
17. Manunta, M., Nichols, B. J., Tan, P. H., Sagoo, P., Harper, J., and George, A. J. T. (2006) Gene delivery by dendrimers operates via different pathways in different cells, but is enhanced by the presence of caveolin. *Journal of Immunological Methods 314*, 134-146.
18. Seib, F. P., Jones, A. T., and Duncan, R. (2007) Comparison of the endocytic properties of linear and branched PEIs, and cationic PAMAM dendrimers in B16f10 melanoma cells. *Journal of Controlled Release 117*, 291-300.
19. Kandyba, A. G., Kozlov, A. M., Somova, O. G., and Dyatlovitskaya, E. V. (2008) A comparative study of sphingolipids in transplanted melanomas with high and low metastatic activity. *Russian Journal of Bioorganic Chemistry 34*, 230-233.
20. Kitchens, K. M., Kolhatkar, I. B., Swaan, P. W., and Ghandehari, H. (2008) Endocytosis inhibitors prevent poly(amidoamine) dendrimer internalization and permeability across Ceco-2 cells. *Molecular Pharmaceutics 5*, 364-369.
21. Perumal, O. P., Inapagolla, R., Kannan, S., and Kannan, R. M. (2008) The effect of surface functionality on cellular trafficking of dendrimers. *Biomaterials 29*, 3469-3476.
22. Mecke, A., Lee, D. K., Ramamoorthy, A., Orr, B. G., and Banaszak Holl, M. M. (2005) Membrane thinning due to antimicrobial peptide binding - An AFM study of MSI-78 in DMPC bilayers. *Biophysical Journal 89*, 4043-4050.
23. Mecke, A., Lee, D.-K., Ramamoorthy, A., Orr, B. G., and Banaszak Holl, M. M. (2005) Synthetic and Natural Polycationic Polymer Nanoparticles Interact Selectively with Fluid-Phase Domains of DMPC Bilayers. *Langmuir 21*, 8588-8590.

24. Mecke, A., Majoros, I., Patri, A. K., Baker, J. R., Banaszak Holl, M. M., and Orr, B. G. (2005) Lipid Bilayer Disruption by Polycationic Polymers: The Roles of Size and Chemical Functional Group. *Langmuir 21*, 10348-10354.
25. Mecke, A., Uppuluri, S., Sassanella, T. J., Lee, D. K., Ramamoorthy, A., Baker, J. R., Orr, B. G., and Banaszak Holl, M. M. (2004) Direct Observation of Lipid Bilayer Disruption by Poly(amidoamine) Dendrimers. *Chemistry and Physics of Lipids 132*, 3-14.
26. Leroueil, P. R., Berry, S. A., Duthie, K., Han, G., Rotello, V. M., McNerny, D. Q., Baker, J. R., Orr, B. G., and Holl, M. M. B. (2008) Wide varieties of cationic nanoparticles induce defects in supported lipid bilayers. *Nano Letters 8*, 420-424.
27. Oberdorster, G., Oberdorster, E., and Oberdorster, J. (2005) Nanotoxicology: An emerging discipline evolving from studies of ultrafine particles. *Environmental Health Perspectives 113*, 823-839.
28. Karoonuthaisiri, N., Titiyevskiy, K., and Thomas, J. L. (2003) Destabilization of fatty acid-containing liposomes by. polyamidoamine dendrimers. *Colloids and Surfaces B-Biointerfaces 27*, 365-375.
29. Zhang, Z.-Y., and Smith, B. D. (2000) High-Generation Polycationic Dendrimers Are Unusually Effective at Disrupting Anionic Vesicles: Membrane Bending Model. *Bioconjugate Chemistry 11*, 805-814.
30. Patri, A. K., Myc, A., Beals, J., Thomas, T. P., Bander, N. H., and Baker, J. R. (2004) Synthesis and in vitro testing of J591 antibody-dendrimer conjugates for targeted prostate cancer therapy. *Bioconjugate Chemistry 15*, 1174-1181.
31. Majoros, I. J., Keszler, B., Woehler, S., Bull, T., and Baker, J. R. (2003) Acetylation of poly(amidoamine) dendrimers. *Macromolecules 36*, 5526-5529.
32. Islam, M. T., Shi, X. Y., Balogh, L., and Baker, J. R. (2005) HPLC separation of different generations of poly(amidoamine) dendrimers modified with various terminal groups. *Analytical Chemistry 77*, 2063-2070.
33. Shi, X. Y., Lesniak, W., Islam, M. T., Muniz, M. C., Balogh, L. P., and Baker, J. R. (2006) Comprehensive characterization of surface-functionalized poly (amidoamine) dendrimers with acetamide, hydroxyl, and carboxyl groups. *Colloids and Surfaces a-Physicochemical and Engineering Aspects 272*, 139-150.
34. Thomas, T. P., Myaing, M. T., Ye, J. Y., Candido, K., Kotlyar, A., Beals, J., Cao, P., Keszler, B., Patri, A. K., Norris, T. B., and Baker, J. R. (2004) Detection and analysis of tumor fluorescence using a two-photon optical fiber probe. *Biophysical Journal 86*, 3959-3965.
35. Banks, P. R., and Paquette, D. M. (1995) Comparison of 3 Common Amine Reactive Fluorescent-Probes Used for Conjugation to Biomolecules by Capillary Zone Electrophoresis. *Bioconjugate Chemistry 6*, 447-458.
36. Shi, X. Y., Banyai, I., Lesniak, W. G., Islam, M. T., Orszagh, I., Balogh, P., Baker, J. R., and Balogh, L. P. (2005) Capillary electrophoresis of polycationic poly(amidoamine) dendrimers. *Electrophoresis 26*, 2949-2959.
37. Shi, X. Y., Majoros, I. J., Patri, A. K., Bi, X. D., Islam, M. T., Desai, A., Ganser, T. R., and Baker, J. R. (2006) Molecular heterogeneity analysis of

poly(amidoamine) dendrimer-based mono- and multifunctional nanodevices by capillary electrophoresis. *Analyst 131*, 374-381.
38. Shi, X. Y., Patri, A. K., Lesniak, W., Islam, M. T., Zhang, C. X., Baker, J. R., and Balogh, L. P. (2005) Analysis of poly(amidoamine)-succinamic acid dendrimers by slab-gel electrophoresis and capillary zone electrophoresis. *Electrophoresis 26*, 2960-2967.
39. Kelly, C. V., Leroueil, P. R., Nett, E. K., Wereszczynski, J. M., Baker, J. R., Orr, B. G., Holl, M. M. B., and Andricioaei, I. (2008) Poly(amidoamine) dendrimers on lipid bilayers I: Free energy and conformation of binding. *Journal of Physical Chemistry B 112*, 9337-9345.
40. Kelly, C. V., Leroueil, P. R., Orr, B. G., Holl, M. M. B., and Andricioaei, I. (2008) Poly(amidoamine) dendrimers on lipid bilayers II: Effects of bilayer phase and dendrimer termination. *Journal of Physical Chemistry B 112*, 9346-9353.
41. Foerg, C., Ziegler, U., Fernandez-Carneado, J., Giralt, E., Rennert, R., Beck-Sickinger, A. G., and Merkle, H. P. (2005) Decoding the entry of two novel cell-penetrating peptides in HeLa cells: Lipid raft-mediated endocytosis and endosomal escape. *Biochemistry 44*, 72-81.
42. Richard, J. P., Melikov, K., Vives, E., Ramos, C., Verbeure, B., Gait, M. J., Chernomordik, L. V., and Lebleu, B. (2003) Cell-penetrating peptides - A reevaluation of the mechanism of cellular uptake. *Journal of Biological Chemistry 278*, 585-590.
43. Spiegel, S. (1988) Insertion of Ganglioside GM_1 into Rat Glioma C6 Cells Renders Them Susceptible to Growth-Inhibition by the B-Subunit of Cholera-Toxin. *Biochimica Et Biophysica Acta 969*, 249-256.
44. Prosa, T. J., Bauer, B. J., Amis, E. J., Tomalia, D. A., and Scherrenberg, R. (1997) A SAXS study of the internal structure of dendritic polymer systems. *Journal of Polymer Science Part B-Polymer Physics 35*, 2913-2924.
45. Wiwattanapatapee, R., Carreño-Gómez, B., Malik, N., and Duncan, R. (2000) Anionic PAMAM Dendrimers Rapidly Cross Adult Rat Intestine In Vitro: A Potential Oral Delivery System? *Pharmaceutical Research 17*, 991-998.
46. Thorén, P. E. G., Persson, D., Esbjorner, E. K., Goksor, M., Lincoln, P., and Norden, B. (2004) Membrane binding and translocation of cell-penetrating peptides. *Biochemistry 43*, 3471-3489.
47. Wadia, J. S., and Dowdy, S. F. (2002) Protein transduction technology. *Current Opinion in Biotechnology 13*, 52-56.
48. Uppuluri, S., Morrison, F. A., and Dvornic, P. R. (2000) Rheology of dendrimers. 2. Bulk polyamidoamine dendrimers under steady shear, creep, and dynamic oscillatory shear. *Macromolecules 33*, 2551-2560.
49. Janiak, M. J., Small, D. M., and Shipley, G. G. (1979) Temperature and compositional dependence of the structure of hydrated dimyristoyl lecithin. *J. Biol. Chem. 254*, 6068-6078.
50. Le Grimellec, C., Friedlander, G., Elyandouzi, E., Zlatkine, P., and Giocondi, M. C. (1992) Membrane Fluidity and Transport-Properties in Epithelia. *Kidney International 42*, 825-836.
51. Vendeville, A., Rayne, F., Bonhoure, A., Bettache, N., Montcourrier, P., and Beaumelle, B. (2004) HIV-1 Tat enters T cells using coated pits before

translocating from acidified endosomes and eliciting biological responses. *Molecular Biology of the Cell 15*, 2347-2360.
52. Schmid, S. L. (1997) Clathrin-coated vesicle formation and protein sorting: An integrated process. *Annual Review of Biochemistry 66*, 511-548.
53. Simons, K., and Ikonen, E. (1997) Functional rafts in cell membranes. *Nature 387*, 569-572.
54. Brown, D. A., and London, E. (1998) Functions of lipid rafts in biological membranes. *Annual Review of Cell and Developmental Biology 14*, 111-136.
55. Parton, R. G., and Richards, A. A. (2003) Lipid rafts and caveolae as portals for endocytosis: New insights and common mechanisms. *Traffic 4*, 724-738.
56. Apodaca, G. (2001) Endocytic traffic in polarized epithelial cells: Role of the actin and microtubule cytoskeleton. *Traffic 2*, 149-159.
57. Fischer, R., Kohler, K., Fotin-Mleczek, M., and Brock, R. (2004) A stepwise dissection of the intracellular fate of cationic cell-penetrating peptides. *Journal of Biological Chemistry 279*, 12625-12635.
58. Bieber, T., Meissner, W., Kostin, S., Niemann, A., and Elsasser, H. P. (2002) Intracellular route and transcriptional competence of polyethylenimine-DNA complexes. *Journal of Controlled Release 82*, 441-454.

Chapter 3

Polyplex-Induced Cytosolic Nuclease Activation leads to Differential Transgene Expression

3.1 Abstract

In this chapter, cytosolic nucleases have been proposed to play an important role in limiting the effectiveness of polyplex-based gene delivery agents. The hypothesis is that polyplex interaction with plasma membrane induces the cellular response by activating cellular nucleases. In order to explore the effect of cell membrane disruption on nuclease activation, nuclease activity upon polyplex uptake and localization, and nuclease activity upon gene expression, we employed an oligonucleotide molecular beacon (MB). The MB was incorporated as an integral part of the polymer/DNA polyplex and two-color flow cytometry experiments were performed to explore the relationship of MB cleavage with Propidium iodide (PI) uptake, protein expression, and polyplex uptake. In addition, confocal fluorescence microcopy was performed to examine both polyplex and cleaved MB localization. The impact of cell membrane disruption was also probed using whole-cell patch clamp measurement of the plasma membrane's electrical conductance. Differential activation of cytosolic nuclease was observed with substantial activity for B-PEI and G5 PAMAM dendrimer (G5), less cleavage for jetPEI™, little activity for L-PEI.

jetPEI™ and L-PEI exhibited significantly greater transgene expression, consistent with the lower amounts of MB oligonucleotide cleavage observed. Cytosolic nuclease activity, although dependent on the choice of polymer employed, was not related to the degree of cell plasma membrane disruption that occurred as measured by PI uptake or whole-cell patch clamp.

3.2 Introduction

The development of safe and efficient nucleic acid delivery systems for use in mammalian cells remains a significant scientific, technological, and clinical challenge. Applications of plasmid DNA (pDNA), antisense DNA (asDNA), and silencing RNA (siRNA) oligonucleotide therapeutics are severely limited due to the absence of safe and efficient vector systems. Despite the outstanding promise of this technology, there are no FDA-approved vector systems for nucleic acid delivery in humans. Of the many existing nucleic acid delivery systems, nonviral-based systems enjoy certain advantages because of their small size, lack of traditional immunogenic epitopes, and avoidance of other viral-based side-effects; however, they are not as efficient with respect to gene expression as viral based systems.[1-3] Nonviral vectors are efficient at delivering the transgene into the cells and can also protect the nucleic acid from degradation; however most of the genetic material is delivered into regions of the cytosol, including endosomes and lysosomes, in a non-functional manner.[4]

Efforts to increase the efficiency of gene delivery vectors have focused on uptake mechanism, endosomal escape, and penetration of the nucleus.[5] Both viral and

nonviral vectors are thought to enter via energy dependent endocytosis pathways that can lead to vector/DNA localization inside endosomes.[2, 6] Before the endosomes become lysosomes, the two vector systems are thought to diverge mechanistically. Viral systems have a dedicated mechanism to transfer nucleic acid into the nucleus, but polyplexes are not known to have such a mechanism.[5, 6] This is thought to contribute to the inefficiency of polymeric vector systems in providing transgene expression. In general, interpretation of mechanistic studies using efficiency of protein expression as an endpoint is difficult because it is quite challenging, or impossible, to separate the transfection steps (i.e., crossing the cell plasma membrane, cytosolic localization, transport to nucleus) and expression steps (i.e., presentation of functional material in the nucleus, optimization of promoters) and to know the impact of any particular change in vector design on each of these hurdles to effective expression.

In addition to the challenges discussed above, there is a common presumption that the cellular environment present over the course of a transfection experiment (typically 12-48 h) is the same for all polymer vector systems tested. In other words, it is assumed that either 1) the cell does not actively respond to the introduction of the polymer/DNA polyplex or 2) if the cell does respond it does so in fashion independent of the polymer employed. This critical, but generally unstated assumption, may lead to incorrect mechanistic conclusions regarding vector optimization if the cells respond in a differential fashion to the polymers and the resulting transfection and expression processes are proceeding in dynamically differing cellular environments. In this study we ask the question, does polyplex

introduction trigger a cellular response that leads to a heightened ability to degrade foreign pDNA? The centrality of this question to developing successful gene therapies is supported by the difficulty of identifying consistent trends as a function of physical properties of the nonviral vectors.[3, 7-9] Work to date has focused on the key problem of how to transport the desired pDNA, asDNA, or siRNA across cellular barriers, but not the possibility of dynamic cellular responses to these barriers being breached. In particular, if the introduction of certain polyplex forms leads to the heightened production and/or activation of cytosolic nucleases, this would represent a major new factor for consideration in the design of nonviral vectors.

The literature contains strong support for the idea that cytosolic nucleases[10] play an important role in the half-life of DNA in the cytosol.[11-17] In a seminal study, Lukacs et al. provided evidence that pDNA is degraded by nucleases constitutively present in the cytosol.[11] Pollard et al. examined complementary DNA (cDNA) degradation in the cytosol and noted that it was Ca^{+2} dependent and inhibited by nuclease inhibitors aurin tricarboxylic acid and Zn^{+2} or by the complexation of the cDNA with poly(ethyleneimine) (PEI).[16] A recent study by Ruponen et al. studied the cytosolic half-life for pDNA delivered by a variety of vectors to CV1 cells and confirmed that unprotected pDNA degraded quickly, but that when protected by cationic lipids or polymers the half-lives could be increased up to a factor of ~20.[12] They also noted that the pDNA release and elimination rates correlated poorly with transgene expression. These studies suggest the possibility that cytosolic nucleases contribute to the degradation of transported DNA, which leads

to decrease in overall transgene expression, before nuclear uptake comes into play. Indeed it has been shown that even nicking the plasmid can lead to significant decrease in transgene expression.[18] Prazeres et al. have explored the effect of cytosolic nucleases by varying the structure of the DNA sequence.[19, 20] They identified regions that could be modified to generate improved nuclease resistance.

In the work described above, efforts were focused on understanding the degradation of pDNA by cytosolic nucleases and how the pDNA could be modified to improve stability. In this report, we focus on the role of the polymer vector. In particular, we test the hypotheses that polycationic polymers differentially activate cytosolic nucleases and that this can lead to decreased transgene expression. We employ a single stranded DNA oligonucleotide molecular beacon (MB)[21] containing a fluorescein derivative 6-FAM on the 5' end and an Iowa Black (IB) quencher at the 3' end (6-FAM-CCTCGTCCATACCCAAGAAGGAAGCGAGG-IB) as a sensitive indicator of cytosolic nuclease activity. The intact single strand forms a hairpin structure leading to quenched fluorescence. The readily cleaved single strand sequence of the MB is a good model for the single stranded "hot spots" in pDNA identified by Prazeres et al. as being particularly susceptible to nuclease attack.[19, 20] Upon exposure to nucleases, the oligonucleotide is cleaved and a fluorescent signal is obtained. The MB was employed for two-color flow cytometry studies comparing 1) MB fluorescence to PI uptake, 2) MB fluorescence to red fluorescent protein (RFP) expression (when mixed at a 10:1 N:P (nitrogen to phosphate molar ratio) ratio with pDNA encoding for RFP) and 3) MB fluorescence to DNA uptake. These polyplex materials were also employed for confocal

microscopy to simultaneously study nuclease activity and polyplex localization and for solution-based experiments to examine the relative degree of nuclease protection afforded by the three polymer vectors.

Nuclease activation as measured by the DNA-based MB was compared to cell plasma membrane permeability as measured by PI uptake and total protein expression levels of RFP. Cell membrane permeability was also measured using whole-cell patch clamp. We examined nuclease activation in the context of cell membrane permeability because our previous studies demonstrated that low concentrations of polycationic polymer vectors induced nanoscale pores in the cell membrane with varying degrees of activity and pore lifetimes.[22-25] A number of the previously published studies on nuclease degradation discussed above employed permeabilization agents (for example, digitonin). This served to further interest us in cell plasma membrane disruption as a possible trigger for nuclease activity. Since protein expression is the end goal of pDNA delivery, we also examined the relationship between protein expression levels and nuclease activity.

The choice of cationic polymer as vector for the transfection and expression of pDNA can have a profound impact on the amount of protein expression observed for the cell population. Polymer vectors are generally designed to optimize and balance the following properties: uptake, protection of the plasmid DNA, transport of the DNA to the nucleus, and release of the DNA to the transcription machinery of the cell.[26, 27] In this study, we compare the impact of selection of polymer vectors, branched-PEI (B-PEI), generation 5 poly(amidoamine) (G5 PAMAM) dendrimer, jetPEI™, and linear PEI (L-PEI), on the activation of nucleases that can cleave

transported pDNA. The experiments were carried out inside the cell as part of a normal polyplex transfection/expression treatment and as model solution-based experiments. For this study, we selected jetPEI™, a commercial form of linear PEI, because it is one of the most effective commercially available polymeric vectors. We chose G5 PAMAM because it is a polymer of roughly similar molecular weight, has an excellent polydispersity index (PDI) (1.01), and is well characterized in terms of numbers of cationic primary amines. L-PEI and B-PEI were selected as non-proprietary PEI comparisons. Polyplexes were made using a 10:1 N:P ratio as this was reasonable compromise for forming functional, low toxicity materials for transfection/expression for this set of four polymers (Figure 3.S1).

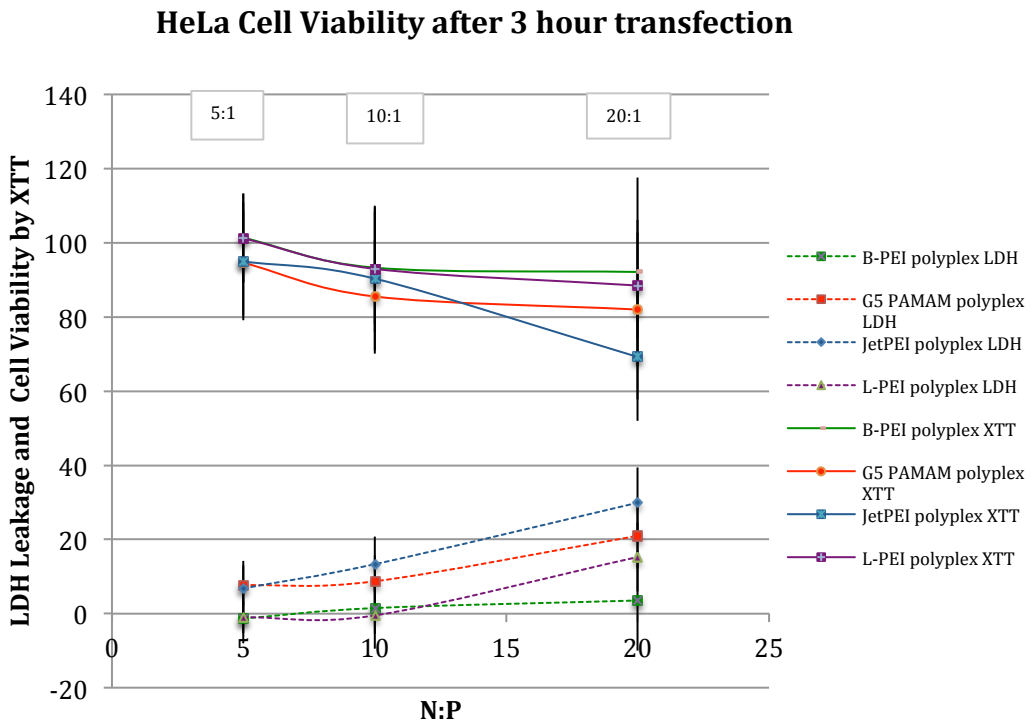

Figure 3.S1. HeLa Cell Viability after 3-hour transfection incubation: Polyplex preparation: 40,000 cells/ well were plated and incubated overnight in 96-wells plate. Wells were rinsed with PBS containing Ca^{2+} and Mg^{2+}. 10 µL Polyplexes at N:P ratio 5:1, 10:1 and 20:1 containing 0.08 µg of Molecular Beacon were then added to 90 µL SFM. 3 hours post-transfection media was removed and added to a replicate 96 wells plate. The media was then used for the LDH assay and the cells were used for the XTT assay. XTT assay: Cells were rinsed with PBS containing Ca^{2+} and Mg^{2+}. 50 µL of PBS containing divalent ions was then added to cells and followed by 50 µL XTT working solution. The plate was then incubated at 37 °C for 4 hours before it was measured. LDH assay: 50 µL of supernatant was incubated with 50 µL of the LDH working solution. The plate was then incubated at 37 °C for 20 minutes and then measured.

For the polymer vectors employed in this study, B-PEI, L-PEI, jetPEI™, and G5 PAMAM, the following conclusions were reached: 1) all four polymer/DNA polyplexes cause substantial cell plasma membrane disruption, 2) B-PEI and G5 PAMAM polyplexes treated cells show substantial nuclease activity whereas L-PEI and jetPEI™ treated cells exhibit significantly less, 3) expressing cells for both L-PEI and jetPEI™ polyplex treated cells show less nuclease activity as compared to

expressing cells for B-PEI and G5 PAMAM polyplexes, 4) the different levels of expression observed are not simply explained by differential polymer protective effects, and 5) the data indicates that the dramatic difference in expression efficiency is related to a significant difference in the extent to which the polymer vectors induce an active nuclease response in the cells. In addition, the DNA cleavage pattern of nuclease present in the cellular cytoplasm is similar to that obtained for S1 nuclease as observed in our agarose gel electrophoresis experiment.

3.3 Materials and Methods

3.3.1 Materials

jetPEI™ was procured from VWR International. In-house GPC characterization of jetPEI™ yielded M_n of 25000 Da and polydispersity index (PDI) of 1.42. B-PEI was obtained from Sigma Aldrich Corporation with M_n of 10,000 and PDI of 2.5. L-PEI was obtained from Polysciences, Inc. with M_n of 23,750 and PDI of 1.04. Stock solutions for G5 PAMAM and B-PEI were made in water at room temperature. L-PEI stock solution was also made in water but was heated to 66°C to dissolve. Minimal essential media (MEM) with glutamine and Earle salts (serum-free media (SFM); #11095) was obtained from life technologies. For suspending cells prior to patch clamp, SFM for suspension culture (SFMII;#11868) from life technologies was employed. Complete media was made by adding 50 mL of fetal bovine serum (FBS) and 5 mL 100x of penicillin-streptomycin to 500 mL SFM. Detachin was purchased from Gelantis Inc. PBS (1X) with and without Ca^{2+} and Mg^{2+} was obtained from Thermo Scientific. Luciferase plasmid DNA, S1 nuclease, and LDH assays kits were

obtained from Promega Corporation. XTT assay kits were obtained from Hoffmann-La Roche Ltd. Salmon sperm DNA was obtained from Ambion. Blank plasmid (plasmid that doesn't express any protein) was obtained from Aldevron, L.L.C. *Label* IT CX-Rhodamine Nucleic Acid Labeling Kit was obtained from Mirus Bio. 2-well coverglass chambers were obtained from Thermo Fisher Scientific, Inc. BD Falcon™ 24 well culture plates were used for flow cytometry experiments. PI and protease inhibitor cocktail were obtained from Sigma-Aldrich and Prolong Gold™ antifade reagent was procured from Invitrogen. NP-40 lysis buffer was procured from Boston BioProducts Inc. pDsRed1-N1 (RFP) was purchased from Clontech Laboratories, Ltd. The MB employed was custom ordered from Integrated DNA Technologies. The sequence is CCTCGTCCATACCCAAGAAGGAAGCGAGG where 5' end modified with 6-FAM™ (Fluorescein) and 3' end with Iowa Black FQ. An EPICS XL-MCL Beckman Coulter flow cytometer was employed. For each sample, two replicates of 10,000 cells each were used; Δ MF and standard error are reported. For confocal microscopy, a Zeiss 510 Meta confocal microscope was used with 63X objective. 351 nm, 488 nm and 543 nm lasers were used to excite DAPI, MB and rhodamine respectively. For both flow cytometry and confocal microscopy using two dyes, independent excitation and emission detection was employed with microsecond delays to avoid potential fluorescence resonance energy transfer (FRET) artifacts.

3.3.2 Porosity vs. MB Fluorescence

Polyplex preparation: Each polymer was diluted in sterile water to obtain an N:P ratio of 10:1. Dilutions of blank plasmid (0.5 μg) and MB (0.5 μg) were prepared and

mixed to obtain a final N:P ratio of 10:1 in the polyplex. The polymer dilutions (25 μL) were added to equal volumes of DNA mixture (25 μL) and incubated at room temperature for 25 min before transfection. Transfection: HeLa cells at 200,000 cells/well in 1 mL of complete media were incubated overnight in 24-well plates for flow cytometry. The cells were transfected with jetPEI™, G5 PAMAM, B-PEI, or L-PEI polyplexes and incubated at 37^{o} C in 440 μL of SFM. After 10 minutes, 10 μL of 5 μg/μL PI was added to each well. After 3 h of polyplex incubation, transfecting media was removed, 500 μL of fresh complete media was added to each well, and cells were incubated at 37 ^{o}C. Flow Cytometry: After 9 h (12 h post transfection) cells were rinsed with PBS without Ca^{2+} and Mg^{2+}, trypsinized, and suspended in 1.8 mL of PBS with Ca^{2+} and Mg^{2+} and centrifuged at 2000 rpm for 5 min. The supernatant was removed and the pellet was re-suspended in 400 μL of PBS without Ca^{2+} and Mg^{2+} ions and kept on ice. In a separate study, we examined the pH stability of the MB and determined that it was stable at neutral to acidic pH values present in the cell (supplementary Figure 3.S2).

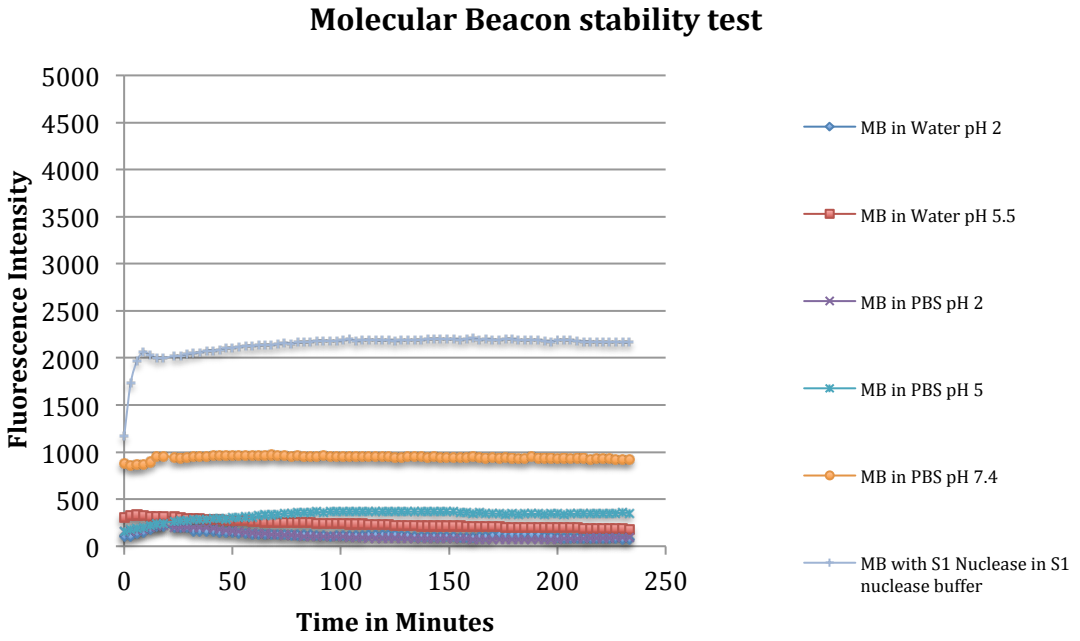

Figure 3.S2. Molecular Beacon stability analysis.: The experiment was carried out in a 96-well plate. Each well contained 0.08 µg of molecular beacon diluted in10 µL water solution. Molecular beacon solution was then added to wells containing 90 µL of water or PBS at pH 2, 5 and 7.4 without S1 nuclease or in S1 nuclease buffer with S1 nuclease. The plate was read at excitation of 485/20 nm and emission of 528/20 nm. Based on this study it can be concluded that molecular beacon is stable at acidic and neutral pH.

3.3.3 Whole-Cell Patch Clamp using Ionflux 16™[28]

Traditional whole-cell patch clamp is very labor intensive. The high throughput IonFlux16™ (IF-16) patch clamp instrument simultaneously traps 320 cells in 16 ensembles of 20. The electrical characteristics of each ensemble of 20 cells are measured using a dedicated amplifier. The changes in cell membrane permeability are measured for the ensemble of cells as a group in eight independently controllable microfluidic environments that allow simultaneous measurement of control cells and the different polyplex formulations. Detailed operation protocols are provided in Figure 3.S3.

A

B

Phase	Main Channel	Traps	Traps and Compounds	Compounds
Preprime	1 psi (0-92 s) 0.3 psi (92-120 s)	5 psi (0-90 s) 1.5 psi (90-115 s)	6 psi (115-120s)	
Prime	1 psi (0-30 s) 0.4 psi (30-55 s)	6 Hg (50-55 s)	5 psi (0-20 s) 2 psi (20-50 s)	Not used
Trap	Pulse: 0 psi for 4.2s 0.25 psi for 0.8 s 15 such pulses	6 Hg (0-85 s)	Not used	Not used
Break	0.2 psi (0-20 s)	6 Hg (0-5 s) 10 Hg (5-15 s) 6 Hg (15-20 s)	Not used	Not used
Data Acquisition	0.16 psi (Duration of experiment)	6 Hg (Duration of experiment)	Not used	6 psi

C

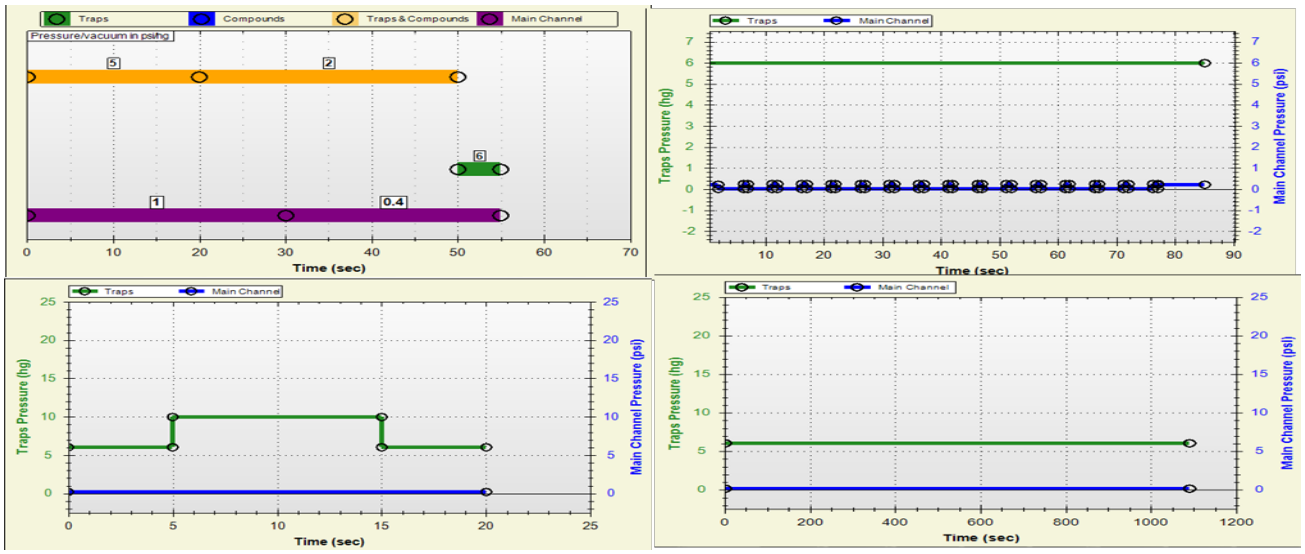

Figure 3.S3. A shows the order and relative durations of the 4 phases in the experiment. B summarizes the pressure settings at the different phases. C is a graphic representation of the pressure settings.

HeLa cells were cultured in 175 cm^2 flasks in complete media at 37 °C and 5% CO_2. The cells were cultured to ~90% confluency (~20-25 million cells). The cells were washed with 10 mL of PBS without Ca^{2+} and Mg^{2+} and suspended by treatment with

5 mL Detachin at 37 °C for 5 minutes. 5 mL of complete media was added and the cells were triturated. The suspension was centrifuged at 1000 rpm for 2 minutes (220 x g) and the supernatant was discarded. The cells were suspended in SFMII supplemented with 25 mM HEPES and penicillin-streptomycin, placed in a 25 cm^2 suspension flask and shaken at 75 rpm for 5 minutes. Employing SFMII as opposed to the regular SFM resulted in a roughly three-fold increase in cell count and was critical for achieving improved seal resistance in each trapping zone. The cells were triturated and counted using a cytometer. The suspension was centrifuged at 1000 rpm for 2 minutes. The cells were suspended in ECS to a concentration of 8 to 12 million cells/mL and loaded in the IonFlux-16™ 96 well microfluidic plate. Polyplexes at N:P ratio of 10:1 were prepared in the same manner and concentrations as prepared for the flow cytometry studies describe above. 50 µL of Polyplexes were added to 450 µL of SFM.

The current vs time trace files were exported and processed using Microsoft Excel and MATLAB. In all cases, initial current magnitudes less than -15 nA were required to indicate patching of sufficient quality for each ensemble of 20 cells. Data for ensembles with starting currents above -15 nA were not included in the analysis. The time averages of current from 4s prior to exposure (60 - 64 s from the beginning) was compared with the time averaged current 600-604 s (665 -669 s from the beginning) following exposure to polymers/polyplexes suspended in SFM. One way analysis of variance (ANOVA) followed by Tukey's multicomparison test was performed to determine the statistical significance of the difference in current changes across different treatments.

3.3.4 RFP Expression vs. MB Fluorescence

Polyplex preparation: Each polymer was diluted in sterile water to obtain an N:P ratio of 10:1. Dilutions of RFP plasmid (0.5 μg) and MB (0.5 μg) were prepared and mixed to obtain a final N:P ratio of 10:1 in the polyplex. The polymer dilutions (25 μL) were added to equal volumes of DNA mixture (25 μL) and incubated at room temperature for 25 min before transfection. Transfection: Hela cells at 200,000 cells/well in 1 mL of complete media were incubated overnight in 24-well plates for flow cytometry. The cells were transfected with jetPEI™, G5 PAMAM, B-PEI, or L-PEI polyplexes and incubated at 37^{o} C in 450 μL of SFM. After 3 h, transfection media was removed and 500 μL of fresh complete media was added to each of them and incubated at 37^{o}C. Flow Cytometry: After 33 h (36 h post-transfection) cells were rinsed with PBS without Ca^{2+} and Mg^{2+}, trypsinized, and suspended in 1.8 mL of PBS with Ca^{2+} and Mg^{2+} and centrifuged at 2000 rpm for 5 min. The supernatant was removed and the pellet was re-suspended in 400 μL of PBS without Ca^{2+} and Mg^{2+} and kept on ice and analyzed using an EPICS XL-MCL Beckman Coulter flow cytometer.

3.3.5 DNA Uptake vs. MB Fluorescence

Polyplex preparation: Each polymer was diluted in sterile water to obtain an N:P ratio of 10:1. Dilutions of Rhodamine labeled blank plasmid (0.5 μg) and MB (0.5 μg) were prepared and mixed to obtain a final N:P ratio of 10:1 in the polyplex. The polymer dilutions (25 μL) were added to equal volumes of DNA mixture (25 μL) and incubated at room temperature for 25 min before transfection. Transfection: Hela cells at 200,000 cells/well in 1 mL of complete media were incubated overnight in

24-well plates for flow cytometry. The cells were transfected with jetPEI™, G5 PAMAM, B-PEI, or L-PEI polyplexes and incubated at 37° C in 450 µL of SFM. After 3 h, transfecting media was removed and 500 µL of fresh complete media was added to each of them and incubated at 37°C. Flow Cytometry: After 9 h (12 h post transfection) cells were rinsed with PBS without Ca^{2+} and Mg^{2+}, trypsinized, and suspended in 1.8 mL of PBS with Ca^{2+} and Mg^{2+} and centrifuged at 2000 rpm for 5 min. The supernatant was removed and the cell pellet was resuspended in 400 µL of PBS without Ca^{2+} and Mg^{2+} and analyzed by flow cytometry. For each sample two replicates were used and fluorescence from 10,000 cells was measured form each replicate.

3.3.6 DNA Protection Assay

The experiment was carried out in 96-well plates. 0.08 µg of MB was added to specific wells with and without jetPEI™, G5 PAMAM, B-PEI, or L-PEI polymers. For polyplex containing samples an N:P ratio of 10:1 was maintained. 5 units of S1 nuclease were used and experiment was done in 100 µL of 1X S1 nuclease buffer. The plate was read at excitation of 485/20 nm and emission of 528/20 nm, the plate reader was kept at 37 °C for the experiment.

3.3.7 Cellular Localization of MB Fluorescence

Polyplex preparation: B-PEI, G5 PAMAM, jetPEI™ and L-PEI polymer were diluted in sterile water to obtain an N:P ratio of 10:1. Dilutions of Rhodamine labeled plasmid (0.5 ug) and MB (0.5 ug) was prepared and mixed to obtain a final N:P ratio of 10:1 in the polyplex. The polymer dilution (25 uL) was then added to equal volumes of

DNA mixture (25 uL) and incubated at room temperature for 25 min before transfection. Transfection: Hela cells at 100,000 cells/well in 1 mL of complete media were incubated overnight in 2-well coverglass chambers for confocal microscopy. The cells were transfected with jetPEI™, G5 PAMAM, B-PEI, or L-PEI polyplexes respectively and incubated at 37° C in 950 uL of SFM. After 3 h, transfecting media was removed and 1 mL of fresh complete media was added to each of them and incubated at 37°C. After 9 h (12 h post-transfection) cells were rinsed with PBS with Ca^{2+} and Mg^{2+}. 2% paraformaldehyde was then used to fix cells for 15 minutes at room temperature. Cells were then given another rinse with PBS with Ca^{2+} and Mg^{2+} and were treated with Prolong gold™ to reduce photobleaching and with DAPI (4',6-diamidino-2-phenylindole) to stain the cell nucleus.

3.3.8 DNA Gel Electrophoresis

A 6-well plate was plated with HeLa cells (ATCC CCL-2) at a count of 500,000 cells/well and incubated overnight at 37 °C. The cells were transfected with polyplexes formed at an N:P ratio of 10:1 between G5 PAMAM and 2 μg of salmon sperm DNA in SFM. The cells were trypsinized and the cytosol was extracted by treating with NP:40 lysis buffer (with protease inhibitors) and incubating on ice for 30 minutes. Using this protocol, complete cell lysis occurs in less than 1 minute (data not shown). The protein concentration of the extract was then measured. Luciferase plasmid DNA was mixed with the extract for 30 minutes at 37 °C and run on 0.9 % agarose gel. Lane 2 contains 0.2 μg of cytosolic protein (from cells only control) and 0.2 μg plasmid DNA. Lane 3 contains 0.2 μg of cytosolic protein from G5

PAMAM polyplex treated cells and 0.2 μg plasmid DNA. Lanes 4 and 5 contain 0.2 units of S1 nuclease and 0.2 μg of plasmid DNA, with S1 nuclease reaction buffer and water as solvent, respectively.

3.4 Results and Discussion

Polyplexes formed using all four polymer vectors at an N:P ratio of 10:1 were exposed to HeLa cells in SFM containing PI. In all cases, cell plasma membrane permeability was measured using PI diffusion into the cell (Figure 3.1, y-axis and Table 3.1). The G5 PAMAM polyplexes and jetPEI™ gave the largest mean fluorescence shifts (Δ MF = 145 (±5) and 131 (±13) respectively) whereas B-PEI and L-PEI showed the least permeability with Δ MF of 71 (±29) and 37 (±3), respectively (Δ MF is calculated by subtracting the Log mean fluorescence value of the control cells from sample cells). Treatment with the four polyplexes yielded significantly different results in terms of the total amount of MB fluorescence obtained with B-PEI and G5 PAMAM polyplexes, Δ MF of 21 (±3) and 15 (±2) respectively, and no shift in Δ MF measured after treatment with jetPEI™ and L-PEI polyplexes (Figure 3.1, x-axis and Table 3.1). When compared at a cell-by-cell level, the behavior of the four polyplexes also differed. For G5 PAMAM and B-PEI most of the cells exhibiting porosity also showed MB fluorescence. jetPEI™ and L-PEI were remarkable for showing 1-2 log shifts in PI intensity for 93% and 46% of cells, respectively, without much evidence of nuclease activation. To ensure that cleavage of MB, which gives rise to fluorescence, is due to nuclease activity and not simply due to changes in pH associated with endosome/lysosome localization, the stability

of MB was tested under a range of pH (supplementary material Figure 3.S2), which shows that the MB is stable at physiological pH values including those associated with lysosomes.

B-PEI polyplex treated cells

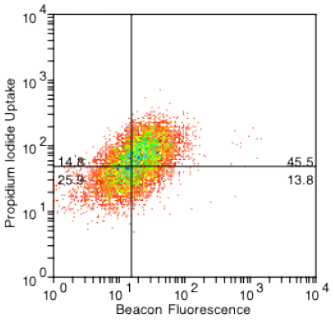

G5 PAMAM polyplex treated cells

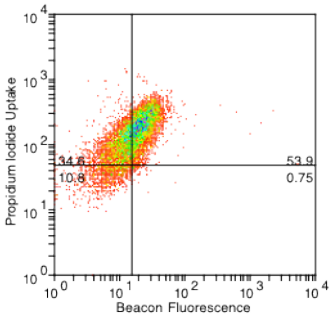

jetPEI™ polyplex treated cells

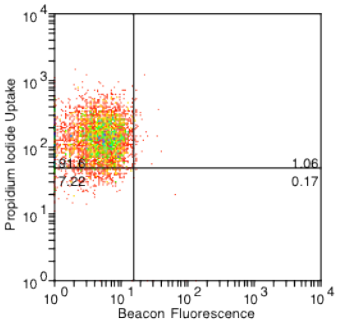

L-PEI polyplex treated cells

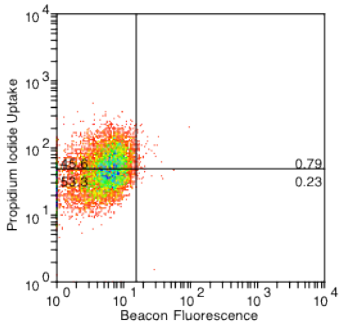

Cells only

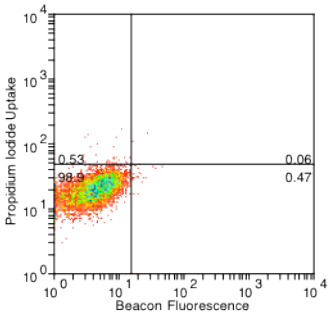

Figure 3.1. Two-color flow cytometry of PI uptake (y-axis) vs MB fluorescence (x-axis) in HeLa cells after 3 h polyplex exposure followed by 9 h incubation. PI uptake is used to indicate cell plasma membrane permeability and MB fluorescence is used to indicate cytosolic nuclease activity.

Table 3.1. Δ MF and standard error for PI uptake and MB fluorescence for samples in Figure 3.1.

Polyplex	PI uptake		MB fluorescence	
	Δ MF (average)	Standard error	Δ MF (average)	Standard error
jetPEI™	131.4	13.3	0.5	0.4
B-PEI	70.8	29.3	21.4	3.4
G5 PAMAM	144.6	5.2	15.3	1.9
L-PEI	37.0	3.4	1.0	0.4

In order to further explore the impact of polyplexes on cell membrane permeability, we then employed whole-cell patch clamp.[28] This allowed us to evaluate the impact of these oligonucleotide delivery materials on the diffusion of small inorganic ions through the cell plasma membrane, as opposed to small organic molecules, as represented by PI (MW = 668). For these experiments, we monitored the change in permeability over the initial ten minutes of polyplex exposure. As a positive control, we first measured the porosity of the cell membrane caused by the polymer vectors alone (Figure 3.2) and obtained data consistent with our previous whole-cell patch clamp studies performed using a traditional glass electrode probing a single cell.[25] All the polymers induced membrane permeability with jetPEI™ and L-PEI inducing the most permeability. We then examined the impact of the polyplexes on cell membrane permeability. As illustrated in Figure 3.2, jetPEI-based polyplexes in SFM generate the largest trans-membrane ion currents, whereas B-PEI, G5 PAMAM, and L-PEI polyplexes do not generate currents that differ significantly from the control cells. The polyplexes generate a solution with less charge density than the polymer vectors alone, since the net positive charge is reduced by the addition of DNA. This is consistent with the reduced ability of

polyplexes to induce membrane permeability when compared to polymers alone. The change in current due to jetPEI™ polyplexes is significantly different from the controls as determined by one-way ANOVA ($P = < 0.001$) followed by Tukey's multiple comparison test ($\alpha = 95\%$). The positive change in currents for cells treated with B-PEI and L-PEI polyplexes are not statistically different from the control. It represents a small improvement in the seal of the cells at the trapping site. This gradual improvement in the seal resistance is observed for all the different treatments. This phenomenon is masked when permeability induced by polymers and polyplexes is high enough. These whole-cell patch clamp experiments were performed in SFM to most closely match the PI-based measure of plasma membrane permeability as well as the expression and uptake experiments. We also examined the impact of the polyplexes on cell membrane using the more traditional patch clamp medium of an extracellular solution (ECS) consisting of 138 mM NaCl, 4 mM KCl, 1.8 mM $CaCl_2$, 1 mM $MgCl_2$, 10 mM HEPES, and 5.6 mM glucose adjusted to pH 7.45 using NaOH (supplementary material Figure 3.S4). In this case, a significant amount of cell plasma membrane permeability is observed for all polyplexes. The SFM primarily differs from ECS in containing up to 2 mM concentrations of amino acids, with the negatively charged L-glutamine being particularly notable, and 0.002 to 0.01 mM concentration of vitamins.

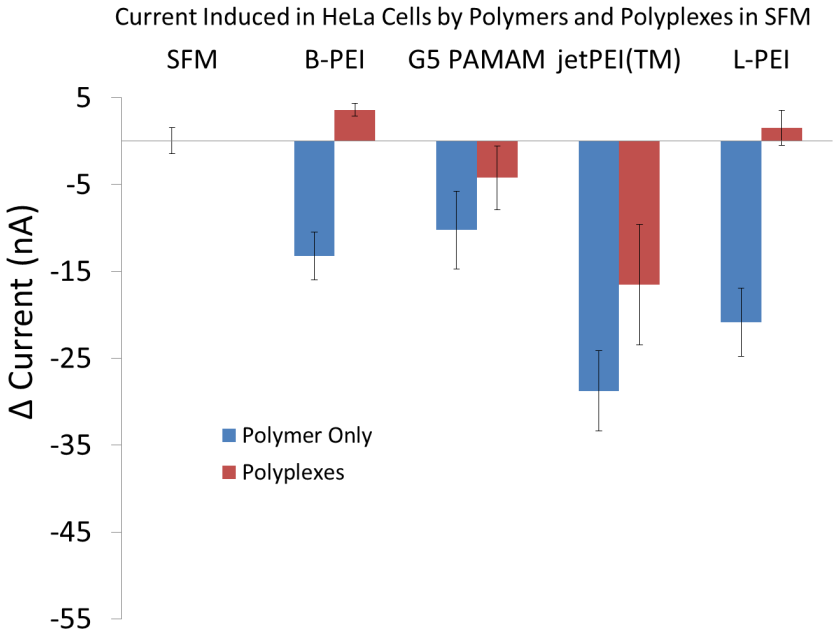

Figure 3.2. Cell plasma membrane currents induced by exposure of HeLa cells to SFM solutions of jetPEI, B-PEI, G5 PAMAM, and L-PEI polymers and polymer/DNA polyplexes. Only the jetPEI polymer and polyplex exhibits evidence for membrane porosity that is significantly different from SFM only controls.

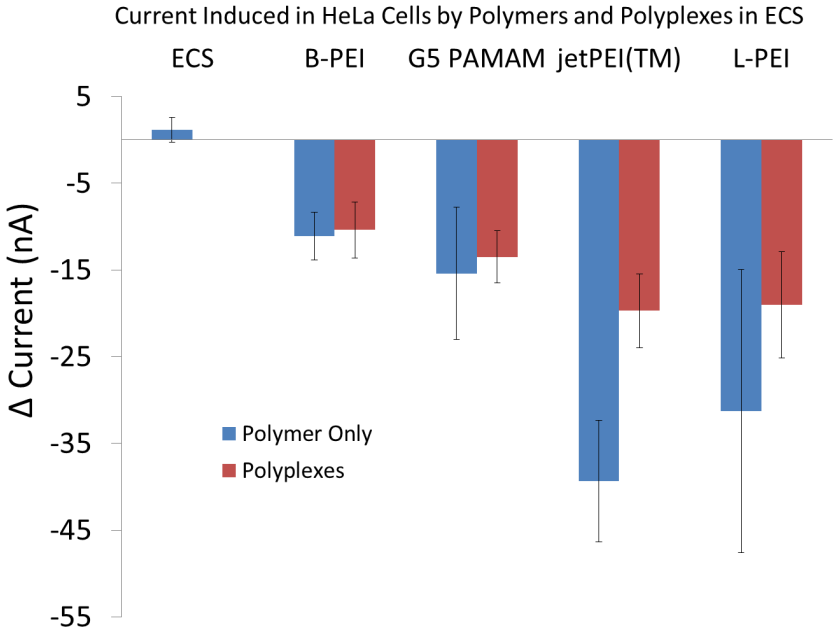

Figure 3.S4. Cell membrane permeability induced by polyplex exposure in ECS.

The relationship between MB fluorescence and protein expression was compared by forming polyplexes at an N:P ratio of 10:1 that contained the MB DNA and RFP-

encoding pDNA in a 1:1 w/w ratio (Figure 3.3 and Table 3.2). Again, G5 PAMAM polyplexes yielded the greatest Δ MF for MB of 49 (±1) whereas B-PEI, jetPEI™, and L-PEI exhibited shifts of 27 (±3), 28 (±3), and 6 (±1), respectively

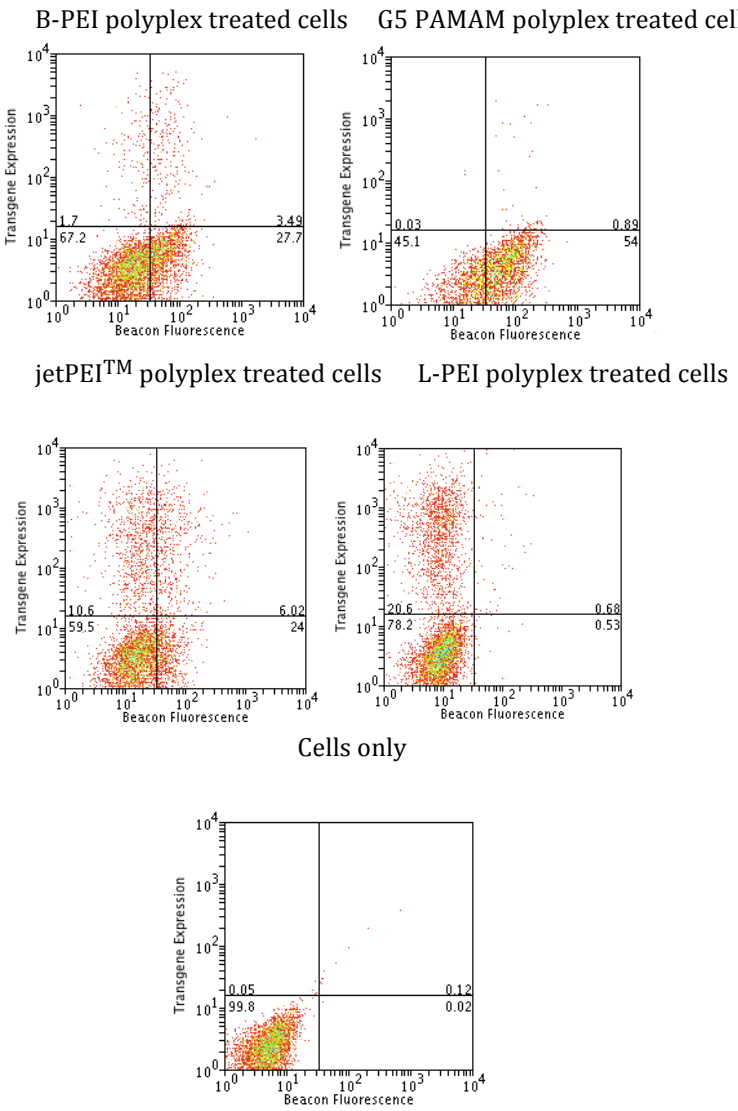

Figure 3.3. Two-color flow cytometry of RFP expression (y-axis) vs MB fluorescence (x-axis) in HeLa cells after 3 h polyplex exposure followed by 33 h incubation. RFP expression is used as the marker of transfected pDNA expression and MB fluorescence is used to indicate cytosolic nuclease activity.

Table 3.2. Δ MF and standard error for MB fluorescence for samples in Figure 3.3.

Polyplex	Expression		MB fluorescence	
	% cells (average)	% Standard error	Δ MF (average)	Standard error
jetPEI	17.2	0.8	28.1	3.0
B-PEI	5.1	0.1	26.7	2.8
G5 PAMAM	0.9	0.1	49.4	1.0
L-PEI	21.2	0.1	5.8	1.0

The change in cellular fluorescence related to RFP expression was qualitatively different than that observed for MB fluorescence or PI uptake. For both MB and PI fluorescence, the entire cell population shifted in response by up to one order in magnitude. By way of contrast, the RFP expression varied by up to three orders of magnitude in fluorescence intensity and was caused by individual cells showing significantly larger signal while the majority of the population exhibited no shift. The G5 PAMAM polyplexes induced RFP fluorescence in less than 1% of the cell population and B-PEI polyplexes showed expression in 5.1% of the population. RFP expression was observed in 17.2% of cells for jetPEI™ with most of this expression occurring in cells exhibiting a small Δ MF for MB fluorescence. The greatest amount of expression was observed for L-PEI, 21.2% of the population, with essentially no Δ MF for MB fluorescence observed. To summarize the results from Figures 3.1 – 3.3, all of the polyplexes cause substantial membrane permeability as measured by PI uptake; however for jetPEI™ and L-PEI, this permeability did not cause an increase in MB fluorescence. Only jetPEI™ polyplexes showed enhanced ion permeability according to whole-cell patch clamp studies. Generally, the L-PEI polyplex-exposed cells that express RFP do not show MB fluorescence and

increasing amounts of MB fluorescence for jetPEI™, B-PEI, and G5 PAMAM correspond to decreased amounts of protein expression.

This data raises a number of interesting questions and the need for related control experiments: 1) Is the large difference in MB fluorescence related to a difference in nuclease activity, or is it actually controlled by a substantial difference in uptake of polyplexes as a function of polymer vector? 2) Is the large difference in MB fluorescence observed accounted for by L-PEI and jetPEI™ providing better protection of the MB DNA? 3) Is the MB fluorescence associated with "intact" polyplexes or with only with degraded DNA that is no longer associated with polyplexes? 4) Finally, if nucleases are involved, what are possible identities of these nucleases?

In order to test any impact of differential DNA uptake on our results we generated 10:1 N:P ratio polyplexes containing a 1:1 w/w ratio of MB DNA and rhodamine-labeled DNA (Figure 3.4 and Table 3.3). The cells were exposed to the polyplexes for 3 h, rinsed, and incubated for an additional 9 h. Similar to the PI and MB fluorescence data, the fluorescence due to DNA uptake also results in an overall population shift with a Δ MF of 1092 (±63), 1277 (±59), 622 (±9), and 1268 (±65) for B-PEI, G5 PAMAM, jetPEI™ and L-PEI, respectively. All four vectors are highly effective at transfection and the differences in MB fluorescence vs plasma membrane porosity and MB fluorescence vs RFP expression are not a function of differential polyplex uptake. The G5 PAMAM polyplex treated cells again exhibited the greatest amount of MB fluorescence, consistent with porosity and expression

studies, with the overall trend remaining for MB ΔMF of G5 PAMAM > B-PEI ~ jetPEI™ > L-PEI.

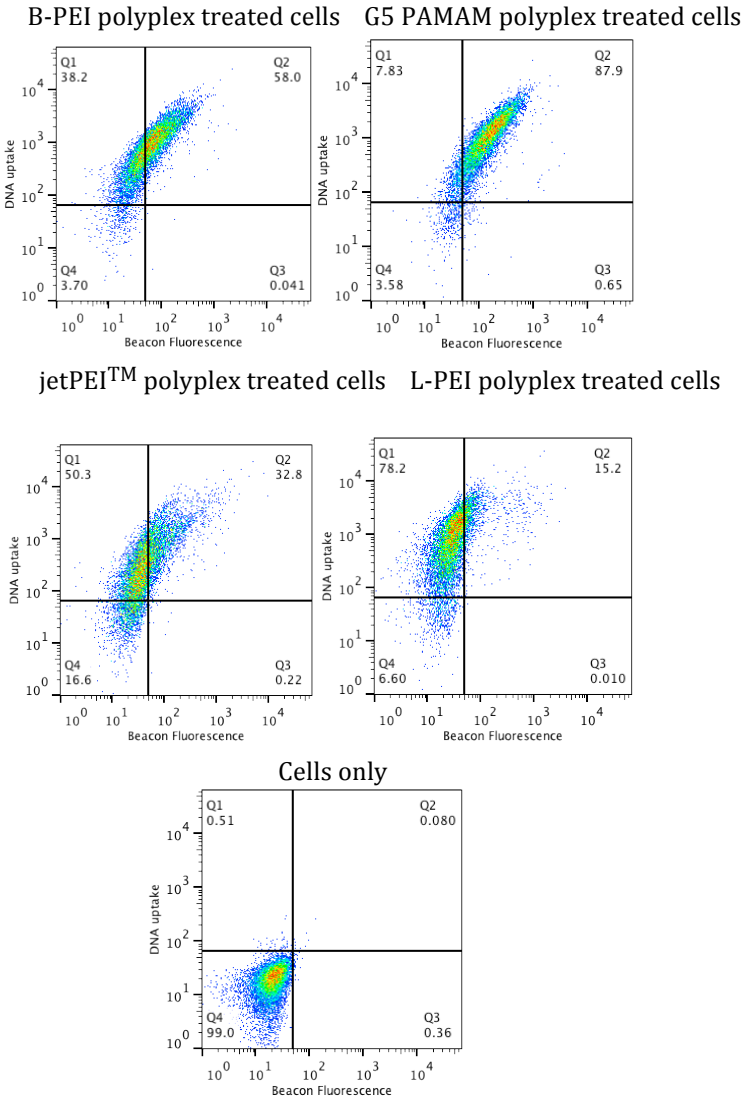

Figure 3.4. Two-color flow cytometry of DNA uptake (y-axis) vs MB fluorescence (x-axis) in HeLa cells after 3 h polyplex exposure followed by 9 h incubation. DNA uptake is measured using a rhodamine labeled DNA plasmid and MB fluorescence is used to indicate cytosolic nuclease activity.

Table 3.3. Δ MF and standard error for DNA uptake for samples in Figure 3.4.

Polyplex	DNA uptake		MB fluorescence	
	Δ MF (average)	Standard error	Δ MF (average)	Standard error
jetPEI	621.6	9.3	43.7	6.5
B-PEI	1091.6	63.0	57.5	6.2
G5 PAMAM	1276.6	58.8	144.5	7.8
L-PEI	1268.1	65.1	21.8	2.5

Having ruled out differential uptake as a mechanism, the significant differences in MB fluorescence observed in Figures 3.1 and 3.3 could be the result of differential nuclease activity in the cells or the result of differential DNA protection offered by the polymers. Indeed, the hypothesis of providing improved DNA protection has often been a goal of synthetic polymer vector design to improve transfection and expression activity.[11, 16, 29] To test if the polymers protected the DNA to different extents, we exposed 10:1 N:P polyplexes to cytosolic extract containing nuclease and to S1 nuclease (*vida infra* for the selection of nuclease). Our controls (Figures 3.5 and 3.S7c) indicate that the MB is stable to the process of polyplex formation and the overall conditions of the nuclease experiment. Cytosolic and S1 nuclease cleavage of the MB with no polymer protection, Figures 3.5 and 3.S5a, indicate the total amount of fluorescence signal that is possible for each experiment.

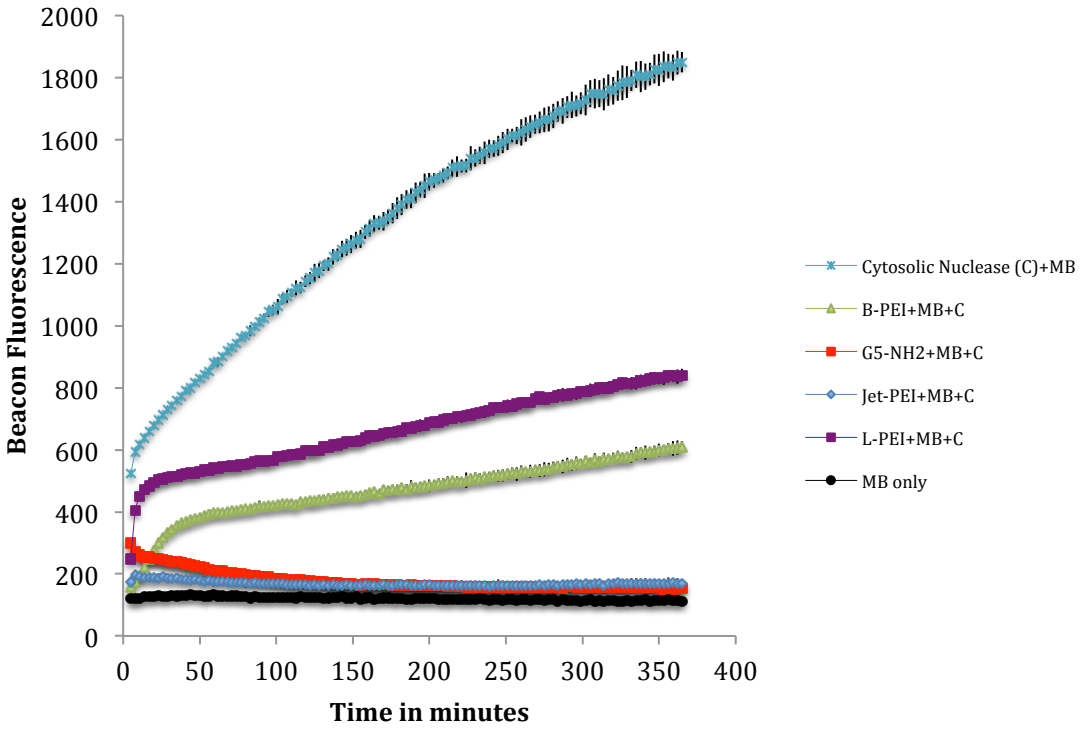

Figure 3.5. Fluorescence of MB after complexing as a 10:1 N:P polyplex with B-PEI, G5 PAMAM, jetPEI™ or L-PEI followed by cytosolic nuclease treatment (5 µg of cytosolic extract). Fluoresence of MB treated with cytosolic nuclease and MB only in water included as controls.

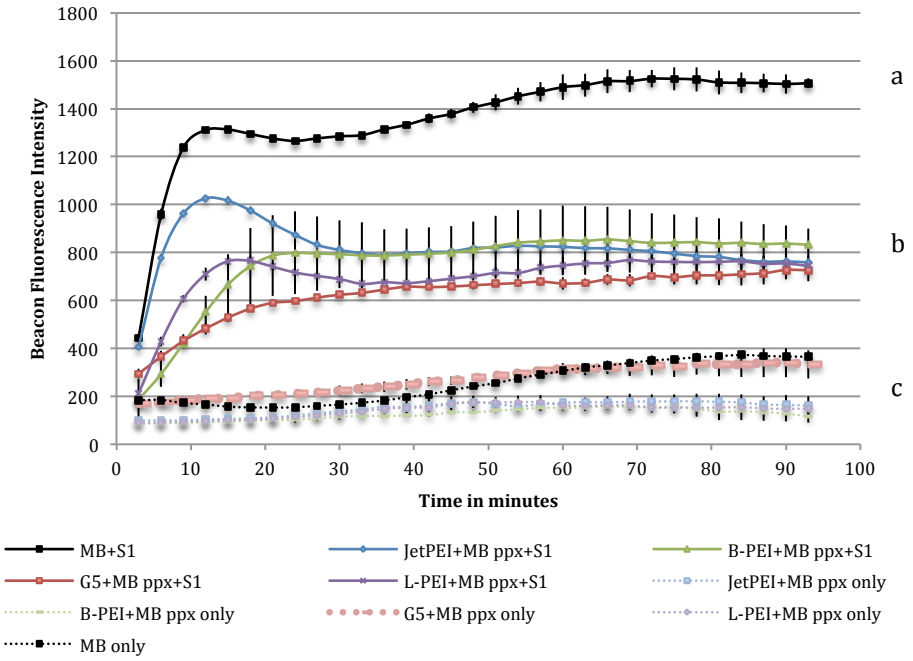

Figure 3.S5: Fluorescence of MB a) after treatment with S1 nuclease b) after complexing as a 10:1 N:P polyplex with L-PEI, B-PEI, G5 PAMAM, or jetPEI™ followed by S1 nuclease treatment c) controls of MB and polyplex with no S1 nuclease added.

For the experiment where the beacon polyplex was exposed to S1 nuclease, all four polymers provide similar protection to the DNA, with jetPEI™ being slightly less protective for the first 20 minutes of the assay (Figure 3.S5b), The inhibition of fluorescence observed between 20 and 40 minutes for the L-PEI and jetPEI™ experiments is consistent with a reduction in fluorescence observed when MB is first cleaved with S1 and then polymer added (data not shown). This type of kinetic behavior is consistent with our recent observations that polyplexes are dynamic species with the pDNA and polymer components in rapid equilibrium that includes the presence of free pDNA.[30]

For the experiment where the beacon polyplex was exposed to cytoplasm containing cytosolic nuclease, we observed a significant difference in protection of the MB as a function of polymer employed. In particular, jetPEI™ and G5 PAMAM provide essentially complete protection as indicated by no increase in fluorescence above the control; however, both L-PEI and B-PEI show a substantial increase in fluorescence consistent with roughly 25-50% of the beacon being cleaved. One limiting case for explaining this data is that nucleases are present inside the cell to which the polyplexes offer differential protection as a function of polymer employed. Another limiting case is that other components are present (ie proteins and/or lipids) that interact with the polyplexes as a function of polymer employed to give differing amounts of MB release. Some combination of these limiting cases is also possible. The second hypothesis of differential release is intriguing with respect to our previous observation of polyplex equilibrium.[30]

To summarize our tests of nuclease activity, the results illustrated in Figure 3.S5 indicate that the four polymers provide a similar level of S1 nuclease protection; however, exposure to cytoplasm containing nucleases shows a significant difference in the level of MB protection (Figure 3.5). In particular, G5 PAMAM and jetPEI™ exhibit no MB degradation whereas B-PEI and L-PEI exhibit substantial fluorescence resulting from MB cleavage. Interestingly, the fluorescence intensity trend observed for this solution based, cell-free test of cytosolic nucleases is L-PEI> B-PEI >> G5 PAMAM ~ jetPEI™, which is significantly different from the ΔMF observed for the in-cell experiments of G5 PAMAM > B-PEI ~ jetPEI™ > L-PEI. The difference in both the S1 nuclease (Figure 3.S7) and the cytosolic nuclease (Figure 3.5) trends with the

consistent trends in MB activity seen in Figures 3.1, 3.3, and 3.4 suggest that neither of these nuclease controls is able to fully capture the in-cell activity. Neither experiment supports the simple hypothesis that the MB fluorescence observed in the flow cytometry studies is due to differential DNA protection facilitated by polymers. We note that one the polymers providing the best protection in Figure 3.5 (G5 PAMAM) provides the least in the flow cytometry studies (Figures 3.1, 3.3, 3.4) and the polymer providing the worst protection in Figure 3.5 (L-PEI) routinely provides the best protection in the flow cytometry studies.

The view of the polyplex as a dynamic and rapid equilibrium between pDNA and polymer[30] raises the question of cellular distribution of the fluorescence as measured by flow cytometry in Figures 3.1, 3.3, and 3.4. Specifically, does the fluorescence arise from polyplexes distributed in a the punctate fashion commonly observed for polymer vectors[31, 32] or from a more diffuse signal from short, dispersed oligonucleotide fragments? Confocal fluorescence microscopy of HeLa cells exposed to polyplexes consisting of MB and B-PEI, G5 PAMAM, jetPEI™, or L-PEI in a 10:1 N:P ratio for 3 h followed by another 9 h incubation indicates a typical punctate transfection pattern for the internalized materials (Figure 3.6). The MB fluorescence appears to remain associated with the polymer and polyplexes, consistent with the decrease in fluorescence exhibited in Figure 3.5. For the B-PEI and G5 PAMAM polyplexes most of the fluorescence observed is green, consistent with the presence of cleaved MB. For the jetPEI™ and L-PEI polyplexes, most of fluorescence observed is red, consistent with the presence of intact MB. These differences in MB cleavage are consistent with those observed by the flow

cytometry experiments (Figures 3.1, 3.3, and 3.4) for L-PEI and G5 PAMAM and suggest an interesting difference for the similar Δ MF shifts seen for B-PEI and jetPEI™.

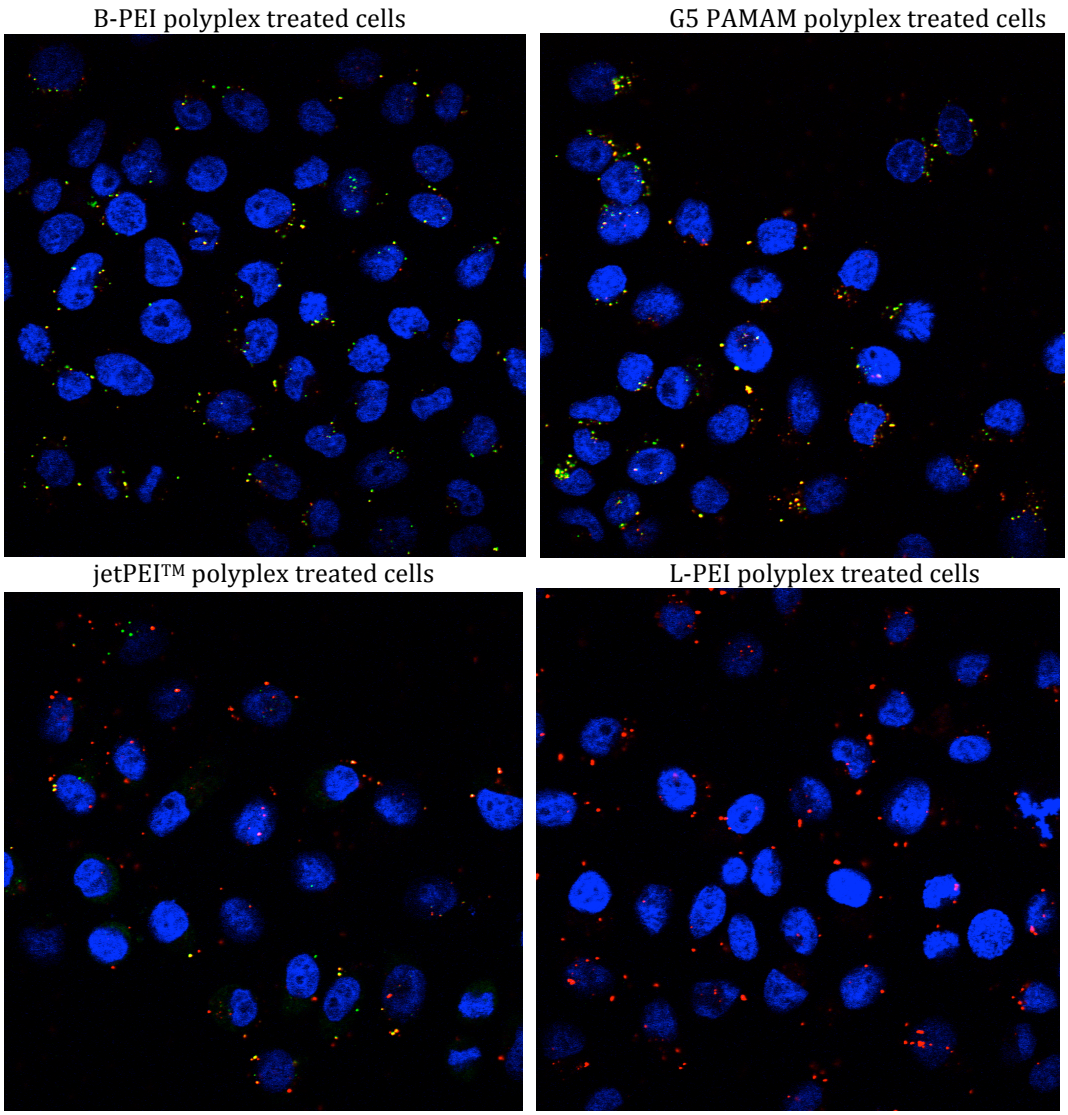

Figure 3.6. Confocal fluorescence microscopy of HeLa cells exposed to polyplexes consisting of MB (to measure nuclease activity), Rhodamine-labeled plasmid (to measure DNA uptake) and polymer in a 10:1 N:P ratio for 3 h followed by another 9 h incubation. Nuclease cleaved MB is shown in green, DNA uptake shown in red and DAPI-stained cell nuclei are shown in blue.

The identity and origin of the nuclease(s) responsible for the degradation of the MB polyplexes is of great interest. The seminal studies by Lukacs et al. suggest that the nucleases are not part of the apoptotic cascade (i.e., not DNAse I, DNAse II, caspase-3, etc.) and support the notion that they are constitutively present in the cytosol.[11] Pollard et al. also noted degradation in the cytosol and reported a Ca^{2+} dependency.[16] Ribeiro et al. have shown how supercoiled plasmid DNA can be degraded by S1 nuclease to yield open-circle and linear topology of the plasmid.[20] By using gel electrophoresis it was also shown that this degradation pattern is consistent with cytosolic nucleases found in CHO cells.

In order to explore the origin of the nuclease in the HeLa cells employed in this study, we exposed HeLa cells to polyplexes generated from G5 PAMAM dendrimer and salmon sperm DNA. G5 PAMAM dendrimer was chosen for this experiment as we have seen it causes maximum MB fluorescence in the cell studies discussed above. Salmon sperm DNA was employed for these polyplexes so that we would not introduce pDNA into the cytoplasm at this step. After 3 h, the cytoplasm from these treated cells was extracted and then incubated with the luciferase plasmid for 45 minutes at 37 °C. The mixture was then run on a 0.9 % agarose gel. Luciferase plasmid was also treated with S1 nuclease in S1 nuclease buffer and in molecular grade water. As illustrated in Figure 3.7, the degradation pattern for the cytoplasm-treated plasmid is identical within the resolution of the gel to that obtained for S1 nuclease. We have also shown that simply treating the luciferase plasmid with the isolated cytoplasm yields the same result. Given the wholesale disruption of the cell in the process used to isolate the cytoplasm, we are unable to separate out the effect

of the polyplex treatment and the cytosol isolation protocol. The experiments also indicate that the nuclease must be constitutively present in the cytosol, as previously proposed by Lukacs,[11] as the cytoplasm isolation protocol lyses the cells in under 1 minute.

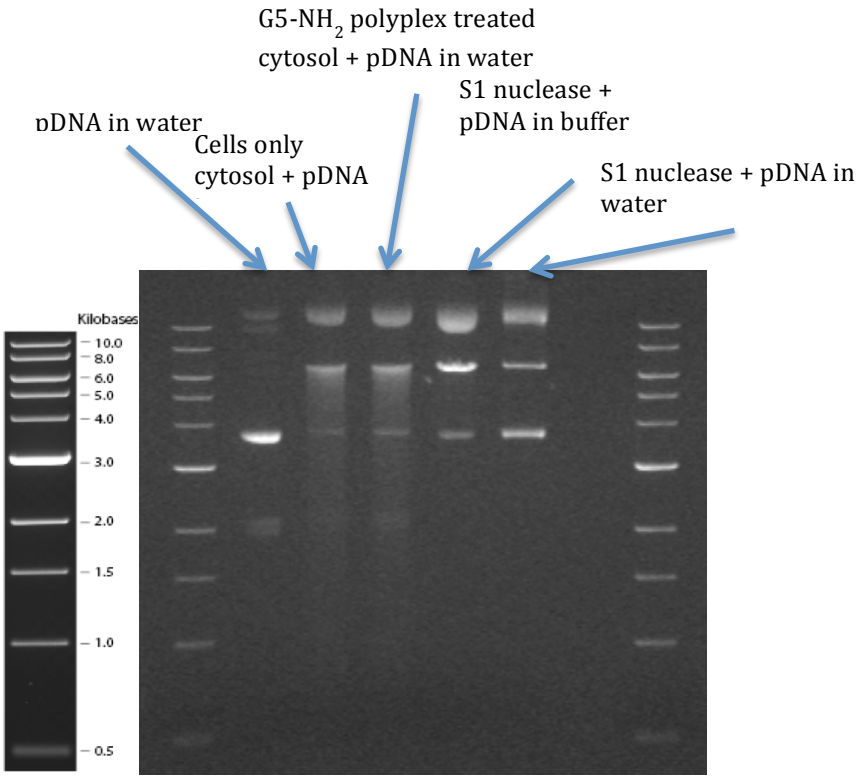

Figure 3.7. Agarose gel electrophoresis showing DNA cleavage pattern of HeLa cytoplasm treated pDNA and S1 nuclease treated pDNA.

Both PI uptake and whole-cell patch clamp measure membrane permeability induced by polyplexes. Whole-cell patch clamp measures the movement of ions across the membrane and thus is sensitive to smaller membrane perturbations than PI. Under the conditions employed in this study, all four polyplexes caused substantial cell plasma permeability as indicated by PI uptake (Figure 3.1). Surprisingly, only JetPEI™ polyplexes exhibited substantial cell permeability as measured by whole-cell patch clamp (Figure 3.2); however, both techniques

indicate that jetPEI™ polyplexes induce the most permeability. There are three major differences between whole-cell patch clamp experiment and PI uptake measured by flow cytometry. First, the whole-cell patch experiment is performed under flow conditions whereas the PI uptake experiment is in quiescent wells. Second, the time frame for the whole-cell patch experiment was 10 minutes whereas the flow cytometry was performed after 9 h exposure. It is possible that polyplexes made using G5 PAMAM, B-PEI and L-PEI induce permeability at time points greater than 10 minutes. Third, the patch clamp experiment measures ion conductance across the cell membrane whereas the flow cytometry experiment examines PI crossing the membrane. Regardless, neither assay demonstrates a relationship between polyplex-induced cell membrane permeability (JetPEI™ ~ G5 PAMAM> B-PEI > L-PEI for PI; JetPEI™ >> G5 PAMAM ~ B-PEI ~ L-PEI for whole-cell patch clamp) with DNA uptake (Figure 3.4) or expression efficiency (Figure 3.3). Overall, materials exhibiting the least amount of in-cell MB fluorescence (L-PEI < jetPEI™ ~ B-PEI < G5 PAMAM) showed the greatest amount of RFP expression. Interestingly, B-PEI and jetPEI™ show the same amount of MB fluorescence at 36 h, and thus apparently similar levels of nuclease activation, yet jetPEI™ gives overall 4x greater RFP expression. Since jetPEI™ is a proprietary form of linear PEI with undisclosed components, we cannot comment further on this difference; however, L-PEI containing no additives shows very little MB fluorescence and also gives the highest expression efficiency.

3.5 Conclusions

The low transgene expression facilitated by polymer gene delivery systems presents a substantial challenge for their use in genetic engineering. In this study we tested the hypothesis that cells respond to polymer-based vector systems by activating cytosolic nucleases that in turn decrease transgene expression. The results of our study indicate that cellular nuclease activity is activated differentially as a function of the polymer employed for polyplex formation. Enhanced levels of nuclease activation are related to lower levels of transgene expression.

3.6 References

1. Smedt, S.C.D., J. Demeester, and W.E. Hennink, *Cationic Polymer based gene delivery systems.* Pharmaceutical Research, 2000. **17**(2): p. 113-126.
2. Pack, D.W., et al., *Design and development of polymers for gene delivery.* Nature Review- Drug Discovery 2005. **4**: p. 581-593.
3. Mintzer, M.A. and E.E. Simanek, *Nonviral Vectors for Gene Delivery.* Chemical Reviews, 2009. **109**(2): p. 259-302.
4. Lechardeur, D., A.S. Verkman, and G.L. Lukacs, *Intracellular routing of plasmid DNA during non-viral gene transfer.* Advanced Drug Delivery Reviews, 2005. **57**(5): p. 755-767.
5. Al-Dosari , M.S. and X. Gao, *Nonviral Gene delivery: Principle, limitations and recent progress.* AAPS Journal, 2009. **11**(4): p. 671-681.
6. Davidson, B.L. and X.O. Breakefiled, *Viral vector for gene delivery to the nervous system.* Nature Review- Neuroscience, 2003. **4**(353-364).
7. Yu, B., et al., *Targeted Delivery Systems for Oligonucleotide Therapeutics.* AAPS Journal, 2009. **11**(1): p. 195-203.
8. Gao, K. and L. Huang, *Nonviral Methods for siRNA Delivery.* Molecular Pharmaceutics, 2009. **6**(3): p. 651-658.
9. Fernandez, C.A. and K.G. Rice. *Engineered Nanoscaled Polyplex Gene Delivery Systems*. in *NanoMedicine Summit on Nanoparticles for Imaging, Diagnosis, and Therapeutics*. 2008. Cleveland, OH.
10. Rangarajan, E.S. and V. Shankar, *Sugar non-specific endonucleases.* Fems Microbiology Reviews, 2001. **25**(5): p. 583-613.
11. Lechardeur, D., et al., *Metabolic instability of plasmid DNA in the cytosol: a potential barrier to gene transfer.* Gene Therapy, 1999. **6**(4): p. 482-497.
12. Ruponen, M., et al., *Intracellular DNA release and elimination correlate poorly with transgene expression after non-viral transfection.* Journal of Controlled Release, 2009. **136**(3): p. 226-231.

13. Shimizu, N., F. Kamezaki, and S. Shigematsu, *Tracking of microinjected DNA in live cells reveals the intracellular behavior and elimination of extrachromosomal genetic material.* Nucleic Acids Research, 2005. **33**(19): p. 6296-6307.
14. Walther, W., et al., *Use of the nuclease inhibitor aurintricarboxylic acid (ATA) for improved non-viral intratumoral in vivo gene transfer by jet-injection.* Journal of Gene Medicine, 2005. **7**(4): p. 477-485.
15. Pampinella, F., et al., *Analysis of differential lipofection efficiency in primary and established myoblasts.* Molecular Therapy, 2002. **5**(2): p. 161-169.
16. Pollard, H., et al., *Ca2+-sensitive cytosolic nucleases prevent efficient delivery to the nucleus of injected plasmids.* Journal of Gene Medicine, 2001. **3**(2): p. 153-164.
17. Ross, G.F., et al., *Enhanced reporter gene expression in cells transfected in the presence of DMI-2, an acid nuclease inhibitor.* Gene Therapy, 1998. **5**(9): p. 1244-1250.
18. Banerjee, S. and D.J. Spector, *Differential effect of DNA supercoiling on transription of adenovirus genes in in vitro.* Journal of General Virology, 1992. **73**: p. 2631-2638.
19. Azzoni, A.R., et al., *The impact of polyadenylation signals on plasmid nuclease-resistance and transgene expression.* Journal of Gene Medicine, 2007. **9**(5): p. 392-402.
20. Ribeiro, S.C., G.A. Monteiro, and D.M.F. Prazeres, *The role of polyadenytation signal secondary structures on the resistance of plasmid vectors to nucleases.* Journal of Gene Medicine, 2004. **6**(5): p. 565-573.
21. Li, J.J., R. Geyer, and W.H. Tan, *Using molecular beacons as a sensitive fluoresence assay for enzymatic cleavage of single-stranded DNA.* Nuclear Acids Research, 2000. **28**: p. e52.
22. Hong, S., et al., *The Interaction of Polyamidoamine (PAMAM) Dendrimers with Supported Lipid Bilayers and Cells: Hole Formation and the Relation to Transport.* Bioconjugate Chemistry, 2004. **15**: p. 774-782.
23. Hong, S., et al., *Interaction of polycationic polymers with supported lipid bilayers and cells: Nanoscale hole formation and enhanced membrane permeability.* Bioconjugate Chemistry, 2006. **17**(3): p. 728-734.
24. Leroueil, P.R., et al., *Nanoparticle interaction with biological membranes: Does nanotechnology present a Janus face?* Accounts of Chemical Research, 2007. **40**(5): p. 335-342.
25. Chen, J.M., et al., *Cationic Nanoparticles Induce Nanoscale Disruption in Living Cell Plasma Membranes.* Journal of Physical Chemistry B, 2009. **113**(32): p. 11179-11185.
26. Merdan, T., J. Kopecek, and T. Kissel, *Prospects for cationic polymers in gene and oligonucleotide therapy against cancer.* Advanced Drug Delivery Reviews, 2002. **54**(5): p. 715-758.
27. Yang, Z., et al., *Amphiphilic Block Copolymers Enhance Cellular Uptake and Nuclear Entry of Polyplex-Delivered DNA.* Bioconjugate Chemistry, 2008. **19**(10): p. 1987-1994.

28. Spencer, C.I., et al., *Ion Channel Pharmacology Under Flow: Automation Via Well-Plate Microfluidics.* Assay and Drug Development Technologies, 2012. **10**(4): p. 313-324.
29. Gebhart, C.L., et al., *Design and formulation of polyplexes based on pluronic-polyethyleneimine conjugates for gene transfer.* Bioconjugate Chemistry, 2002. **13**(5): p. 937-944.
30. Prevette, L.E., et al., *Intrinsic Dynamics of DNA-Polymer Complexes: A Mechanism of DNA Release.* Molecular Pharmaceutics, 2012. **9**: p. 2743-2749.
31. Hong, S., et al., *The Role of Ganglioside GM_1 in Cellular Internalization Mechanisms of Poly(amidoamine) Dendrimers.* Bioconjugate Chemistry, 2009. **20**: p. 1503-1513.
32. Qi, R., et al., *The Mechanism of Polyplex Internalization into Cells: Testing the GM1/Caveolin-1-Mediated Lipid Raft Mediated Endocytosis Pathway.* Molecular Pharmaceutics, 2010. **7**(267-279): p. 267-279.

Chapter 4

Quantification of Cytosolic Plasmid DNA Degradation Using High-Throughput Sequencing: Implications for Gene Delivery

4.1 Abstract

Although cytosolic DNA degradation plays an important role in decreasing transgene expression, their plasmid degradation pattern remains largely unexplored. Herein, we use Illumina dye sequencing to provide degradation site information for S1 and cytosolic nucleases. S1 nuclease provides a positive control for comparison between the agarose gel method and the sequencing approaches. In addition to identifying the plasmid bacterial origin of replication (*OriC*) as the highest probability cut region, consistent with agarose gel results, the sequencing approaches yielded information about previously unknown cut sites. The poly(A) region between the β–lactamase gene and the CMV promoter was identified as most likely cut site for plasmid treated with cytosol from polyplex-treated cells. The second most likely site, at the 5' end of the β–lactamase gene, was identified by gel electrophoresis and by sequencing. Additional sites were detected in the *OriC* regio*n*, the SV40/poly(A) region, the luciferase gene, and the CMV promoter. Sequence analysis of plasmid treated with cytosolic nucleases from control cells

showed the greatest cut activity in the *OriC* region, the β–lactamase gene, and the poly(A) region following the luciferase gene. Additional regions of cut activity include the SV40 promoter and the β–lactamase poly(A) termination sequence. Both cytosolic nucleases and the S1 nuclease showed substantial activity at *OriC*. This analysis reveals regions of the luciferase plasmid DNA (pDNA) sequence that are important for effective transgene expression and sensitive to degradation. This provides new targets for improving plasmid and/or polymer design to optimize the likelihood of protein expression.

4.2 Introduction

Delivery of oligonucleotides, including antisense DNA (asDNA) and silencing RNA (siRNA), and plasmid DNA (pDNA) is a promising strategy in the field of medicine with possible applications including diagnosis, vaccines and disease management.[1] The big range of applications and potential impact on common, life threatening diseases like diabetes mellitus and metastatic neoplasm,[1] led to a predicted pharmaceutical industry of $16.8 billion/year by 2020-2025;[2] however, almost 15 years after this prediction gene therapy is only a small fraction of this multi-billion dollar market projection. This lack of market availability and penetration arises primarily because of safety and efficiency issues for current nucleic acid delivery systems.[3, 4] In addition to gene therapy, many other nucleic acid manipulation techniques like asDNA and siRNA can greatly benefit from safe and efficient delivery systems.[1, 3] Development of non-viral delivery systems such as polycationic polymers present a unique and unprecedented opportunity to genetic engineers.[5, 6] Polymers allow a significant amount of customization,

provide a high surface moiety to volume ratio, and are relatively safe when compared to viral systems;[7] [8] however, they still have the major drawback of low transgene expression. Incomplete understanding of cellular uptake mechanisms[9, 10], inefficient endosomal escape,[11-13] and poorly designed and understood nuclear uptake[13, 14] are thought to be the major reasons limiting optimization. [3, 13]

Recent work by Lechardaur et al.[15] and Pollard et al.[16] indicated the activity of cyotosolic nucleases plays a significant role in limiting expression efficiency. Our recent work has shown that differential transgene expression facilitated by jetPEI™, linear PEI, and generation 5 poly(amidoamine) (G5 PAMAM) dendrimer can be explained by activation of cytosolic nucleases that degrade the plasmid into a non-functional form.[17] Characterizing the activity pattern of these cytosolic nucleases is a key step needed to develop better synthetic strategies for polymers capable of delivering, protecting, and releasing the plasmid. Substantial efforts have been expended to make the plasmid less susceptible to nuclease degradation via backbone, codon, and poly(A) modifications and by removing viral DNA components.[18, 19]

In this study, high-throughput sequencing is used to identify and quantify labile sites on a pGL4.51 luciferase expressing plasmid that are susceptible to cytosolic nucleases. S1 nuclease was used both to validate the experimental protocols and to develop a comparison to the published cleavage pattern determined using agarose gel electrophoresis.[18, 19] High-throughput sequencing not only identifies more labile sites than previously observed using agarose gel electrophoresis, it also

provides information about the relative degree of degradation per site and significantly greater resolution of the site location in the plasmid sequence. Many of the cleavage sensitive sequences lay in homopurine and homopyrimidine regions of the synthetic/viral poly(A) regions and the plasmid's bacterial origin of replication (*OriC*); however, labile sites were also identified in the reporter and the antibiotic resistance genes required for stable expression.[20] Many of the labile sites identified in the plasmid correspond to regions that are indispensible for plasmid functionality.

Human epithelial carcinoma cells (HeLa cells) were used based on previous studies exploring the role of cytosolic nucleases.[15, 18] S1 nuclease was used as the control nuclease in this study because it has already been shown that customizing plasmid sequences on the basis of S1 nuclease activity can improve plasmid stability in vitro studies.[18, 19] The luciferase expression plasmid was selected because it is widely used in gene expression studies in mammalian cells and understanding the susceptibility to cytosolic nucleases should be useful for a broad range of research groups. The plasmid also contains the commonly employed selective Neomycin gene to select for permanently transgene expressing mammalian cells.

4.3 Materials and Methods

HeLa cells (Catalogue #CCL-2) were obtained from American Type Culture Collection (ATCC). S1 nuclease and 10x S1 nuclease buffer, salmon sperm DNA (ssDNA), and luciferase plasmid (pGL4.51) were purchased from Promega Corporation. A circular map of the plasmid is provided in the supplemental material (Figure 4.S1). NP-40 lysis buffer was procured from Boston BioProducts Inc. and

protease inhibitor cocktail was obtained from Sigma-Aldrich. The BCA protein assay kit was purchased from Thermo Fisher Scientific, Inc. The Gel extraction kit was purchased from Qiagen (Catalogue #28706). 10xBlueJuice™ gel loading buffer was obtained from Life Technologies Corporations (Catalogue # 0816-015). Three restriction endonucleases SacI (Catalogue #R3156S), DraIII (Catalogue #R3510S) and StuI (Catalogue #R0187S) were obtained from New England BioLabs®, Inc. The Serum free media (SFM) employed in this study was Minimal Essential Media (MEM) with glutamine and Earle salts obtained from life technologies. Complete media was made by adding 50 mL of fetal bovine serum (FBS) and 5 mL of 100X penicillin-streptomycin to 500 mL of MEM. An Illumina HiSeq 2000 (Illumina, Inc.) was employed for all sequencing experiments. Initial sequence alignment was completed with the help of Bowtie. Integrated Genomic Viewer was used to view the aligned sequence. MATLAB™ was employed to generate heat-maps of nuclease activity. PAMAM dendrimer was purchased from Dendritech, Inc. In-house characterization revealed M_w as 28910 and polydispersity index (PDI) as 1.01. Titration showed 116 amines per dendrimer.

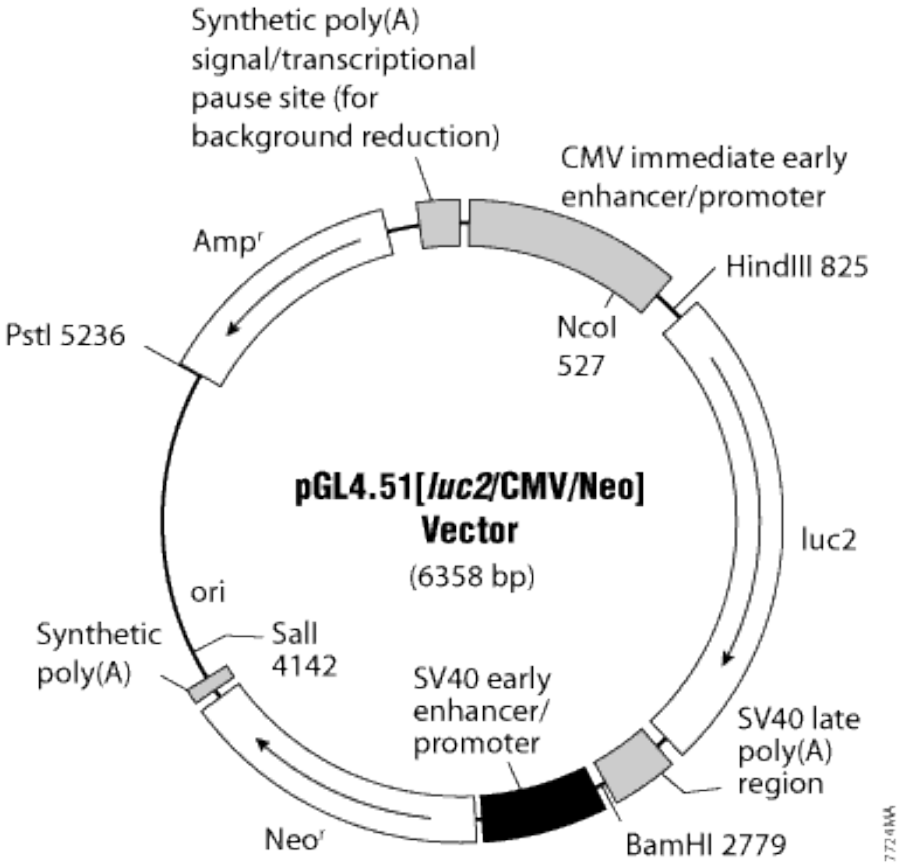

Figure 4.S1: Circular plasmid map pGL4.51 employed in the presented study. Courtesy: Promega Corporation.

Transfection and cytosol extraction: 500,000 HeLa cells/well were cultured in a 6 well plate with 1.5 mL of complete media at 37 °C overnight. Subsequently, cells were treated in duplicate with 10:1 nitrogen to phosphorus (N/P) ratio of G5 PAMAM polyplexes (2 µg ssDNA, 15.13 µg G5 PAMAM, 100 µL water) for 3 h in 0.9 mL SFM. After 3 hours the transfection media was replaced with 1.5 mL complete media and the cells were incubated for another 1 h. Cells were then washed with PBS without Ca^{2+} and Mg^{2+} and incubated with 200 µL 0.1% trypsin for 5 minutes at 37 °C. 1.8 mL of cold PBS (4 °C) with Ca^{2+} and Mg^{2+} ions was added to each well to stop trypsin activity. Duplicates were pooled together and cells were centrifuged at

1200 rpm. To obtain cell lysates, the cell pellet was suspended in 200 μL of ice-cold cell lysis buffer and incubated for 30 minutes on ice. Afterwards, the samples were centrifuged at 3,000 rpm for 5 minutes at 4 °C and the supernatants were collected. A BCA assay was used to assess and normalize protein concentration in subsequent experiments. 20 μg of pDNA was incubated with 10 μg of the cytosol lysate in 100 μL of water for 30 minutes at 37 °C. The control lysates from non-treated cells were prepared identically except no polyplexes were added in the initial step. S1 nuclease cleavage sample were prepared by adding 10 units of S1 nuclease to 20 μg of pDNA in 100 μL of water and 1X S1 nuclease buffer for 30 minutes at 37 °C. The negative control was prepared using 20 μg of pDNA re-suspended in 100 μL of water and employed using the same incubation conditions.

For Illumina dye sequencing, samples containing 100 μL of the plasmid reaction mixture were treated with cell extracts (polyplex-treated cells or untreated cells) or S1 nuclease and optimized using the Qiagen gel extraction kit (the 100 μL of reaction mixture was used in place of excised gel) to change the buffering media to 10 mM Tris-Cl at pH 8.5 for downstream sequencing. In addition, a plasmid-only control was brought through the identical procedure.

For agarose gel electrophoresis, 10 μL of the plasmid reaction mixtures described above were added to each well in 1X BlueJuice™ gel loading buffer. The gel electrophoresis was performed on a 0.9% agarose gel containing ethidium bromide at 60 V for 3 hours.

For the restriction nuclease analysis presented in Figure 4.2, agarose gel electrophoresis was performed using 10 μL of the S1 nuclease and luciferase

plasmid reaction mixture in 10 parallel lanes (under the conditions used for this mixture in Figure 4.1, lane 5). The linear topology 6.4 kB form of the luciferase plasmid was then cut out from gel and purified using a gel extraction protocol (explained below). 0.2 μg of the isolated 6.4 kB linear plasmid was incubated with either 2 units of SacI, DraIII or StuI restriction endonucleases in the supplied reaction buffer for 60 minutes at 37 °C. Control digests were performed with these restriction endonucleases and using the luciferase plasmid under same conditions. SacI, DraIII and StuI endonucleases were used because they each have a single restriction site in the plasmid sequence, which provides enough resolution to map the pDNA. The endonuclease treated samples were analysed on 0.9% agarose gel containing ethidium bromide at 60 V for 3 hours.

Gel extraction protocol (employing buffers QG, PE and EB supplied with the kit): The region containing the linear form of pDNA was excised from the agarose gel and weighed. The excised gel was then incubated with 3 volumes of buffer QG (1 volume of QG buffer is 100 μL for 100 μg of gel) at 50 °C for 10 minutes. Afterwards, 1 volume of isopropanol was added to the mixture. This sample was then applied to a QIAquick column and centrifuged at 13,000 rpm for 1 minute; the flow-through was discarded. To remove the trace amount of gel left on the column, 0.5 mL of buffer QG was centrifuged through the column for 1 minute at 13,000 rpm and the flow-through was discarded. 0.75 mL of buffer PE was added to the QIAquick column. The buffer was left on the column for 5 minutes after which the column was centrifuged at 13,000 rpm for 1 minute and the flow-through was discarded. The QIAquick column was centrifuged again to discard any remaining PE buffer. To

elute the DNA, 30 μL of buffer EB (for the Illumina sequencing) or water (for the restriction endonuclease experiment) was added to the column and the column was allowed to stand for 2 minutes before being centrifuged at 13,000 rpm for 1 minute. The flow-through was collected and the DNA concentration measured using a spectrophotometer.

4.4 Results and Discussion

4.4.1 Cleavage Sites as Determined by Agarose Gel Electrophoresis

The degradation pattern resulting from treatment of luciferase plasmid with S1 nuclease or the nucleases present in cytosol was first studied using agarose gel electrophoresis. Figure 4.1 illustrates that upon treatment with either S1 or cytosolic nucleases the supercoiled pDNA degrades into two major forms, a linear plasmid (6.4 kB) and nicked plasmids (appearing as ~10 kB fragments as compared to the linear DNA size ladder). The gel also shows substantial streaking suggesting the presence of other sites susceptible to nuclease cleavage. The major band of the 6.4 kB linear plasmid was extracted from the gel and incubated with either Sac1, DraIII, or StuI endonucleases (Figure 4.2). These three restriction endonucleases, which cut at the 735, 2006, and 3212 bp sites, respectively, provide the redundancy necessary to define the primary S1 cut site. The pattern obtained with all three endonucleases indicated a S1 cut site located at the 5000 ± 500 bp position of the pDNA. This site is close to the homopurine/homopyrimidine rich plasmid *OriC* region, consistent with previous work that showed homopurine regions are susceptible to S1 nuclease degradation.[19]. In previous work two predominant cut

regions, defined as hot spots, were found the in poly(A) sequence and in *OriC*. [19] In this paper we show that gel electrophoresis method has low sensitivity for cut site detection and that high-throughput sequencing can be used to determine S1 nuclease and cytosolic nuclease labile regions in pDNA. The presence of discrete bands of linear DNA in Figures 4.1 and 4.2 also indicate that endonuclease cleavage preferentially occurs at supercoiled pDNA as opposed to the linear DNA form.

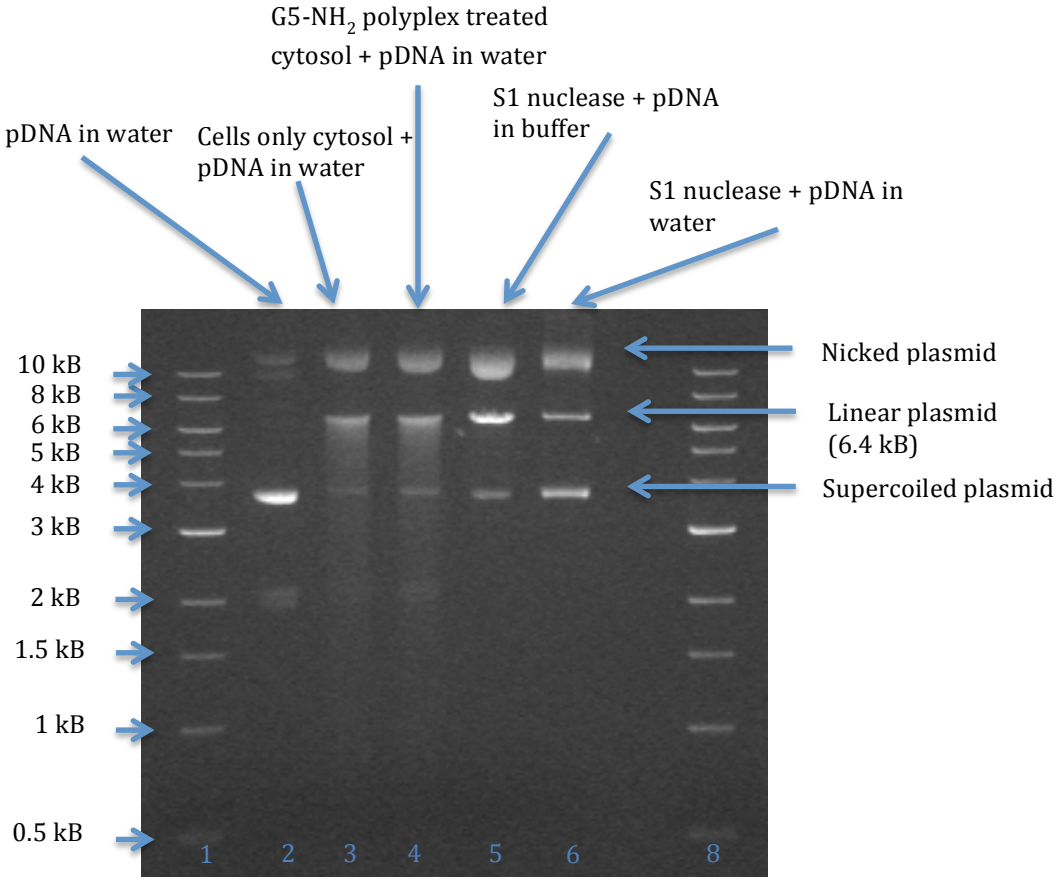

Figure 4.1. Agarose gel electrophoresis showing the DNA cleavage pattern of HeLa cytosol and S1 nuclease treated luciferase pDNA. Lanes 1 and 8) 10 kB DNA ladder. Lane 2) pDNA in water. Lane 3) pDNA treated with cells only cytosol in water. Lane 4) pDNA treated with cytosol in water from cells exposed to G5 polyplexes. Lane 5) pDNA treated with S1 nuclease in S1 nuclease buffer. Lane 6) pDNA treated with S1 nuclease in water. In lanes 3-6, both the nicked and linear topology of the plasmid can be seen.

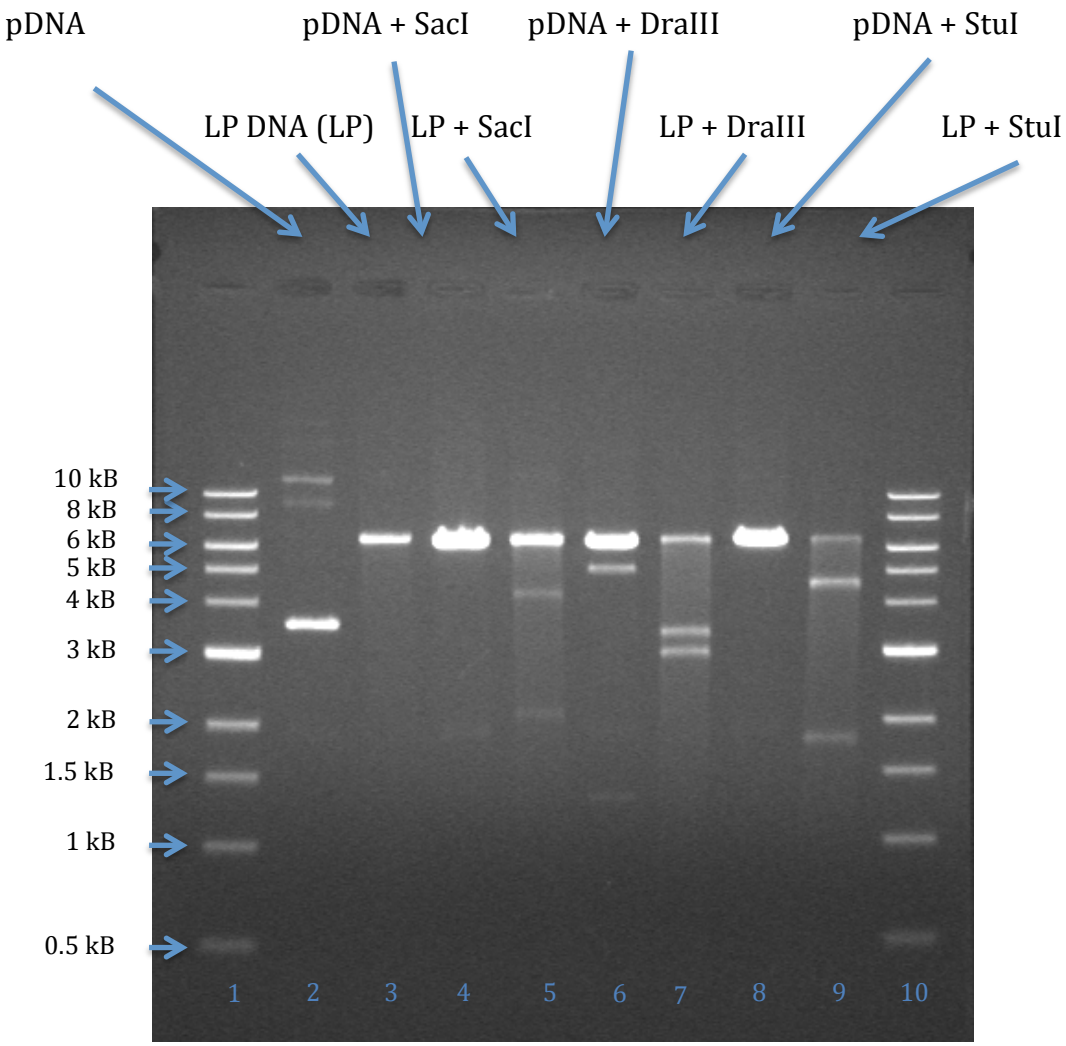

Figure 4.2. Endonuclease treatment of 6.4 kB linear plasmid (LP). Lanes 1 and 10; 10 kB DNA ladder. Lane 2) pDNA in water. Lane 3) LP in water. Lanes 4, 6, 8) pDNA treated with SacI, DraIII and StuI, respectively. Lanes 5, 7, 9) LP treated with SacI, DraIII and StuI, respectively.

is

The analysis presented in Figures 4.1 and 4.2 provided a useful start to understanding nuclease activity against plasmids in cells; however, two aspects of the experiment could benefit from substantial improvement. First, the inherent resolution of the gel electrophoresis method (~500 bp) prevents a detailed sequence determination of where the pDNA was cut. This limits the extent to which one can understand the S1 and cytosolic nucleases activity and to make

comparisons between them. Second, it seemed unlikely, particularly giving the streaking in Figure 4.1, that a single cleavage sequence existed for either cytosolic nucleases or the S1 nuclease, suggesting that the gels did not have the desired level of sensitivity. In addition to these concerns, Sanger sequencing is limited by the choice of primers. Given this set of concerns and challenges, the high-throughput Illumina dye sequencing method was employed to explore the range of cellular nuclease cuts introduced on the pDNA.[21] We employed S1 nuclease as both a positive control, in comparison to the gel work, and to learn more about the S1 activity. There are number of advantages of using high-throughput Illumina dye sequencing for the cytosolic nuclease experiments. The development of the specific sequencing primer sets as well as the need to perform multiple gels for the analysis of restriction enzyme patterns for each cut site of interest is avoided (as illustrated in Figure 4.2). In addition, the high-throughput sequencing also provides higher resolution of the cut site location. Lastly, high-throughput sequencing defines the degree of cutting over a region (*vida infra*), as opposed to the notion of a singular base pair location. This observation is important both for design of more robust plasmids and for the design of polymers that might protect these regions.

4.4.2 Cleavage Sites as Determined by High-Throughput Sequencing

High-throughput Illumina dye sequencing was performed in three steps.[21] The first step was library preparation where the treated and control luciferase pDNA samples were randomly broken into smaller fragments with sonication, adenylated, connected to adapter oligonucleotides, size-selected, and purified. Next, the materials underwent cluster generation where each library of fragments was

clonally amplified. The final step was sequencing, which was accomplished for each cluster using fluorescent deoxyribonucleotides (dNTPs). Each dNTP addition (50 bases) was recorded for every cluster on the lane.

Heat maps were used to visualize both the location and extent of nuclease cut on the luciferase pDNA (Figures 4.3-4.5). Each panel provides data for the specified range of pDNA cutting efficiency. Sample normalization for S1 nuclease, untreated cytosol and G5 polyplex-treated cytosol samples was accomplished using the untreated pDNA control. First the readcount for each base was normalized by the average readcount for that sample. For each base in nuclease-treated samples, the normalized base readcount was divided by the normalized readcount from untreated pDNA control. This ratio was used for heat map generation. The greyscale vertical lines indicate the percentage of plasmids cut at that location. White regions indicate a cut frequency lower than or equal to the lowest value of the specified range. A black line indicates a cut extent equal to the highest value of the range. For each figure, panel A illustrates the full set of data. The range in panel B is defined to focus on approximately the top 15 cut regions. The range in panel C is chosen to focus on the top 3-5 cut regions for easiest comparison to agarose gel electrophoresis data. At the bottom of each figure, a luciferase gene functional map is provided in registry with the heat map to facilitate comparison of cut sites to the different regions of the pDNA plasmid.

The heat map in Figure 4.3 illustrates the activity of S1 nuclease in water on pDNA. Panel A indicates the locations were 0 to 45% of the plasmids were cut. There are few “white” regions corresponding to sequences where no cuts were detected,

suggesting that the nuclease is promiscuous with respect to the types of base sequences suitable for a cleavage location. Panel B illustrates only sites in which 25-45% of the plasmids were cleaved and Panel C illustrates sites in which only 28-45% of the plasmids were cleaved. Information regarding each cut site, including % AT content, function of plasmid region, cut location and width and fraction of plasmids cut is summarized in Table 4.1 for the top 15 regions (Figure 4.3b). These regions include four cuts (S1-4) in the luciferase gene, a cut in the SV40 promoter/enhancer (S5), cuts in three locations on the Neomycin gene (S6-8), cuts at three sites on the origin of replication region (S9-11), and three sites on ampicillin gene (S13-15). Cuts S9-11 at *OriC* are consistent with the primary region previously determined by agarose gel electrophoresis[19] and illustrated in Figure 4.1. The homopurine/homopyrimidine rich sites like poly (A) and *OriC* have been reported as susceptible to S1 nucleases using gel electrophoresis;[19, 22] however, using high-throughput sequencing we have found many additional labile regions not previously identified. These findings challenge the long held hypothesis that S1 nuclease only attacks single stranded secondary structures of DNA.[18, 19, 22]

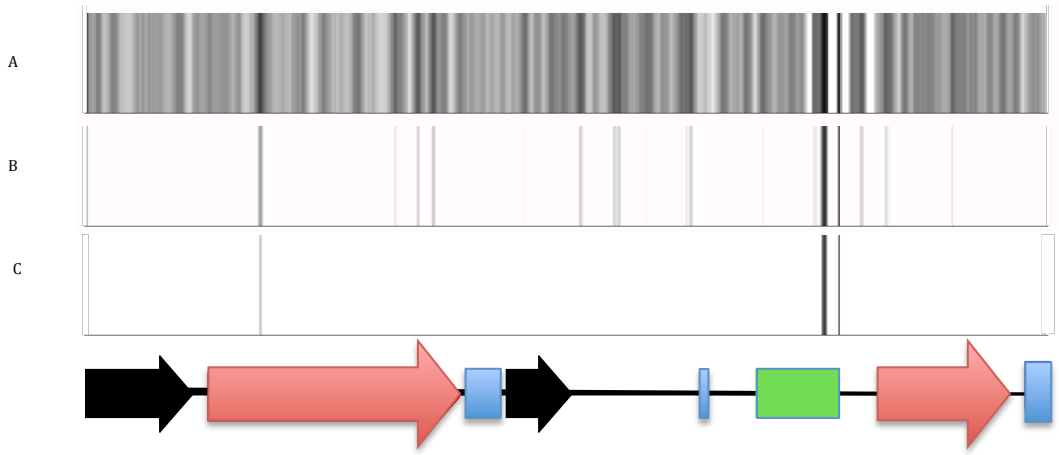

Black: CMV early promoters/enhancers
Red: Genes
Blue: Poly(A) sequence
Green: *OriC*

Figure 4.3. Heat maps showing frequency of cuts on the luciferase pDNA resulting from the S1 nuclease digest in water. White color indicates the percentage of plasmids cut is between zero and the lower part of the cut range listed. Black color indicates the percentage cut is the maximum value for that cut range. Greyscale indicates cut percentages between these extrema. Panel A shows the full range of labile sites, Panel B represents labile regions that have frequency of cuts between 25-45% (showing ~15 most cut regions). Panel C shows ~top 5 cut regions between 28-45%. The luciferase functional map is provided in registry with the heat map to facilitate comparison of cuts sites to the different regions of the plasmid.

Table 4.1. Summary of the top 15 regions of the luciferase plasmid cut by S1 nuclease, as illustrated in Figure 4.3B.

Region	% AT content	Function	Cut Location and width(bp)	Percent extent of cut (average, maximum)
S1	43	Luciferase gene	1142-1187 (46)	29, 33
S2	50	"	2042-2067 (26)	26, 27
S3	36	"	2195-2217 (22)	27, 29
S4	25	"	2292-2319 (28)	28, 30
S5	55	SV40 promoter	2903-2913 (11)	25, 26
S6	39	Neomycin gene	3261-3296 (36)	27, 29
S7	32	"	3489-3544 (56)	28, 29
S8	38	"	3967-4018 (52)	27, 29
S9	53	*OriC*	4474-4484 (15)	26, 26
S10	54	"	4812-4910 (99)	31, 41
S11	78	"	4974-4990 (17)	35, 38
S12	48	Close to *OriC*	5062-5076 (14)	25, 26
S13	67	Ampicillin gene	5116-5145 (30)	27, 29
S14	47	"	5283-5325 (43)	26, 28
S15	53	"	5725-5741 (17)	26, 28

Similar to Figure 4.3, the heat map in Figure 4.4 illustrates the activity of cytosolic nucleases overlaid on the luciferase pDNA functional map. Panels A-C provide data for nuclease activity from cytosol obtained for cells treated with G5 polyplexes. In a previous study, we demonstrated that the nuclease activity is polyplex dependent and is negatively related to the level of protein expression.[17] G5 polyplexes were selected because they induced the maximum level of nuclease activity and gave the minimum level of expression. We also prepared lysates from cells that had not been treated with polyplexes in order to establish the "background" level of nucleases. The data presented in panels D-F, although important and informative, must be treated with caution in ascribing nuclease levels in a normal, functional cell. Caveats may include the neoplastic origin of HeLa cancer cell line and that the cytosol was obtained by cell lysis, a procedure which may itself trigger nuclease activity. [23] [24]

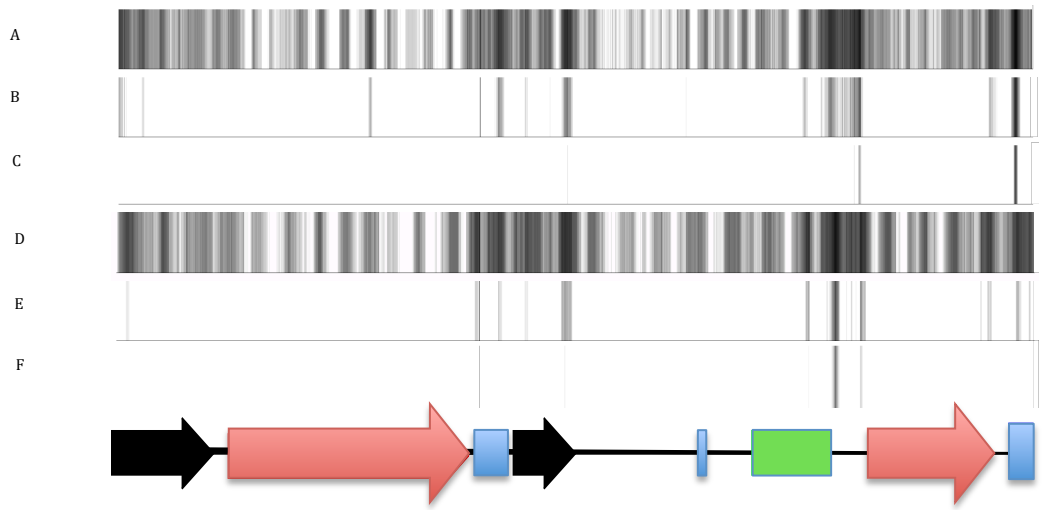

Figure 4.4. Heat maps showing frequency of cuts on the luciferase plasmid resulting from cytosolic nuclease treatments. White color indicates the percentage of cut is between zero and the lower part of the cut range listed. Black color indicates the percentage of cut is the maximum value for that cut range. Greyscale indicates cut percentages between these extrema. Panels A, B and C show labile cut regions for G5 polyplex-treated cell cytosol treatment. Panel A shows the full range of labile sites, Panel B represents labile regions that have a frequency of cuts between 41-65% (showing ~15 most cut regions). Panel C shows ~top 5 cut regions between 52-65%. Panels D, E and F represent cells-only cytosol treatment. Panel D shows the full range of labile sites, Panel E represents labile regions that have a frequency of cuts between 50-75% (showing ~15 most cut regions) and Panel F shows ~top 5 cut regions between 59-75%.

Panels A and D show all the labile sites present in 0-65% and 0-75% extent of cut range for the G5 polyplex-treated and untreated cells, respectively. Similar to S1 nuclease, the cytosolic nucleases are promiscuous and attack numerous regions in addition to the most common cuts in the poly(A) and viral enhancer/promoter regions of the pDNA. Panels B and E represent the 15 most labile regions lying in the range of 41-65% and 50-75% for G5 polyplex-treated and untreated cell cytosolic samples, respectively. Panels C (52-65% extent of cut) and F (59-75%

extent of cut) represent the most labile regions and are most useful for comparison to gel electrophoresis data.

Table 4.2 summarizes the top 15 most labile regions obtained with the cytosol from untreated cells (data in Figure 4.4e). Cytosolic nucleases in this cytosol produce four cuts in the viral CMV enhancer/promoter region, one cut in the luciferase gene, three cuts in the poly(A) regions, two cuts on *OriC*, and three cuts on the ampicillin gene.

Table 4.2. Summary of the top 15 regions of the luciferase plasmid cut by cells only cytosolic nucleases (as illustrated in Figure 4.4E).

Region	% AT content	Function	Cut Location and width(bp)	Percent extent of cut (average, maximum)
C1	67	CMV promoter	62-113 (52)	51, 53
C2	57	"	321-327 (7)	51, 53
C3	50	Luciferase gene	2483-2520 (38)	55, 63
C4	62	SV40 poly A	2573-2580 (8)	51, 53
C5	73	"	2633-2683 (51)	53, 57
C6	62	SV40 promoter	2831-2859 (29)	52, 54
C7	44	"	3081-3160 (80)	58, 61
C8	45	*OriC*	4774-4804 (31)	58, 61
C9	50	"	4915-5022 (103)	58, 71
C10	50	Close to *OriC*	5060-5063 (4)	52, 53
C11	62	"	5075-5126 (52)	51, 56
C12	86	Ampicillin gene	5148-5196 (49)	57, 62
C13	58	"	5991-6002 (12)	52, 55
C14	42	"	6025-6066 (42)	54, 57
C15	70	Synthetic Poly(A)	6217-6273 (57)	54, 59

Table 4.3. Summary of the top 15 regions of the luciferase plasmid cut by G5 polyplex-treated cells cytosolic nucleases (as illustrated in Figure 4.4B).

Region	% AT content	Function	Cut Location and width(bp)	Percent extent of cut (average, maximum)
G1	57	CMV promoter	-4 – 33 (37)	45, 49
G2	83	"	38-55 (18)	42, 44
G3	37	"	141-148 (8)	41, 42
G4	75	"	150-181 (32)	41, 45
G5	56	Luciferase gene	1738-1764 (27)	44, 48
G6	73	SV40 poly A	2610-2686 (71)	45, 55
G7	54	SV40 promoter	2827-2850 (24)	42, 44
G8	25	"	3002-3005 (4)	42, 44
G9	47	"	3083-3156 (74)	48, 54
G10	33	Neomycin gene	3947-3949 (3)	41, 41
G11	33	Close to *OriC*	4359-4361 (3)	41, 41
G12	48	*OriC*	4748-4797 (50)	43, 48
G13	59	"	4882-5182 (300)	47, 59
G14	51	Ampicillin gene	6051-6109 (51)	44, 49
G15	72	Synthetic poly(A)	6208-6275 (60)	52, 61

Similar to Table 4.2, Table 4.3 shows top 15 labile sites for cytosol from G5 polyplex treated cells (data in Figure 4.4b). Three cuts are observed in the viral enhancer/promoter regions, one cut in the luciferase gene, two cuts in the poly(A) sequence, two cuts near *OriC*, one cut in the ampicillin resistance gene, and one cut in the neomycin gene.

Cytosol nuclease activity from untreated cells and G5 polyplex treated cells display significant similarities. The top 15 labile regions for cytosolic samples can be divided into three major regions: the viral promoter/enhancer sequence, poly(A) sequences, and *OriC*. There are also some cut regions in the luciferase reporter and the selective neomycin resistance gene. Cuts in viral promoter/enhancers, poly(A) sequences, and the transgene can severely abrogate transgene expression[18, 25]. The multiple cuts in the selective neomycin and ampicillin resistance genes point to

the additional challenge in efforts to establish the cell lines with a stable plasmid expression. The bacterial origin of replication (*OriC*) is necessary for plasmid replication in bacteria[26] though it has little functional role in eukaryotes. [27] The discovery that *OriC* is one of the most degraded regions for S1 (Table 4.S1) and cytosolic nucleases (Tables 4.S2 and 4.S3) suggests that eukaryotic cells may recognize *OriC* as a marker for foreign DNA.

Table 4.S1: Top 20 most cut sites for S1 nuclease in luciferase plasmid. S10_X represents cut site belonging to S10 region from Table 4.1.

Site	Location	Function	Percent extent of cut
S10_1	4883	Origin of replication	42
S10_2	4884	"	41
S10_3	4885	"	41
S10_4	4886	"	41
S10_5	4887	"	41
S10_6	4888	"	41
S10_7	4889	"	41
S10_8	4890	"	41
S10_9	4891	"	41
S10_10	4877	"	40
S10_11	4892	"	40
S10_12	4893	"	40
S10_13	4894	"	40
S10_14	4895	"	40
S10_15	4879	"	39
S10_16	4880	"	39
S10_17	4881	"	39
S10_18	4896	"	39
S10_19	4874	"	38
S10_20	4876	"	38

Table 4.S2: Top 20 most cut sites for untreated cells cytosolic nucleases in luciferase plasmid. C9_X represents cut site belonging to C9 region from Table 4.2.

Site	Location	Function	Percent extent of cut
C9_1	4984	Origin of Replication	71
C9_2	4985	"	70
C9_3	4983	"	69
C9_4	4982	"	68
C9_5	4979	"	67
C9_6	4980	"	67
C9_7	4981	"	67
C9_8	4978	"	66
C9_9	4993	"	66
C9_10	4994	"	66
C9_11	4995	"	66
C9_12	4976	"	65
C9_13	4977	"	65
C9_14	4986	"	65
C9_15	4988	"	65
C9_16	4989	"	65
C9_17	4990	"	65
C9_18	4991	"	65
C9_19	4992	"	65
C9_20	4975	"	64

Table 4.S3: Top 20 most cut sites for G5 polyplex treated cells cytosolic nuclease. G15_X and G13_X represents cut site belonging to G15 and G13 regions respectively from Table 4.3.

Site	Location	Function	Percent extent of cut
G15_1	6235	Synthetic Poly (A)	61
G15_2	6236	"	61
G15_3	6237	"	61
G15_4	6234	"	60
G15_5	6238	"	60
G15_6	6239	"	60
G15_7	6240	"	60
G15_8	6241	"	60
G15_9	6242	"	60
G15_10	6243	"	60
G15_11	6244	"	60
G15_12	6245	"	59
G15_13	6246	"	59
G15_14	6247	"	59
G15_15	6232	"	59
G15_16	6233	"	59
G13_1	5151	Origin of Replication	59
G13_2	5152	"	59
G15_17	6248	Synthetic Poly (A)	59
G15_18	6249	"	59

In summary, we have detected a greater number of labile regions suceptabile to cleavage for cytosolic extracts than for S1 indicating that cytosol contains additional nucleases. This observation is consistent with the hypothesis that S1 type nucleases are part of a group of cytosolic nucleases targeting the pDNA at the predominately homopurine/homopyrimidine sequences.[18] [19]

In other studies, treatment with G5 PAMAM polyplexes lead to the highest cytosolic nuclease activation leading to a decrease in transgene expression[17]. In Figure 4.5 we showed that G5 PAMAM polyplex treated cytosol has activity similar to control cytosol with several notable, and possibly significant differences, especially in the luciferase transgene. The labile region in the luciferase gene is one of the top 15 most labile regions for G5 polyplex treated cytosol; however, it is not for untreated cells cytosol. This may contribute to poor luciferase transgene expression facilitated by G5 PAMAM polyplexes. This is consistent with the hypothesis that G5 PAMAM polyplexes induce heightened activation of cytosolic nuclease, therefore decreasing the transgene expression[17]. In making this comparison, it is important to note that cells were lysed for the sequencing experiments, which may lead to changes in the activity of cytosolic nucleases.

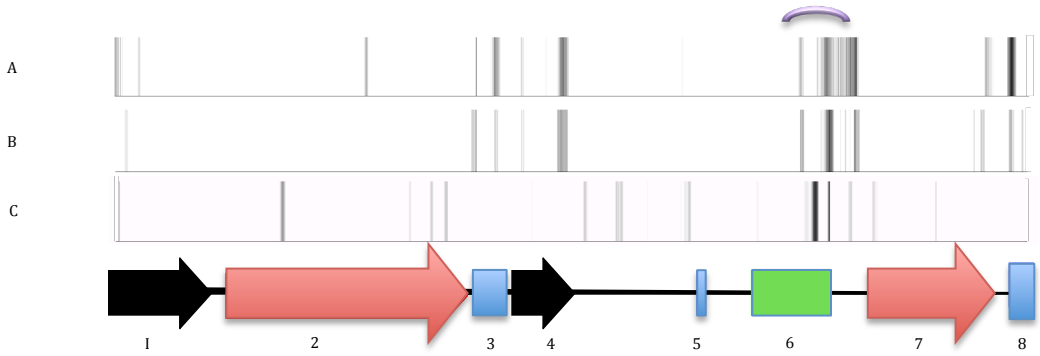

1: CMV immediate early promoters/enhancers
2: Luciferase gene
3: SV40 poly(A) sequence
4:SV40 early promoters/enhancers
5 and 8: Synthetic poly(A) sequence
6: *OriC*
7: Beta-Lactamase coding region
Purple crescent: agarose gel result for S1 nuclease

Figure 4.5. Heat map comparison between cytosol nuclease samples and S1 nuclease. (A) G5 polyplex-treated cytosol cut regions with 41-65% cuts (B) cells-only cytosol cut regions with 50-75% cuts (C) S1 nuclease cut regions with 25-45% cuts.

4.4.3 Consensus Analysis

Apart from showing the position of labile sites, sequencing also provides a unique opportunity to evaluate homology between the labile sites. To study and quantify homology between the labile sequence for S1 and cytosolic sample, a consensus sequence was developed by performing a multiple sequence alignment of the most labile region of the cytosolic samples and the S1 nuclease sample (S10, C9, G13 in Tables 4.1, 4.2 and 4.3, respectively). The consensus sequence AGCTCTTGATCCGGCAAACAAACCACC was then used to calculate similarity for other labile sequence locations. Tables 4.S4, 4.S5, and 4.S6 show the analyses performed for S1 nuclease, control cytoplasm and the G5 polyplex treated cells cytoplasm samples, respectively. Low sequence homology between the consensus sequence and labile region for S1 nuclease and cytosolic samples supports the hypothesis that nuclease are not primary DNA sequence specific, and can be considered promiscuous with respect to the base pair sequence.

Table 4.S4: S1 nuclease treatment: pairwise alignment using consensus sequence.

Region	Size	Identity to consensus
S1	46	16/46
S2	26	13/26
S3	22	10/22
S4	28	10/28
S5	11	6/11
S6	36	12/36
S7	56	9/56
S8	52	20/52
S9	15	11/15
S10	99	18/99
S11	17	4/17
S12	14	3/14
S13	30	9/30
S14	43	16/46
S15	17	13/17

Table 4.S5: Cytoplasmic extract from HeLa cells only treatment: pairwise alignment using consensus sequence.

Region	Size	Identity to consensus
C1	52	17/52
C2	7	2/7
C3	38	11/38
C4	8	7/8
C5	51	16/51
C6	29	8/29
C7	80	11/80
C8	31	11/31
C9	108	27/108
C10	4	3/4
C11	52	14/52
C12	49	14/49
C13	12	9/12
C14	42	14/42
C15	57	10/57

Table 4.S6: Cytoplasmic extract from G5 polyplex. HeLa cells treatment: pairwise alignment using consensus sequence.

Region	Size	Identity to consensus
G1	37	15/37
G2	18	1/18
G3	8	6/8
G4	32	7/32
G5	27	15/27
G6	71	16/71
G7	24	12/24
G8	4	3/4
G9	74	12/74
G10	3	2/3
G11	3	2/3
G12	50	20/50
G13	300	27/300
G14	51	12/51
G15	60	8/60

4.5 Conclusions

Agarose gel electrophoresis and Illumina dye sequencing confirm that cytosolic nucleases cleave luciferase pDNA, rendering it as non-functional template for expression, and that S1 nuclease cuts at high homopurine/homopyrimidine regions of the plasmid[18, 19]. To the best of our knowledge, this is the first time high-throughput sequencing has been used to study degradation effects of S1 and cytosolic nucleases on pDNA. Interestingly, the most susceptible cut region for S1 nuclease overlaps the susceptible region for cytosolic nucleases, consistent with the hypothesis that S1 type nucleases are part of the cytosolic nuclease milieu. Lack of significant homology between labile sequences and a consensus sequence (Table 4.S4, 4.S5 and 4.S3) suggests that these nucleases are highly promiscuous. In addition, our agarose gel results are consistent with the hypothesis that S1 and cytosolic nucleases are more likely to cleave supercoiled pDNA than the linear form

of DNA. Our data further indicates that since many of susceptible sites lie in the indispensible functional units of pDNA there is a limit to DNA sequence optimization. To overcome this challenge, further research is needed on polymers designed to protect these labile regions from degradation during the transport of pDNA into the cell and to the nucleus.

4.6 References

1. Scholz C, Wagner E Therapeutic plasmid DNA versus siRNA delivery: Common and different tasks for synthetic carriers. Journal of Controlled Release 2012; **161**: 554-565
2. Hess P, Cooper D Impact of Pharmacogenomics on the Clinical Laboratory. Molecular Diagnosis 1999; **4**: 289-298
3. Liu C, Zhang N Nanoparticles in gene therapy principles, prospects, and challenges. Prog Mol Biol Transl Sci 2011; **104**: 509-662
4. D. L, G.L. L Intracellular Barriers to Non-Viral Gene Transfer. Current Gene Therapy 2002; **2**: 183-194
5. Smedt SCD, Demeester J, Hennink WE Cationic Polymer Based Gene Delivery Systems. Pharmaceutical Research 2000; **17**: 113-126
6. Benns JM, Choi J-S, Mahato RI*, et al.* pH-Sensitive Cationic Polymer Gene Delivery Vehicle: N-Ac-poly(l-histidine)-graft-poly(l-lysine) Comb Shaped Polymer. Bioconjugate Chemistry 2000; **11**: 637-645
7. Luo D, Saltzman WM Synthetic DNA delivery systems. Nature Biotechnology 2000; **18**: 33-37
8. Lungwitz U, Breunig M, Blunk T*, et al.* Polyethylenimine-based non-viral gene delivery systems. European Journal of Pharmaceutics and Biopharmaceutics 2005; **60**: 247-266
9. Hong S, Rattan R, Majoros InJ*, et al.* The Role of Ganglioside GM1 in Cellular Internalization Mechanisms of Poly(amidoamine) Dendrimers. Bioconjugate Chem 2009; **20**: 1503-1513
10. Qi R, Mullen DG, James R. Baker J*, et al.* The Mechanism of Polyplexes Internalization into Cells: Testing the GM1/Caveolin-1-Mediated Lipid Raft Mediated Endocytosis Pathway. Molecular Pharmaceutics 2010; **7**: 267-279
11. Varkouhi AK, Scholte M, Storm G*, et al.* Endosomal escape pathways for delivery of biologicals. Journal of Controlled Release 2011; **151**: 220-228
12. Cho YW, Kim J-D, Park K Polycation gene delivery systems: escape from endosomes to cytosol. Journal of Pharmacy and Pharmacology 2003; **55**: 721-734

13. Lechardeur D, Verkman AS, Lukacs GL Intracellular routing of plasmid DNA during non-viral gene transfer. Advanced Drug Delivery Reviews 2005; **57**: 755-767
14. Dean D, Strong D, Zimmer W Nuclear entry of nonviral vectors. Gene Therapy 2005; **12**: 881-890
15. Lechardeur D, Sohn KJ, Haardt M*, et al.* Metabolic instability of plasmid DNA in the cytosol: a potential barrier to gene transfer. Gene Therapy 1999; **4:** 482-497
16. Pollard H, Toumaniantz G, Amos J-L*, et al.* Ca2+-sensitive cytosolic nucleases prevent efficient delivery to the nucleus of injected plasmids. The Journal of Gene Medicine 2001; **3**: 153-164
17. Rattan R, Vaidyanathan S, Wu G*, et al.* Polyplex-Induced Cytosolic Nuclease Activation leads to Differential Transgene Expression. Molecular Pharmaceutics; submitted
18. Azzoni AR, Ribeiro SC, Monteiro GA*, et al.* The impact of polyadenylation signals on plasmid nuclease-resistance and transgene expression. The Journal of Gene Medicine 2007; **9**: 392-402
19. Ribeiro SC, Monteiro GA, Prazeres DMF The role of polyadenylation signal secondary structures on the resistance of plasmid vectors to nucleases. Journal of Gene Medicine 2004; **6**: 565-573
20. Condreay JP, Witherspoon SM, Clay WC*, et al.* Transient and stable gene expression in mammalian cells transduced with a recombinant baculovirus vector. 1999; **96**: 127-132
21. Meyer M, Kircher M Illumina Sequencing Library Preparation for Highly Multiplexed Target Capture and Sequencing. Cold Spring Harbor Protocols 2010; **2010**: pdb.prot5448. DOI: 10.1101/pdb.prot5448
22. Hoffman EK, Trusko SP, Murphy M*, et al.* An S1 nuclease-sensitive homopurine/homopyrimidine domain in the c-Ki-ras promoter interacts with a nuclease factor. Proceeding in National Academy of Science 1990; **87**: 2705-2709
23. Hallick RB, Chelm BK, Gray PW*, et al.* Use of aurintricarboxylic acid as an inhibitor of nucleases during nucleic acid isolation. Nucleic Acids Research 1977; **4**: 3055-3064
24. Solymosy F, Fedorcsák I, Gulyás A*, et al.* A New Method Based on the Use of Diethyl Pyrocarbonate as a Nuclease Inhibitor for the Extraction of Undegraded Nucleic Acid from Plant Tissues. European Journal of Biochemistry 1968; **5**: 520-527
25. Rao BS Regulation of DNA replication by homopurine/homopyrimidine sequences. Molecular and Cellular Biochemistry 1996; **2**: 163-168
26. Mott ML, Berger JM DNA replication initiation: mechanisms and regulation in bacteria. Nature Reviews Microbiology 2007; **5**: 343-354
27. Nasheuer H-P, Smith R, Bauerschmidt C*, et al.* Initiation of Eukaryotic DNA Replication: Regulation and Mechanisms. Progress in Nucleic Acid Research and Molecular Biology 2002; **72**: 41-93

Chapter 5

Conclusions and Future Directions

In this dissertation, I've examined cellular internalization mechanisms for polycationic polymers used in nucleic acid delivery systems and also how cell responds to the polymer/DNA polyplexes once they are inside cells. In chapter 2 it was shown that contrary to literature reports, [1] GM_1 mediated endocytosis doesn't play an important role in G7 PAMAM dendrimer internalization. The false positive results that the other investigations reported, reproduced by our laboratory as well, was due to a previously unappreciated interaction between G7 PAMAM dendrimer and the endocytosis marker CTB. Our study was successful because it was performed with the help of a unique and indispensably functional marker called GM_1. C6 cells were employed in this experiment because of their unique characteristic of inherently lacking GM_1 but still possessing all downstream requirements for successful GM_1 mediated endocytosis. [2] C6 cells can be made to undergo GM_1 mediated endocytosis by simple overnight incubation with GM_1. [2] This unique characteristic of C6 cells resulted in the reported binary experiment where C6 cells without and with GM_1 did not show differential G7 PAMAM dendrimer uptake. This supports the hypothesis that GM_1 mediated endocytosis is not the primary pathway for G7 PAMAM dendrimer internalization. Subsequent

repetition of this study with G7 polyplexes by Qi et al. also resulted in the conclusion that GM_1 mediated endocytosis is not the primary internalization pathway for PAMAM dendrimer polyplexes. [3] In chapter 2, only G7 PAMAM dendrimer was tested. One way to improve this study is to test polyplexes made by B-PEI, L-PEI and jetPEI™. As all these polymers facilitate different level of gene expression testing if they require GM_1 mediated endocytosis to transfect can provide important information about role of GM_1 in successful gene expression.

The overall goal of chapters 3 and 4 is to improve our understanding of intracellular response to polyplexes that lead to decrease transgene expression. In these chapters I examine the downstream processes that happen once polyplexes are inside cells. Work by Pollard et al. [4] and Lechardeaur et al. [5] showed that foreign DNA inside cells is rapidly degraded. This leads to the hypothesis that cells respond to the polyplexes by activating cytosolic nucleases. These active nucleases then degrade the transported nucleic acid and, in case of pDNA, lead to a decrease in downstream gene expression. Another important observation from this study was that the level of nuclease activation is directly dependent on the specific polymer used to make polyplexes.

In this study a variety of polycationic polymers with different molecular architecture were used. This is the first time molecular architecture of polymer has been related to nuclease activation inside cells bearing direct impact on the transgene expression. Having the missing link between polymer system and expression is a great tool as this nuclease activation can be easily measured with the

help of molecular beacon. Specific polymers can now be designed to mimic L-PEI in terms of nuclease activation to in turn facilitate good transgene expression. Nuclease activation may not be a bad consequence for some nucleic acid delivery systems like asDNA and siRNA delivery. asDNA and siRNA are oligonucleotides that have been shown to have many important applications in therapeutics and are functional in cytoplasm. [10-13]

An optimum polymer system for asDNA and siRNA will be characteristically different from polymer vectors for pDNA delivery. An optimum polymer for oligonucleotide delivery should hypothetically allow DNA to be in a less-bound form, so that it's available for the downstream processes in the cytosol. Studying nuclease activation facilitated by polymers transporting oligonucleotide and how that impacts the efficacy of these oligonucleotides will provide unprecedented knowledge to help design better polymer systems asDNA and siRNA delivery.

Nuclease activity in these systems will represent greater cytosolic enzyme interaction, which can be very important for success of these systems. asDNA and si RNA may require downstream enzyme interaction in the cytosol for them to be functional. Polymer systems can be designed that allow cytosolic enzyme interaction but specifically inhibit nuclease activity if required.

Some specific experimental ways to improve our understanding of cytosolic nucleases: one way to take this study forward is to examine if there is a direct one to one relationship between cytosolic nuclease activation and gene expression. If decreasing nuclease activity inside cells leads to increase in gene expression by polyplexes, it will indicate that nuclease activation is a primary reason for low gene

expression. One way to address above the hypothesis is by adding nuclease inhibitors during polyplex treatment. The presence of nuclease inhibitors will decrease nuclease activation measured by MB fluorescence thus increasing gene expression. This experiment is different from other published studies[6-9] because here we will have a direct measurement of nuclease activity which none of the previous studies had.

One important question that arises from chapter 3 is where the foreign DNA degradation happens inside the cell. To address this question, an experiment can be designed with fluorescent markers specific to organelles like Endoplasmic Reticulum, Golgi bodies and lysosomes. These markers can be covalently bound to the DNA in the polyplex sample and once they are inside the cell their colocalization with MB can be measured and monitored.

Another question that remained unanswered in chapter 3 is the induction pathway for cytosolic nuclease activation. One of the conclusions of chapter 3 is that membrane permeability facilitated by polycationic polymer is not related to nuclease activation. Experiments can be designed that tests other polymer characteristic like charge per particle and how that relates to nuclease activation and ultimately gene expression. This experiment can help in selecting optimum charge/particle to get minimum nuclease activation and in turn getting maximum expression.

The aim of chapter 4 is to improve our understanding of cytosolic nucleases. In this study, high-throughput sequencing was used to fingerprint cytosolic nucleases as well as S1 nuclease. With the help of high-throughout sequencing, previously

unreported labile sites were found that were susceptible to S1 nuclease.[14-16] Interestingly, the most susceptible cut region for S1 nuclease overlaps with the susceptible region of cytosolic nucleases, consistent with the hypothesis that S1 type nuclease are part of the cytosolic nuclease milieu. No significant homology was observed between these labile sequencing suggesting that these nucleases are promiscuous in nature. Additionally, gel results indicate that S1 and cytosolic nuclease are more likely to cleave supercoiled DNA than the linear form of the DNA. A lot of work has been dedicated to improve nucleic acid sequence to make it nuclease resistant but as many of these sites lie in indispensable functional parts of pDNA, there is a limit to DNA sequence optimization. Understanding labile regions where DNA gets degraded can help design novel polymer vector systems that protect these sites and ultimately improving the downstream gene expression.

This study can be improved by sequencing the transported DNA itself by high-throughput sequencing. By sequencing the transported DNA and using other polymer used in nucleic acid delivery, this experiment can answer questions and concerns raised in chapter 4. There are studies showing that once the pDNA is nicked it becomes non-functional in terms of gene expression. [17] Sequencing experiments are very well poised to test this hypothesis. One way sequencing can address this hypothesis is by separating nuclear extract from cytosolic extract, and then sequencing the transported pDNA in each fraction. If the sequencing shows that nuclear fraction pDNA is less degraded as compared cytosolic fraction pDNA then it will support the above hypothesis.

Degradation pattern for L-PEI and jetPEI™ like polymers that facilitate good transgene expression can be used as gold standards. New polymer candidates can then be quickly compared. The shortlisted candidates can then be checked using in cell MB experiments to measure their efficacy before moving onwards with in-vivo animal studies.

5.1 References

1. Manunta, M., et al., *Gene delivery by dendrimers operates via a cholesterol dependent pathway.* Nucleic Acids Research, 2004. **32**: p. 2730-2739.
2. Spiegel, S., *Insertion of ganglioside GM1 into rat glioma C6 cells renders them susceptible to growth inhibition by the B-subunit of cholera-toxin.* Biochimica et Biophysica Acta, 1988. **969**: p. 249-256.
3. Qi, R., et al., *The Mechanism of Polyplexes Internalization into Cells: Testing the GM1/Caveolin-1-Mediated Lipid Raft Mediated Endocytosis Pathway.* Molecular Pharmaceutics, 2010. **7**: p. 267-279.
4. Pollard, H., et al., *Ca2+-sensitive cytosolic nucleases prevent efficient delivery to the nucleus of injected plasmids.* The Journal of Gene Medicine, 2001. **3**: p. 153-164.
5. Lechardeur, D., et al., *Metabolic instability of plasmid DNA in the cytosol: a potential barrier to gene transfer.* Gene Therapy, 1999. **4**(482-497).
6. Ross, G.F., et al., *Enhanced reporter gene expression in cells transfected in the presence of DMI-2, an acid nuclease inhibitor.* Gene Therapy, 1998. **5**(9): p. 1244-1250.
7. Desigaux L, et al., *Nonionic amphiphilic block copolymers promote gene transfer to the lung.* Human Gene Therapy, 2005. **16**: p. 821-829.
8. Freeman, D.J. and R.W. Niven, *The influence of sodium glycocholate and other additives on the in vivo transfection of plasmid DNA in the lungs.* Pharmaceutical Research, 1996. **13**: p. 202-209.
9. Glasspool-Malone, J. and R.W. Malone, *Marked enhancement of direct respiratory tissue transfection by aurintricarboxylic acid.* Human Gene Therapy, 1999. **10**: p. 1703-1713.
10. Gary, D.J., N. Puri, and Y.-Y. Won, *Polymer-based siRNA delivery: Perspectives on the fundamental and phenomenological distinctions from polymer-based DNA delivery.* Journal of Controlled Release, 2007. **121**: p. 64-73.
11. Murata, M., et al., *Novel DNA/polymer conjugate for intelligent antisense reagent with improved nuclease resistance.* Bioorganic & Medicinal Chemistry Letters, 2003. **13**(22): p. 3967-3970.
12. Rakoczy, P.E., *Antisense DNA technology.* Methods in Molecular Medicine, 2001. **47**: p. 89-104.

13. Raymond, M.S., et al., *Cancer siRNA therapy by tumor selective delivery with ligand-targeted sterically stabilized nanoparticle.* Nucleic Acids Research, 2004. **32**(19): p. 149-158.
14. Ribeiro, S.C., G.A. Monteiro, and D.M.F. Prazeres, *The role of polyadenytation signal secondary structures on the resistance of plasmid vectors to nucleases.* Journal of Gene Medicine, 2004. **6**: p. 565-573.
15. Azzoni, A.R., et al., *The impact of polyadenylation signals on plasmid nuclease-resistance and transgene expression.* The Journal of Gene Medicine, 2007. **9**: p. 392-402.
16. Hoffman, E.K., et al., *An S1 nuclease-sensitive homopurine/homopyrimidine domain in the c-Ki-ras promoter interacts with a nuclease factor.* Proceeding in National Academy of Science, 1990. **87**: p. 2705-2709.
17. Banerjee, S. and D.J. Spector, *Differential effect of DNA supercoiling on transription of adenovirus genes in in vitro.* Journal of General Virology, 1992. **73**: p. 2631-2638.

Chapter 6

The Endocutter*: A Gastrointestinal Medical Device That Cuts Clots, Cuts Cost and Saves Lives

6.1 Abstract

A major problem in the endoscopic treatment of upper gastrointestinal (GI) bleeding is the removal of blood clots inside the stomach.[1-3] The ineffectiveness of existing methods to remove blood clots quickly during active bleeding events has led to the development of the Endocutter. This device is designed to be used in conjunction with the endoscope's existing suction power, chopping up blood clots and similar stomach content before they enter the narrow instrument channel. The device is effective in facilitating the removal of blood clots in a short time span, reducing procedure risk by limiting the number of endoscope reinsertions, and eliminating the need to perform second endoscopy procedures. Furthermore, the Endocutter aims to be cost-effective by reducing patient length of stay and saving the hospital $2,000 - $3,000 per procedure.[4] Most importantly, the Endocutter aims to decrease mortality rates by reducing the number of second endoscopies.

*A team of four engineers invented Endocutter: Rahul Rattan, Tareef Jafferi, Zachary T. Weingarden and Raghunath Sai Katragadda. Apart from working in a collaborative team, my individual responsibility included prior art and patentability analysis, medical device standard research, reimbursement and FDA approval analysis.

6.2 Problem Description

During an episode of upper GI bleeding, an endoscope is passed through the patient's esophagus and into the GI tract for a visual assessment of the bleeding location,[2] this procedure is called gastroduodenoscopy. A major problem in endoscopic management of upper GI bleeding is the difficulty to identify the bleeding source, which is often obscured by overlying blood and clots.[1-3] Traditional efforts of removing blood clots are via lavage (i.e. using large bore gastric tubes or suction through large channel therapeutic endoscopes). [1, 2] These methods often fail to dislodge blood clots that are adherent to the base of the bleeding site. Another method is to remove clots mechanically with a snare.[2] Physicians are generally reluctant to use this latter technique because of the risk of induced bleeding.[2] A clot dissociating composition comprising of hydrogen peroxide and a surfactant can also be used;[3] however, this process is time-consuming and the delay in treatment can lead to serious consequences. These problems have fueled the search for quicker and cost-effective ways to remove blood clots from stomach during gastroduodenoscopy.

6.3 Objective Statement

The Endocutter is an accessory that is compatible with any large instrumental endoscope. The device is to be used in conjunction with the endoscope's existing suction power, chopping up blood clots and similar stomach content before they enter the narrow instrument channel. It consists of a motor with a spinning blade shaft encased in a clear polycarbonate shell that can be attached at the distal end of the endoscope and powered via wiring through the instrument channel. The blade

is recessed and surrounded by the shell in order to protect the stomach lining from contact with the blade. The motor is sufficiently small to be placed on the end of the endoscope while preserving the visual field and use of the instrument channel. The Endocutter allows the physician to quickly locate the bleeding site without the need for repeated endoscope reinsertions or extended patient stay.

6.4 Prototype of the Final Design

The final prototype has been designed to maintain functionality of the endoscope while ensuring safety and effectiveness. The CAD models of the prototype (Figure 6.9.1) are designed using the software CATIA V5R17. The prototype is comprised of five components integrated in the complete design. These components are the protective polycarbonate casing, rubber attachment, electric motor, blade connector, and blade. The wiring for the prototype includes male and female connectors soldered to the wires, allowing them to be passed through the instrument channel of the endoscope. The end terminals of the wires are connected to a switch that is integrated with a battery. The physician can power the battery-operated motor using this switch. The prototype is 30 mm long with an outer diameter of 14.6 mm (similar in diameter to dual-channel endoscopes). The polycarbonate casing is 25 mm long, 1 mm thick, and transparent to maximize the field of vision. The motor holder has an inner diameter of 6 mm and a curvature angle of 270 degrees to secure the motor in place. It is mounted on a stem that spans the 15 mm motor holder. The motor itself is 6 mm in diameter, 15 mm in length, and is placed 3 mm from the tip of the casing. The blade is connected to the shaft using a blade connector placed over the shaft. The blade has dimensions of 10

mm in length, 1 mm in width, and 0.1 mm in thickness and is passed over the spindle and glued using industrial stainless steel adhesive. A rubber attachment is fixed over the other end of the casing and secures the prototype at the distal end of the endoscope.

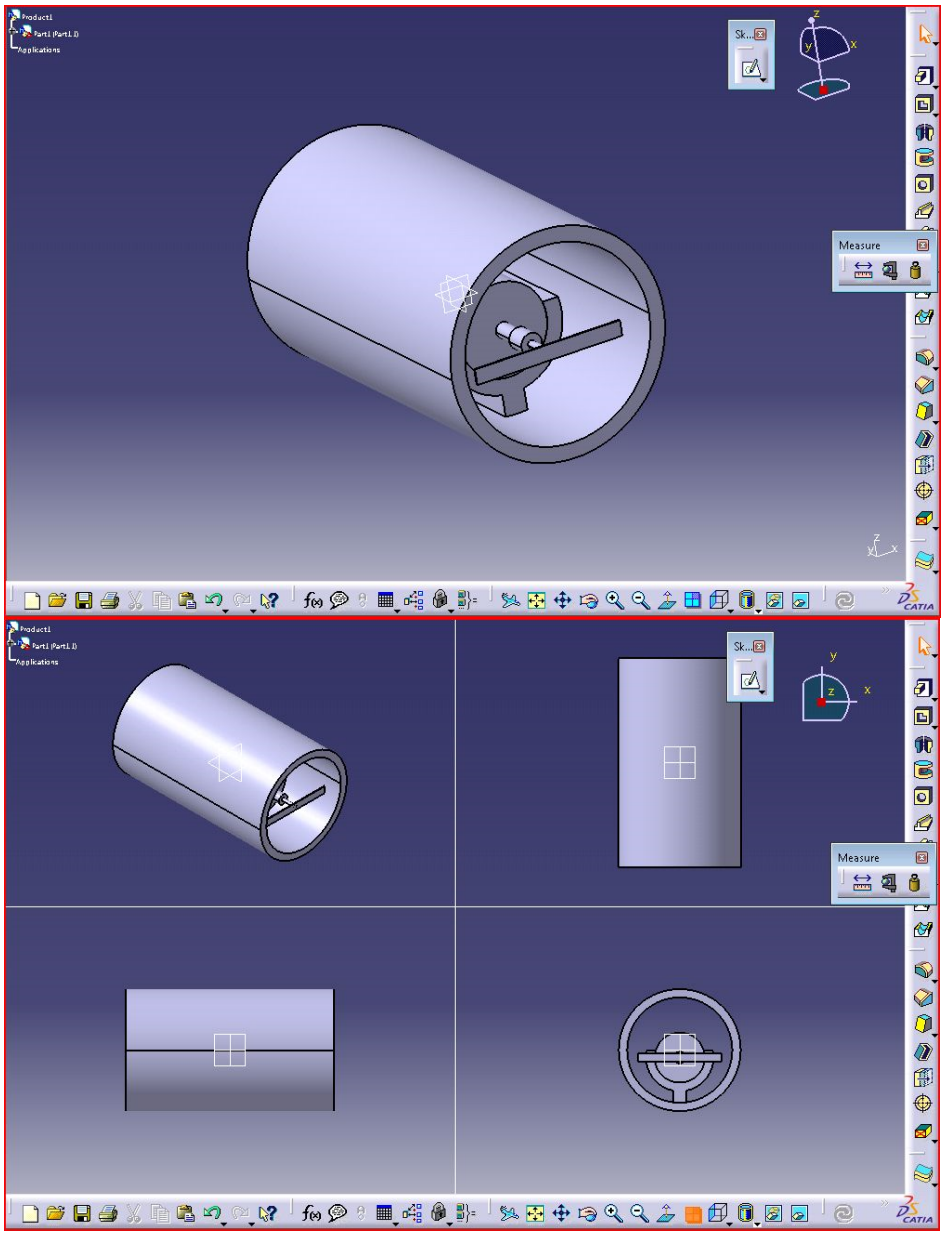

Figure 6.1. Below are CAD representations of the polycarbonate attachment with the motor in place.

6.5 Intellectual Property

6.5.1 Prior Art

An exhaustive patent search revealed no endoscopic attachments or accessories that incorporated a micro-motor. Searches for similar endoscope attachments or clot removal methods yielded the following patents and patent applications:

6.5.1.1. Endoscopic apparatus with integrated hemostasis device [5] (Application No.10/955,908)

6.5.1.2. Multichannel endoscope[6] (Patent No. 4146019)

6.5.1.3. Clot dissolving method[7] (Patent No. 5846567)

6.5.1.4. Method and apparatus for removing blood clots and other objects[8] (Patent No. 5947995)

6.5.1.5. Method and associated device for removing clot[9] (Patent No. 5520635)

There are no existing patents that include the features of the Endocutter. It can therefore be concluded that there is little risk for patent infringement.

6.5.2 Patentability Analysis

This device is patentable as it meets these three criteria:

6.5.2.1. **Novel**: This is the first device to incorporate a motorized cutting tool with an endoscope for gastroduodenoscopy procedures.

6.5.2.2. **Non-obvious**: This device is specifically designed to use mechanical power and suction while still preserving the functions of an endoscope.

6.5.2.3. Utility: This device presents a method that efficiently removes clots and improves the overall effectiveness of the procedure.

Utility patent for Endocutter was filed in December 2011.

6.6 Applicable Standards

Applicable standards have been divided into the following components (Table 6.10.1):

6.6.1. Process standards: These standards specify the controls and methods to be used to manage all aspects of a manufacturing business, including design requirements and evaluation of potential design hazards.

6.6.2. Standard testing methods: These standards specify material safety tests and acceptance criteria that must be satisfied for a biocompatible device.

6.6.3. Performance standards: These standards describe performance attributes for the device.

Table 6.1. Standards applicable to the Endocutter.

Process standards	Standard testing methods	Performance standards
ISO 10993: 2003	ISO 10993-1:2003	ISO 8600-6:2005
ISO 14971:2007	IEC 60601	ISO 15223:2000
ISO 14937:2000		ISO 15225:2000
ISO 11137-1:2006		ISO 11607-2:2006
EN ISO 14155-1,2:2003		CEN/TR 15133:2005

6.7 FDA Regulatory Pathway

The Endocutter falls under 876:4300,[10] endoscopic electrosurgical unit and accessories. It is a class II device and non-exempt for GMP.[10] The submission type would be 510(k) premarket approval, where the device must be compared to previously marketed devices to support the substantial equivalency claims.[10] To prove substantial equivalence, it must be shown that the device has the same intended use as a predicate or does not raise new questions of safety and effectiveness.

Predicate devices for substantial equivalence are:

6.7.1. X-SIZERS Catheter System: [11] This device is a cardiovascular device used to mechanically remove clots from blood vessels, aided with suction, making it substantially equivalent, as the Endocutter clears clots by using mechanical methods and suction.

6.7.2. Auto-Band Ligator: [12] This device is an attachment to the endoscope tip. It has a number of bands that can be ejected and snapped around blood vessels, veins, or arteries that have burst. This device is substantially equivalent, as it is also an endoscope attachment.

As Endocutter is a potential license out technology the team has decided to not pursue FDA regulatory pathway, as it will not add much value to the final product.

6.8 Conclusion and Future Directions

Exit strategy for Endocutter is a potential license out. Currently, I am trying to find potential licensees for Endocutter with the help of Office of Technology Transfer at the University of Michigan. The prototyping for Endocutter has come to an end as of

February 2012 and at the present moment there are no ongoing negotiations for Endocutter with potential licensees.

6.9 References

1. Stollman, N.H., et al., *The uncleared fundal pool in acute upper gastrointestinal bleeding: implications and outcomes.* Gastrointestinal Endoscopy, 1997. **46**(4): p. 324-327.
2. Cappell, M.S. and D. Friedel, *Acute Nonvariceal Upper Gastrointestinal Bleeding: Endoscopic Diagnosis and Therapy.* The Medical Clinics of North America, 2008. **92**: p. 511-550.
3. Lennon, A.M. and A.N. Kalloo, *Hydrogen Peroxide in Upper Gastrointestinal Bleeding: A Coming of Age?* Digestive Diseases and Sciences, 2010. **55**(2): p. 223-225.
4. Dasta, J.F., et al., *Daily cost of an intensive care unit day: the contribution of mechanical ventilation.* Critical Care Medicine, 2005. **33**(6): p. 1266-1271.
5. Couvillon, L., *Endoscopic apparatus with integrated hemostasis device*, USPTO, Editor 2006, Couvillon Lucien A Jr: US.
6. Bass, M. and R.M. Dwyer, *Multichannel endoscope*, USPTO, Editor 1979, University Of Southern California: US.
7. Kalloo, A.N. and P.J. Pasricha, *Clot dissolving method*, USPTO, Editor 1998, Chek-Med Systems, Inc.: US.
8. Samuels, S.L.W., *Method and apparatus for removing blood clots and other objects*, USPTO, Editor 1999, Shaun Lawrence Wilkie Samuels: US.
9. Gelbfish, G.A., *Method and associated device for removing clot*, USPTO, Editor 1996, Gary A. Gelbfish: US.
10. FDA, *Code of Federal Regulations Title 21*, 2012, FDA: http://www.accessdata.fda.gov/scripts/cdrh/cfdocs/cfCFR/CFRSearch.cfm?fr=876.4300.
11. ev3-Inc., *510(k) Premarket Notification for X-SIZER CATHETER SYSTEM*, 2004, FDA: http://www.accessdata.fda.gov/cdrh_docs/pdf2/K021096.pdf.
12. Scandimed-International, *510(k) Premarket Approval for Auto-Band Ligator* 2008, FDA: http://www.accessdata.fda.gov/cdrh_docs/pdf8/K081142.pdf.